ACTIVE MAGNETIC BEARING
DESIGN AND CHARACTERIZATION
FOR HIGH TEMPERATURE APPLICATIONS

THÈSE N^O 3616 (2006)

PRÉSENTÉE LE 6 SEPTEMBRE 2006

À LA FACULTÉ DES SCIENCES ET TECHNIQUES DE L'INGÉNIEUR

Institut de production et robotique

SECTION DE MICROTECHNIQUE

ÉCOLE POLYTECHNIQUE FÉDÉRALE DE LAUSANNE

POUR L'OBTENTION DU GRADE DE DOCTEUR ÈS SCIENCES

PAR

Luc BURDET

ingénieur en microtechnique diplômé EPF
de nationalité suisse et originaire de Ursins (VD)

acceptée sur proposition du jury:

Prof. Y. Perriard, président du jury
Prof. R. Siegwart, directeur de thèse
Dr B. Aeschlimann, rapporteur
Prof. G. Schweitzer, rapporteur
Prof. H. Bleuler, rapporteur

ÉCOLE POLYTECHNIQUE
FÉDÉRALE DE LAUSANNE

Lausanne, EPFL
2006

Acknowledgements

This thesis is the result of the work I carried out at the Autonomous System Lab at the Swiss Feredal Institute of Technology in Lausanne (EPFL). I would like to express my sincere gratitude the following people, who made this work possible:

- Prof. Roland Siegwart: for giving me the opportunity to work at his laboratory, for scientific freedom and his advise.

- Dr. Beat Aeschlimann: for being my supervisor, for his guidance and support, his patience, for many helpful comments and his friendship.

- Co-examiners: Prof. Gerhard Schweitzer, Prof. Hannes Bleuler and Prof. Yves Perriard

- The State Secretariat for Education and Research: for the financial support [9].

- Thomas Maeder and Giancarlo Corradini: for all the discussions about high temperature materials and for the realization of the position sensors.

- Alfons Traxler: for giving me the opportunity to work at the company Mecos Traxler AG.

- Philipp Buehler: for his advice, his great help for the position sensor development, electronics and for his endless discussions and his great interest to all high temperature technical aspects.

- Manuela Joehl, Matthias Kohler, Suzanne Bolli, Florian Loesch and Markus Dietrich: for their great help for the realization of the test rig.

iv

Résumé

Cette thèse est née d'un des plus grands marchés actuels: l'aviation. En effet, ce marché dans lequel la concurrence et les sommes mises en jeux sont extraordinaires, nécessite un besoin constant d'améliorations notamment techniques pour augmenter sa compétitivité.

Les turbines d'avion ont une influence non négligeable sur la consommation de kérozène et sur la maintenance des avions, donc sur les coûts du transport aérien. La thèse présentée ici traite du sujet et est supportée par la communauté européenne [9].

Cette thèse débute par une introduction situant ce travail dans les mondes économique et technique actuels. Les avantages d'un tel système sont donnés, ainsi que la contribution scientifique des recherches qui ont été menées.

Une introduction sur les palier magnétiques est donée, de manière à ce que les éléments clefs du dimensionnement d'un tel système soient compréhensibles pour des lecteurs de tous horizons. La force maximale pouvant être produite par des paliers magnétiques est en grande partie limitée par l'échauffement lié aux pertes du système. Un modèle thermique du palier valide pour les hautes températures a été implémenté. Une partie expérimentale a permis la validation de ce modèle sur une large gamme de températures.

La construction d'un palier magnétique nécessite différents types de matériaux; des matériaux magnétiques doux, des conducteurs électriques, des isolants électriques ainsi que plusieurs matériaux de fixation. Des tests ont été menés et un catalogue répertorie les matériaux disponibles pour la conception de systèmes électro-magnétiques fonctionnant à haute température.

Les paliers magnétiques fonctionnent pour la majorité des cas avec des capteurs de position. Des capteurs de position à courants de Foucault

ont été développés. Ils ont été réalisés avec des bobines imprimées sur un substrat en céramique, en utilisant la technologie des couches épaisses. Des mesures pratiquées à haute température montrent les propriétés de ces capteurs. Des problèmes de migration d'argent ont rencontrés entre les soudures de fils, lors de tests effectués à haute température. Diverses solutions ont été testées dans le but de stopper cette migration de l'argent.

Les matériaux exposés à haute température ont malheureusement une durée de vie parfois limitée. Une études des problèmes menant aux dysfonctionnements liés à une exposition à la haute température est présentée. Certains dysfonctionnements provoquent des détériorations détectables par le palier magnétique. Un exemple de détection d'éventuels courts-circuits dans les bobines d'actuateur est développé.

Finalement un prototype de palier magnétique comprenant cinq degrés de liberté a été construit. Un four développé pour l'occasion permet de créer un environnement à haute température. Les caractéristiques du palier pendant la lévitaion ont été mesurées à partir de la température ambiante jusqu'à 550°C.

Mots-Clés

AMB, palier magnétique actif, haute température, turbine d'avion, modèle thermique, matériau magnétique doux, saturation magnétique, bobine, actuateur, isolation, capteur de position, courants de Foucault, couches épaisses, céramique, argent, migration, four, lévitation, stabilité.

Abstract

This thesis is motivated by one of the largest markets: aviation. This market, in which competition and investments are extraordinary, requires constant technical improvements in order to increase its competitivness.

Jet engines have an important influence on fuel consumption and servicing of airplanes, thus on the transportation cost. The present work was supported by the European Community [9].

This thesis investigates the use of active magnetic bearings for jet engines. It is expected that magnetic bearings could considerably reduce losses and service intervals in jet engines. The present work concentrates on the design and characterization an active magnetic bearing for applications at high temperature.

The report begins with an introduction locating the accomplished work into the current economic and technical context. The advantages of such system are given, as well as the scientific contribution of the research which has been undertaken.

An introduction to magnetics bearing is given, so that the key elements of the dimensioning of such a system are comprehensible for readers of all horizons. The maximum force produced by magnetic bearings is mainly limited by the heating related to the losses in the coils. A thermal model for high temperature magnetic bearings has been implemented. An experimental part allowed the validation of this model for a wide temperature range.

The construction of a magnetic bearing requires various types of materials; soft magnetic materials, electrical conductors, electrical insulators as well as several fixation materials. Tests have been carried

out and a catalogue lists the materials available for high temperature magnetic bearings.

Position sensors are usually used in magnetic bearings. Eddy current position sensors have been developed. They were realized with coils printed on a ceramics substrate by using thick-film technology. Measurements done at high temperature show the great characteristics of these sensors. Problems of silver migration between the wire weldings have been encountered during tests carried out at high temperature. Various solutions have been tested with the aim of avoiding the silver migration.

The materials exposed at high temperature have unfortunately sometimes a limited lifespan. Studies of failures related to an exposure at high temperature have been done. Some failures are detectable by the magnetic bearing. An example of detection of possible short-circuits in the actuator coils is presented.

Finally a prototype of an active magnetic bearing system with five degrees of freedom has been built. A furnace especially developed, makes it possible to create environments at high temperature. The characteristics of the active magnetic bearing have been measured during levitation at ambient temperatures from $25\,^{\circ}$C up to $550\,^{\circ}$C.

Key words

AMB, active magnetic bearing, high temperature, jet engine, aero-engine, thermal model, soft magnetic material, magnetic saturation, coil, actuator, insulation, position sensor, eddy current, thick layers technology, ceramics, silver migration, furnace, levitation, stability.

Contents

Chapter 1

Introduction

The introduction of this thesis presents first the motivation and framework of this project. An overview of the industrial needs, from which this project is born, is shown in section 1.1.

Section 1.2 gives the state-of-the-art in high temperature magnetic bearing research. The contribution of this thesis is presented in section 1.3. Finally in section 1.4, the whole dissertation is outlined.

1.1 Frame of This Work

The world's aero-space industry showed the last years losses in gigantic proportion (several tens of billions Dollars [36]). The air-transport market is very competitive and complicated. Growth is nevertheless continuous. Rolls-Royce forecasts a growth by an average of 5% per year over the period of 1998 to 2017 [37]. Some cost, as for example kerosene price, are not controllable by aircraft companies. Nevertheless, maintenance cost and kerosene consumption can be reduced by improving technical components in aircraft gas turbines engines.

Active magnetic bearings (AMB) have been successfully used in various applications for several decades. They show great abilities to work under extreme conditions, such as vacuum, high rotation speed or at high temperature [40]. AMB are used today in applications such as turbo-molecular pumps, turbo expanders, textile spindles, machine

tool spindles [42], hard disk drives [2] and magnetically levitated vehicles (MAGLEV). The idea here is to use magnetic bearings in aircraft jet engine.

Advantages of Jet Engine Running on Magnetic Bearings

Current jet engine systems are supported by ball bearings and dampers, which are limited in speed and temperature ($<260°$C). Additionally, these systems require complicated secondary cooling paths and an intricate lubrication system. These components significantly increase the weight, complexity and cost of the aircraft.

A way to improve the jet engine is to make it more electrical [37]. The concept is to replace lubrication, hydraulic and pneumatic systems by a single powerful electrical generator, and electrical components.

Since magnetic bearings can operate at high temperature, the whole system can be dramatically improved. Because there are no contacting parts in magnetic bearings, the lubrication system can be eliminated. Studies have shown than a jet engine with AMBs weights up to 5% less that the equivalent engine with conventional bearings.

By removing lubrication in the bearings, oil emissions are reduced, which provides direct environmental benefits. The removal of oil in the system makes it more fire safe as well.

Since AMB are non-contact bearings, the friction losses are eliminated. This provides a direct improvement in terms of kerosene consumption. Furthermore a non-contact system avoids fatigue and wear, which occur with ball bearings. The operating speed and the efficiency can be increased as well.

Magnetic bearing is an active system, thus it provides several advantages over a passive one. The controller can compensate unbalance and control the rotor behaviour actively at critical speeds. System monitoring is then possible by using the AMB as a sensor, which provides indications about the changes in shaft dynamics. This system diagnosis enables to reduce the maintenance cost by increasing the intervals between engine services.

An European research project named *MagFly* has been created with the goal of developing a smart jet engine using magnetic bearings. Part of it was to develop AMBs working at high temperature. The present work has been supported by *MagFly* [9].

1.2   State of the Art

A first European project named Active Magnetic Bearing in Aircraft Turbo-machinery (AMBIT) [48, 50, 45, 49], laid the groundwork for the present research.

The objectives of AMBIT were to investigate and to demonstrate the feasibility of an active magnetic bearing that works at up to 540°C. A one-degree-of-freedom high temperature AMB rig was built as well as a five-degree-of-freedom prototype with a high temperature radial bearing.

The AMBs developed in AMBIT satisfied the requirements, but problems were encountered with overheating and coil short circuits. Position sensors for high temperature applications were developed [47] during this project.

Previous work done by others, in the seventeenth research was done [22] for aero-space applications. Research was done on the mechanical properties of iron-cobalt alloys [12, 11] for high temperature electromechanical machines. Short term tests on magnetic and mechanical properties of iron-cobalt alloys was done for magnetic bearing applications [20]. Tests on systems developed for high temperature applications done at room temperature have been presented in [25, 28]. Glenn H. Research Center works presently on a high temperature AMB, which is composed of a single radial bearing located at the center of a shaft mounted on ball bearings [26, 27].

Work has been done as well on fault tolerant systems in view of an integration in turbo-machinery systems [10] and recently for a combined magnetic-hydrostatic bearing [17] has been proposed.

However, no work with a 5 degree-of-freedom system running at 550°C has been reported until now.

The major application of AMBs nowadays are turbo-molecular pumps. The advantages of AMBs compared to conventional bearings can be very significant. They work without emission of lubricant, without emission of particles due to friction and without wear and are moreover very reliable. A lot of systems are running for more than ten years without maintenance. All these advantages make AMBs being a highly attractive alternative to the existing jet engine ball bearings.

1.3   Contribution of this Thesis

Building a product, which is ready to be inserted in an aero-engine, is obviously out of reach of this work. However, the field of this thesis is quite new, and only few publications are available until this day. The contributions of this thesis are the following:

- In the context of this thesis the first 5 axis AMB running at environment temperatures up to 550˚C has been developed and tested.

- A modular finite elements thermal model with low computation time has been implemented and validated for high temperature AMBs.

- Materials for the design of high temperature electromechanical systems have been tested and reported.

- Thick-film low cost eddy current position sensors for 550˚C applications have been developed.

- An analyse of failures related to high temperature applications is presented and illustrated with the simulation of a reported case.

1.4   Structure of this Thesis

This thesis is structured as follows. Chapter 2 gives an overview of the basics of AMB theory. The information given here should enable non-specialists in magnetic bearing to get the main purposes, and give them the possibility to understand the next chapters.

Chapter 3 gives the high temperature aspect in high temperature electro-mechanical designs. Materials, especially magnetic, conductive and electrical insulations have been tested and are described in this chapter.

Chapter 4 presents an innovative way of position sensing. Sensors, working from room temperature up to 550˚C, have been realized with printed coils on ceramic substrates. Construction details, sensing principle and measurements are given in this chapter.

Chapter 5 describes a thermal model developed for high temperature magnetic bearings. Temperature is the main force limitation of electro-mechanical systems.

In chapter 6 reliability aspects are studied. Faults which can occur in AMB because of high temperature exposure are outlined. A strategy of fault detection using the AMB as diagnosis tool is discussed.

Chapter 7 presents the result of the whole thesis. It describes the construction and characterization of a high temperature AMB prototype. This chapter is probably a good starting point for the readers interested first in a quick survey of this thesis. Concrete solutions are given in it. Nevertheless for a better understanding of the reasons of the technical choices, the related chapters have to be consulted. Readers with no knowledge on AMBs should start reading with the first section of chapter 2.

Chapter 2

AMB Basics

Books and publications have been already written on the topic of active magnetic bearings. A lot of literature is available at this day, namely in the proceedings of the ISMB[1]. This introduction does not provide a complete theory about AMB. Nevertheless, an overview of the AMB theory is given in order to give the non-specialist readers the bases for the next chapters of this thesis.

This introduction is mainly based on the book *Active Magnetic Bearings* [41] and the book chapter [38] entitled *Industrial Magnetic Bearings - Basics and Applications*.

2.1   AMB General Schema

This section provides a general overview of active magnetic bearings. The main components as well as the basic working principle are presented.

2.1.1   Working Principle

Figure 2.1 shows the basic components of a magnetic bearing and its working principle. A magnetic rotor is suspended by an electromagnet. In order to get an active control of the rotor, its position is

---

[1]International Symposium of Magnetic Bearings
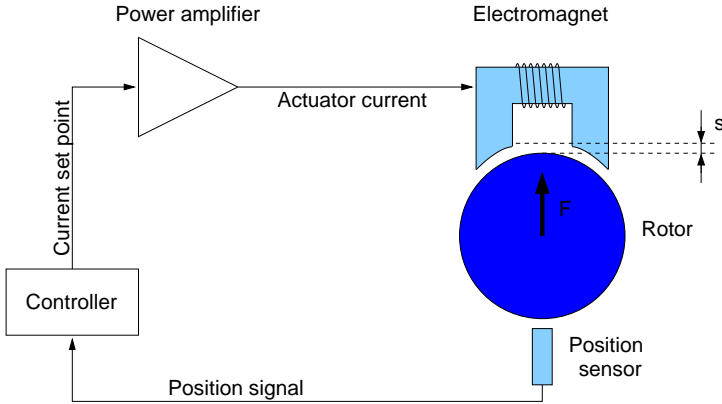
Figure 2.1: Function principle of the active magnetic bearing.

measured by a position sensor. The position signal is then treated by a controller, which gives a current set point. This signal is then amplified by the power amplifier, in order to get the necessary actuator current. A closed loop control is thus realized and the system can be stabilized.

This single actuator enables the levitation along only one axis and only in one direction. In AMB systems, several actuators are used in order to control the rotor levitation along several degrees-of-freedom (DOF). Actuators are typically arranged as pairs facing each-other. This enables to attract the rotor in two opposite directions along one axis (see subsection 2.2.2).

2.1.2 AMB components

The basic AMB components are shown in figure 2.1. Electromagnets are composed of a soft magnetic core and electrical coils. They look somewhat like the stator of an electrical motor.

Iron Core

The iron core is a material conducting the magnetic field to the air gap. Its magnetic permeability has to be high, as well as its magnetic saturation. In order to minimize eddy current losses, the core usually consists of insulated lamination sheets.

Windings

The current through the winding is the source of magnetic field. The winding is made of an insulated conductor wound on the soft magnetic core. In order to improve the efficiency of the AMB, the conductor has to have a low electrical resistance and must be wound with a high fill-factor.

Rotor

The rotor, in standard constructions, is realized with a lamination packet shrinked on a non magnetic shaft. Tight manufacturing tolerances are needed in order to avoid unbalances. The mechanical properties of the rotor lamination have to be good, in order to overcome the centrifugal stress due to high speed rotation.

Position Sensors

In most applications, there are position sensors in AMBs. Since AMBs are actively controlled regarding to the sensor signal, the control performance strongly depends on the sensor performance. Several sensor types are used in AMBs: inductive, eddy current, capacity and optical displacement sensors.

Controller

Today controllers are mainly based on digital technology. They provide a great flexibility and high computation speed. Digital controllers enable principally an adaptative control, unbalance compensation and provide a great tool for system diagnosis. For real time processing, Digital Signal Processors (DSPs) are used.

AMBs are controlled in closed-loop. Different methods such as PD, PID, optimal output feedback or observer based state feedback are in use.

Power Amplifiers

The power amplifiers convert the control signals into control currents. Switching amplifiers are usually used because of their low losses. The amplifier is often the limiting component in an AMB system.
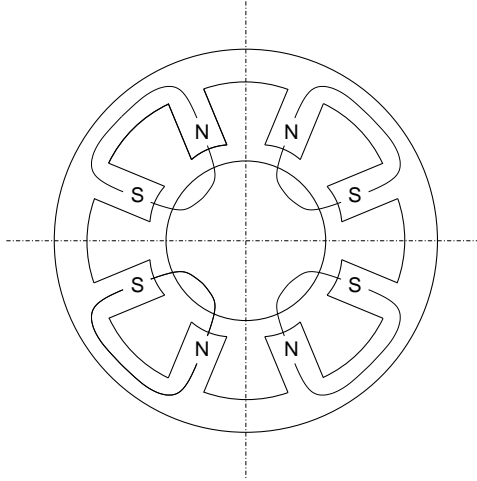
Figure 2.2: Magnetic poles configuration for a NS-SN-NS-SN heteropolar radial bearing.

Amplifiers with voltage or flux density control may improve AMB performance in certain cases, but are not yet widely used.

2.1.3 AMB Configuration

A lot of AMB radial bearings have four mangetic poles. That means that the bearing is able to attract the rotor along two orthogonal axis, and in both directions. Figure 2.2 shows the configuration of an heteropolar NS-SN-NS-SN radial bearing. Doing so brings the advantages that the axis are decoupled.

Actually only three poles are sufficient for a radial bearing. This configuration is not commonly used because of the coupling between the axis. The tendency in jet engine industry is to build radial actuators with 6 poles. These bearings are able to guarantee the levitation even in case of total failure of an actuator axis.

In order to minimize rotor losses configurations with homopolar radial bearings are possible. Other AMB configurations using permanent magnets have been developed. More information about AMB configurations are available in the already cited books [41, 38].
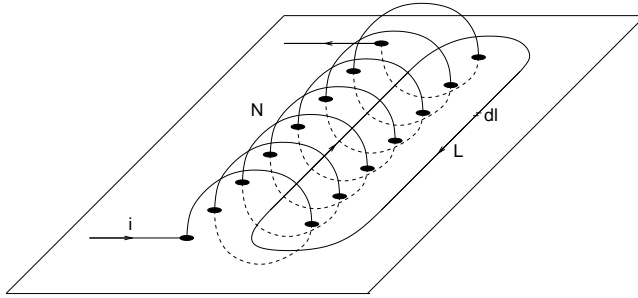
Figure 2.3: Air solenoid.

2.2 Theoretical Models

This section gives an introduction to AMB design rules. First a magnetic model is presented, and the relation giving the force of a single actuator is presented. AMB actuator force-current relation can be linearized for a pair of actuators around the working point. A mathematical development yields the well known linear AMB equation. Finally an overview of the losses in AMB is given.

2.2.1 Magnetic Model

Magnetomotive Force

The magnetic field is generated by an electrical current. *Ampère's circuital law* (equation 2.1) gives the relation between the *magnetic field H* [A/m] and the current sum enclosed by the closed integration path L [m].

$$\oint H \cdot dl = Ni \tag{2.1}$$

where N is the turn number of the coil and i the current going through, as drawn on figure 2.3.

Soft Magnetic Material Magnetization

The *magnetic flux density B* [T] is given by the following relation:

$$B = \mu_r \mu_0 H \qquad\qquad (2.2)$$

Here μ_0 represents the permability of air ($\mu_0 = 4\pi \cdot 10^{-7}$ [H/m]) and μ_r represents the iron core relative permeability.

When a magnetic field is applied on a material, the generated magnetic flux densitiy B depends on the material properties. *Diamagnetic* materials do have a $\mu_r < 1$, for *Paramagnetic* $\mu_r > 1$, which means that the field B generated is higher than the flux density in the vacuum.

Ferromagnetic material, which are used for the realization of magnets, have a $\mu_r \gg 1$, and are available for high temperature[2] applications. However the temperature has to be kept lower than the *Curie temperature*, beyond which the materials loose ferromagnetic properties.

Ferromagnetic materials show non-linear characteristics. Their magnetization depends on their history, and can be represented on a $B-H$ diagram (figure 2.4). When an unmagnetized material sample is put whithin a homogeneous field H, the magnetization flux B increases rapidly, according to a new magnetization curve. If H keeps increasing, the material reaches its magnetic saturation, and B then only increases with a slope μ_0.

When the outer field is reduced to $H = 0$, the flux density does not run reversibly along the new curve. The plotted relationship will follow a similar curve as for the magnetization, but back toward the zero flux density. This behaviour is called *magnetic hysteresis.* At $H = 0$, the flux density on the demagnetization curve is not zero. The material has been magnetized and the remaining flux densitiy B_R is called *remanent flux density* or *remanence.* In order to get $B = 0$, a field H_C, called the *coercitive field,* is necessary.

Force of a Single Actuator

The aim of the present subsection is to determine the magnetic force produced by a single actuator. Figure 2.5 shows a magnet and the main geometrical characteristics required to calculate the AMB force.

---

[2]Here high temperature means $T \gg 373°K$. A confusion should not be done with high temperature superconductor magnets, which have today a maximum operating temperature of about $130°K$.
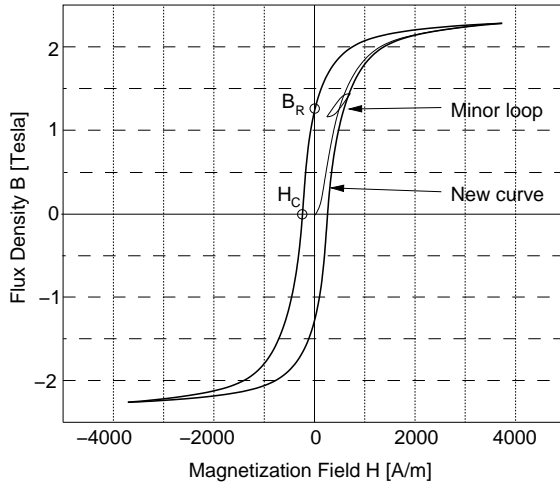
Figure 2.4: Magnetization curve B-H of a soft magnetic material (here AFK 502).
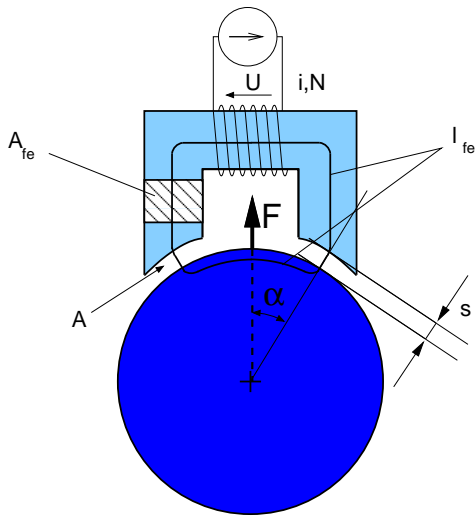
Figure 2.5: Magnetic force of an AMB.

Typically it can be assumed that the magnetic flux Φ [T·m^2], in the stator cross-section A_{fe} [m^2] is constant along the whole loop. Furthermore $A_{fe} = A_a$ (A_a is the cross-section of the air-gap) can be assumed. Thus,

$$\Phi = B_{fe}A_{fe} = B_aA_a \tag{2.3}$$

So

$$B_{fe} = B_a = B \tag{2.4}$$

The magnetic path can be decomposed into two parts, the field in the air, and in the soft magnetic material.

$$Ni = H_{fe}l_{fe} + 2H_as \tag{2.5}$$

where s [m] is the air gap between stator and rotor. The average magnetic path length in the lamination is l_{fe} [m].

From equations 2.5 and 2.2, and after solving for B the relation 2.6 gives the flux density.

$$B = \mu_0\frac{Ni}{\left(\frac{l_{fe}}{\mu_r} + 2s\right)} \tag{2.6}$$

Since the iron relative permeability $\mu_r \gg 1$, the magnetization of the iron can often be neglected, and the relation can be simplified:

$$B \approx \mu_0\frac{Ni}{2s} \tag{2.7}$$

Now the AMB force is obtained by considering the energy stored in the air gap and is given by equation 2.8:

$$F = \frac{B_a^2 A_a}{\mu_0} \tag{2.8}$$

The angle between the force direction and the center of the cross-section A is determined by α. For common four poles radial AMBs,

which means eight actuator teeth, α is 22.5°. Equations 2.7 and 2.8 yield the force for one actuator:

$$F = \frac{1}{4}\mu_0 N^2 A_a \frac{i^2}{s^2} \cos\alpha = k\frac{i^2}{s^2}\cos\alpha \qquad (2.9)$$

$$k = \frac{1}{4}\mu_0 N^2 A_a \qquad (2.10)$$

Inductance L in the Magnetic Circuit

The static inductance L of the magnetic circuit is given by:

$$L = \frac{N\Phi}{i} \qquad (2.11)$$

which, with equations 2.3, 2.6 and 2.11, yields

$$L = N^2 \mu_0 A_a \frac{1}{\left(\frac{l_{fe}}{\mu_r} + 2s\right)} \qquad (2.12)$$

2.2.2 Relation Between Current and Force

In order to be able to produce magnetic force along two opposite directions, the actuators are usually arranged in pairs (figure 2.6). This enables a full control of the rotor along one axis.

For a pair of magnets, the force F_x [N] represents the force difference between the positive and the negative directions. For this case, the actuator currents are defined as the sum of a bias current i_0 [A] and a control current i_x [A] for the positive actuator, and the difference $i_0 - i_x$ for the negative actuator. The air gaps are defined by the deviation x [m] and the nominal air gap s_0 [m], thus the terms $(s_0 - x)$ and $(s_0 + x)$ are inserted.

$$F_x = F_+ - F_- = k\left(\frac{(i_0 + i_x)^2}{(s_0 - x)^2} - \frac{(i_0 - i_x)^2}{(s_0 + x)^2}\right)\cos\alpha \qquad (2.13)$$

with $k = \frac{1}{4}\mu_0 N^2 A_a$
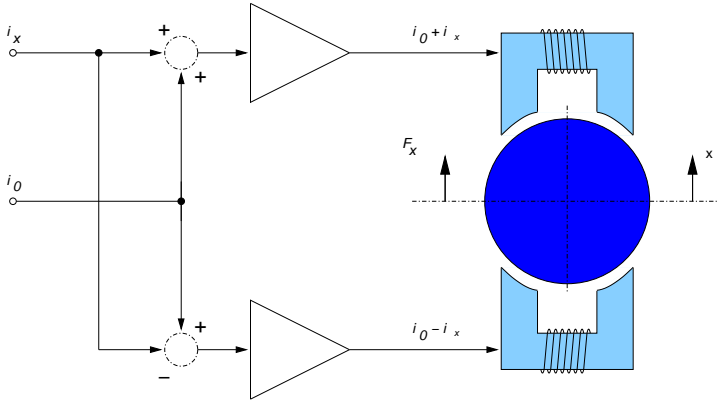
Figure 2.6: Pair of electromagnets for positive and negative force.

By considering that $x \ll s_0$ and $i_x \ll i_0$, equation 2.13 can be linearized using Taylor's series. It yields the typical AMB relation 2.14:

$$F_x = \frac{4ki_0}{s_0^2}(\cos\alpha)i_x + \frac{4ki_0^2}{s_0^3}(\cos\alpha)x = k_i i_x + k_s x \qquad (2.14)$$

$$k_s = k_i \frac{i_0}{s_0} \qquad (2.15)$$

The coefficient k_s is the open-loop stiffness. It is less than zero, so the AMB has an inherent negative stiffness. This negative stiffness leads to an open-loop instability.

The force-current coefficient k_i is the actuator gain.

2.2.3   Losses

Magnetic bearings are contact-free, consequently there is no friction. The equations presented previously do not take the losses into account. Losses in magnetic bearings are the following: hysteresis, flux leakage, saturation of the iron and eddy current. The breaking torque in AMBs is however much smaller than the torque due to friction losses in conventional bearings.

Hysteresis Losses

Magnetic losses P_{fe} [W] are due to hysteresis and eddy currents losses. They depend on the rotor speed, the magnetic material, and the direction of the flux vector B [T] over the rotor circumference. Hysteresis losses are due to the remagnetization of the magnetic material in the $B - H$ curve. At each loop the energy diminishes by $W_h = V_{fe}A_{BH}$, with A_{BH} [T·H] area of the hysteresis loop, V_{fe} [m^3] volume of the iron. Losses are proportional to the frequency of remagnetization f_r [Hz], if the flux in sheets is sinusoidal and distributed evenly.

$$P_h = k_h f_r B_m^{1.6} V_{fe} \qquad (2.16)$$

Eddy Current Losses

When the flux density in a conductive material changes, eddy currents are generated. They are minimized by using an iron core made of insulated sheets or particles. Eddy currents losses P_e [W] in laminated iron, ρ [Ω/m] is the specific electrical resistance of the iron, e [m] stands for the thickness of the sheets, f_r [Hz] for remagnetization frequency, B_m [T] for the maximum flux density or the amplitude of the flux density respectively.

$$P_e = \frac{1}{6\rho}\pi^2 e^2 f_r^2 B_m^2 V_{fe} \qquad (2.17)$$

Resistance Losses

The main losses in the stator are resistance losses in the actuator windings. They are dependent on the square of the coil current and the wire resistance:

$$P_{Cu} = Ri^2 \qquad (2.18)$$

The electrical resistance R [Ω] of a wire is given by:

$$R = \rho\frac{A}{l} \qquad (2.19)$$

ρ [Ω/m] is the resistivity, A [m^2] the cross sectional area of the wire and l [m] the length of the wire. For[3] $T > 0°$C:

$$\rho = \rho(T) = \rho_0(1 + \alpha_1 T + \alpha_2 T^2) \qquad (2.20)$$

Where T [°C] is the temperature, α_1, α_2 [K^{-1}] are temperature coefficients. The electrical resistance is considered as linear over a small temperature range, typically from 0°C to 100°C. On a large temperature range, the electrical resistance temperature dependence has to be considered as quadratic.

Air Losses

Air losses are dependent on the square of the rotation speed. Experimentally they have been determined by comparing losses in air and vacuum environments.

Amplification Losses

Losses in AMB systems are generated by the digital circuitry and the power amplifiers. Switching amplifiers are usually used. The efficiency of the power amplifier is situated around 95-98%. For example, typical amplifiers, as the ones used in chapter 7 are able to deliver 50V and 6A, the power losses per actuator is about 12W.

2.3 Summary

Active magnetic basics has been given in this chapter. The working principle, the description of the components as well as the AMB configuration give an understanding of the system. The major equations leading to the AMB linearized equation have been taken in review. This chapter ends with the system losses.

Although the theory presented here does not cover the vast field of AMB, it enables non-specialists to understand how AMBs work, especially how the AMB prototype of chapter 7 has been developed.

---

[3]For temperatures below 0°C, a term $\alpha_3 T^3$ should be added in equation 2.20.

Chapter 3

High Temperature Aspects for AMB Design

Industrial needs give specifications, which a system has to fulfill. In the field of gas turbines, new objectives for AMBs are given, so that they work at 538˚C (1000˚F). At that temperature range, physical properties and chemical reactions take place in very different proportions than at room temperature. High life span and reliability are consequently the critical points to be proven and to be tested.

The present work has not been restrained to one working solution. Suitable solutions for high temperature applications with their limitations in performance, time and temperature are shown in this chapter in a general way.

First an overview of technical difficulties specific to high temperature mechatronic systems (section 3.1) gives the readers an opportunity to get an idea of the different design aspects. Links to the different chapters and sections are given by this way. Research on magnetic material is presented in subsection 3.2 and subsection 3.3 shows a solution catalogue about coil fabrication.

3.1 Overview of High Temperature Aspects in AMB Design

This section gives an overview of construction difficulties related to high temperature electromechanical system. Related aspects are only listed in this section and references are given to find detailed information in the appropriate chapters. This section starts with physical aspects, then chemical aspects, to conclude with more practical points for high temperature electromechanical designs.

Thermal expansion

Thermal expansion or more precisely difference of thermal expansion between different materials is a very relevant topic. Several ceramics and metal are necessary to build mechatronic systems. In order to ensure a good alignment at both room and high temperature and to avoid high mechanical stress or clearance with fastening parts, precautions are needed. Details about construction solutions that have been chosen for a prototype are described in section 7.1. Subsection 7.2.1 describes how the stator laminations are kept centered. Subsection 7.2.3 shows how radial ceramic sensors are kept centered inside a metal housing.

Electrical Properties

In electromechanical systems good electrical conductors are needed. The temperature coefficients of electrical resistance are relevant as well (equations 2.19 and 2.20). Tests on conductor materials are shown in the subsection 3.3.2 and electrical properties of some metals are given in appendix A.

Oxidation

The working atmosphere plays an important role on the material behaviour. Oxidation occurs of course at room temperature, but at high temperature, this reaction is much accelerated. Using appropriate materials or working in non oxidant atmosphere slow down this phenomena. Each part of the system has to be well chosen to keep the

life span long enough. This point is treated in the sections concerning material.

Diffusion

When two components are in contact, chemical reactions take place between them. Many materials are inert at room temperature, but no longer at high temperature. For example, diffusion in nickel-clad copper wire (subsection 3.3.2) shows changing conductive properties at high temperature with the time.

Magnetic Properties

Magnetic properties depend on the temperature in a non-linear way. Iron is no longer ferromagnetic when heated up above the so-called *Curie temperature*. This temperature is actually not set so precisely. Properties decrease slowly in function of the temperature and above a specific point they decrease dramatically; this point is the *Curie temperature*. Special FeCo alloys have been developed for high temperature applications. They feature high saturation and good high temperature capability. They need a heat treatment to reach the best magnetic properties and they show some ageing. Material tests are shown in section 3.2.

Electrical Insulations

Over temperatures of 260°C only few plastics can survive, thus electrical insulations have to be realized with other materials. Good electrical insulators are also ceramics and glass. Most of the ceramics are stable at temperature over 1000°C and some glasses can achieve work in such conditions. Nevertheless formability of these non-ductile materials makes them complex to use. Solutions are shown in subsection 3.3.3.

Mechanical properties

Elastic modulus of metals changes with temperature and decreases until liquefaction down to zero. Designing and controlling a system, which works from room to high temperature must take into account

these stiffness changes. All the computations have to be verified for all temperature ranges.

Materials should not remain under high stress. Creeping becomes important at high temperature. Creep aspects must be taken into account during the design process. All metallic parts have to fulfill their function for a minimal known time at a given temperature.

Realization of construction details

Common solution for room temperature for example: gluing, welding, binding or connecting wires together are not trivial at high temperature. This point is probably the least formal of this thesis, thus solving these kind of problems involve mainly practical knowledge. Testing and experimenting is the key point of this design aspect. Realization of a prototype needs to find such solutions. Section 7.1.2 deals with that matter.

3.2   Magnetic Materials

The Aerospace Industry has a need of efficient soft magnetic alloys for high temperature applications [22, 4, 8]. Research has been led for a few decades, but the required specifications are more and more difficult to fulfill. Typical specifications for high temperature uses are obviously having excellent magnetic, high mechanical properties and advantageous electrical properties, but even in function of temperature and time.

Information about temperature and long term behavior is quite difficult to produce. It often depends on the experimentation and is valid only for very special conditions. Richard T. Fingers [12, 11] shows measurements on the mechanical behavior of high temperature magnetic material in his PhD dissertation. Kondoleon and al. [20] show some research concerning soft magnetic alloys magnetic properties for high temperature applications. Long-term tests of this paper are limited to some hours. Further emphasis is needed and long-term measurements in a furnace are necessary to find the consequences of ageing. In the present work an accentuation is done with magnetic properties, the mechanical aspect have already been treated in Fingers dissertation.
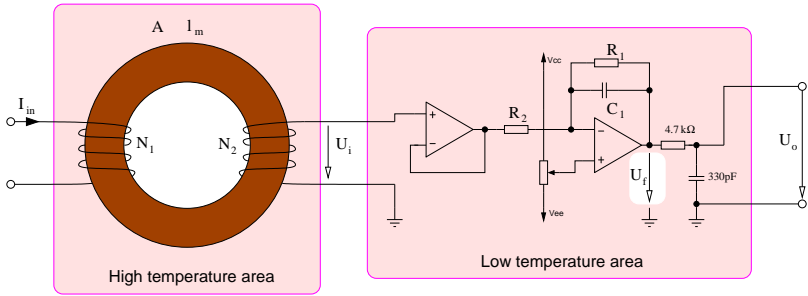
Figure 3.1: Setup for magnetic property measurement at high temperature.

3.2.1 Testing Procedure

The aim of the tests presented here is to measure the magnetic properties in function of temperature and time. The measurement setup has to be able to acquire the B-H properties of magnetic materials at high temperature.

This setup is based on the principle of a transformer. A soft magnetic torus with a first winding stage (N_1) and a second winding stage (N_2) is put in a furnace. The magnetic field $N_1 I$ does not depend on the temperature. For this purpose N_1 is supplied by a current source, which enables to get rid of the changing wire resistance effect.

The measured signal has to be temperature independent, so the voltage produced on N_2 should not be disturbed by any electrical resistance effect. For this purpose a voltage follower at the input of the measurement circuit avoids distortion and current in the second winding.

A small circuitry has been built to integrate the signal analogically in order to get the result of Ampere's theorem. Such a device can measure only the AC part of the signal, so a potentiometer enables to adjust the reference voltage. The measured signal is however adjusted more precisely by software subtracting the middle value of whole B-H curve, which should be zero. Figure 3.1 shows this setup, where l_m is the middle length of the flux path and A is the metal cross section of the magnetic torus.

The induction is given by:

$$H = \frac{N_1 I}{l_m} \tag{3.1}$$

The transfer function of this system is:

$$G(s) = \frac{U_f}{B} = \frac{R_1}{R_2} N_2 A \frac{s}{R_1 C_1 s + 1} \tag{3.2}$$

The gain is:

$$gain = \frac{N_2 A}{C_1 R_2} \tag{3.3}$$

So B is directly obtained with:

$$B = U_0 \frac{C_1 R_2}{N_2 A} \tag{3.4}$$

and the cut-off frequency is adjustable with C_1:

$$f_c = \frac{1}{2 \Pi R_1 C_1} \tag{3.5}$$

Measurements are taken after different times and at different temperatures. Different materials have been tested using this setup.

3.2.2　Fe-49%Co-2%V

Tests with a FeCo soft magnetic alloy, named AFK 502[1] (49% Fe, 49% Co, 2%V), have been done. This material is equivalent with Hiperco 50[2] and Vacoflux 50[3]. Figure 3.2 shows the phase diagram of Fe-Co. For a composition of 50% Co (weight) in the Fe, Curie temperature of this metal is between 950 and 980˚C. The phase γ is not magnetic and the phase α has very good magnetic properties.

The presence of Vanadium increases the ductility, facilitates the metallurgical transformation and increases its electrical resistance. After

---

[1]Imphy Ugine SA
[2]Carpenter
[3]Vacuumschmelze
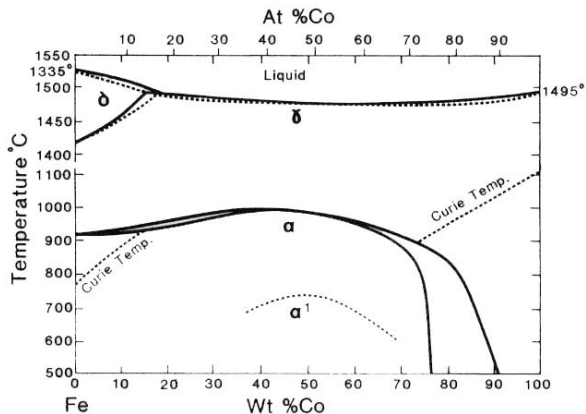
Figure 3.2: Phase Diagram of Fe-Co.

machining, this material has to be heat treated, in order to remove the tensions due to machining and to confer on the metal its optimal magnetic characteristics. The heat treatment cycle is 2 to 3 hours at 850°C in a dry and pure hydrogen atmosphere, or under vacuum, then cooling of 250°C/h in the same atmosphere.

The phase diagram of this alloy (figure 3.3) shows that in the region between 500 and 630°C, there is an equilibrium with a phase α^1 and γ_2 with very unfavorable magnetic properties due to γ_2. This material should not be used in this region of temperature to keep its best characteristics [51].

An attempt has been made to retreat aged material with the above-given procedure, in order to regenerate its best magnetic properties. The result is not satisfying, the properties are even worse after the second heat-treatment than only after ageing.

Magnetic Properties

Tests have been done to show how the material behaves after an exposure at 550°C during the period of 1500h. The magnetic characteristics have been measured after 0, 800 and 1500 hours. The right part of figure 3.4 shows the magnetic properties of AFK 502 at 550°C. It can be observed that the saturation level decreases, but the shape of the
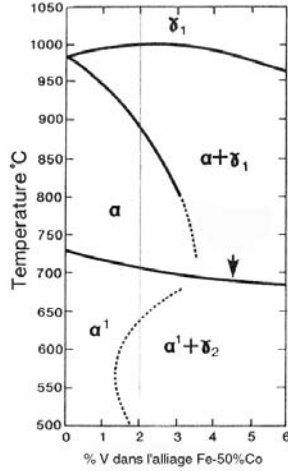
Figure 3.3: Phase Diagram of V in Fe-50%Co.

curve remains almost the same. The left part of figure 3.4 shows the same piece of material as shown on the right part , but cooled down to room temperature. The saturation level and the permeability decrease too. The losses due to the hysteresis are not becoming higher with time for a given temperature.

Figure 3.5 shows the same curve than figure 3.4, but with an other disposition. Here B-H curves are shown before and after cooling down for 0 and 1500 hours, respectively left and right part of the figure. New material has slightly lower saturation level at high temperature than at room temperature. However the permeability remains constant. Losses are on the contrary lower at high temperature. After 1500 hours the behavior of the material is quite different. The saturation at high temperature is higher and the permeability is higher than at room temperature.

The saturation of the material just after the final heat treatment at room temperature is 2.3 T. After 1500 hours at 550°C it is also still about 1.75 T (figure 3.6) , which is still acceptable for a soft magnetic alloy. It should be noticed that the force of the AMB is relative to the square of the magnetic field, so it remains in this case only 42% of the nominal force.
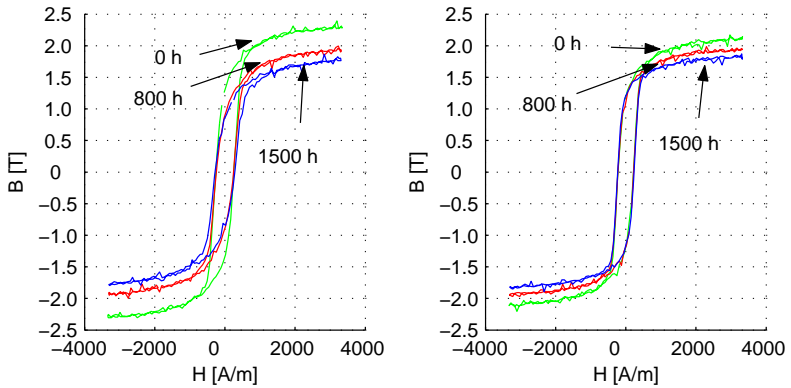
Figure 3.4: B-H curve of AFK 502 at 25°C (after cooling down, left) and 550°C (right) at three different times of exposure at 550°C.
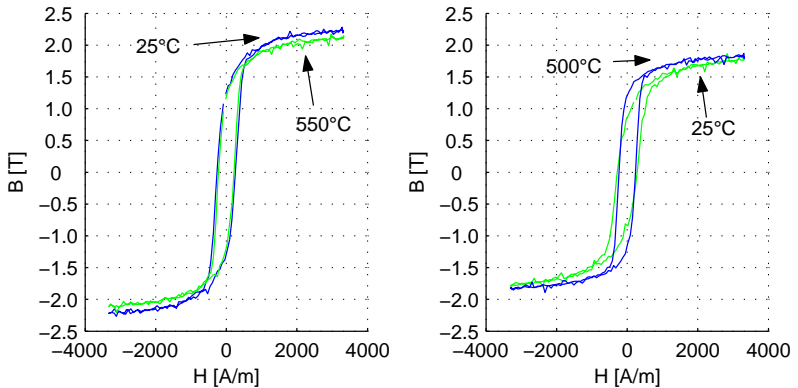
Figure 3.5: Magnetic measurements after 0 (left) and 1500 hours (right) exposure at 550°C. Curve of measurements done at high temperature and after cooling down are shown.
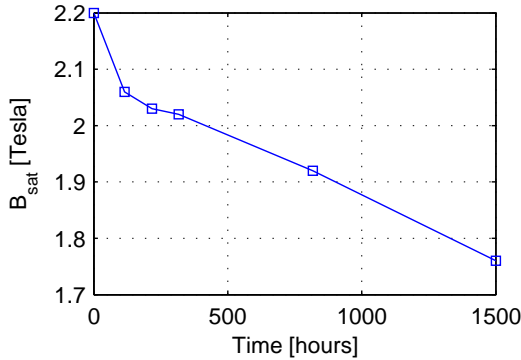
Figure 3.6: Saturation of AFK 502 after exposure at 550˚C.

Mechanical Properties

Now that the magnetic capabilities have been proven, mechanical properties have to be characterized at high temperature in function of the time. Research of Fingers [12] shows a study on the mechanical properties of Hiperco 50[4]. This material has the same chemical composition and the same heat treatment process as AFK 502.

Creep behaviour becomes very critical beyond 540˚C. This study shows that at 540˚C, in order to avoid too much creep-strain, the stress should be kept much below 310 kPa continuously and should never exceed 550 kPa. Working at 550˚C furnace temperature means that the magnetic material inside the AMB will reach even a higher temperature. Tests done by Fingers at 593˚C already show a very bad creep-strain behaviour beyond 207 kPa. In order to keep the life span of the system reasonably high, internal stresses should be much lower than these values.

3.2.3   FeSi

Tests with FeSi[5] has been done at high temperature. Figure 3.7 shows the magnetization of FeSi at 25˚C and at 575˚C. This figure shows a

---

[4]Carpenter Corporation
[5]N020, Thyssen-Krupp
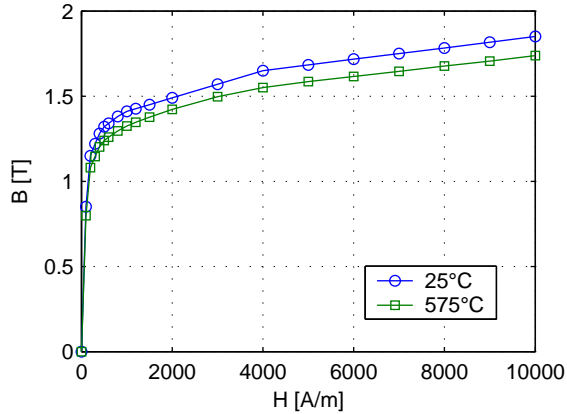
Figure 3.7: Magnetization of FeSi at 25˚C and 575˚C.

low diminution of the saturation at high temperature. Long term tests (500 hours) did not show ageing on the magnetic properties. FeSi seems to be more stable at high temperature. Nevertheless, it linearity magnetic region of only one Tesla, makes is less interesting for high performance AMB. Curie temperature of FeSi is 750˚C, but above 600˚C its magnetic properties are already dramatically reduced. FeSi has an yield strength of 180 MPa at room temperature.

3.2.4 Outlook

Magnetic properties, saturation, permeability and losses of AFK 502 have been tested at high temperature. The measurements show that the saturation decreases significantly in function of the time, however after 1500 hours, the magnetic properties are still good enough to make an AMB working. Therefore these characteristics have to be taken into account during the design phase. The maximal force, which is proportional to the square of the magnetic field, is significantly reduced throughout time.

It seems very difficult to predict the material behavior after a long time of use with changing temperatures. Experimental tests have to be performed in realistic condition of use in order to acquire some data. On-line measurement should be done as well, in order to estimate the remaining life span, and the AMB force.

3.3   Actuator Coils

Now that is was demonstrated that soft magnetic alloy have capabilities to work at high temperature, it must be shown how to induce the magnetic field. For this purpose electrical coils are used, which are wound around the stator. The aim is to get the highest possible current density in the coil, thus to increase the efficiency. Specifications for coils are:

- Good electrical properties

- Reliable electrical insulations

- High heat transfer capabilities

- Compact fastening parts

- High life-span.

Because of losses, coils work at even higher temperature than the ambient one. As seen in chapter 5 the hottest spot of the whole machine is located in the coils. In this section different solutions of high temperature actuator coils are shown. Table 3.1 gives an overview of possible alternatives for the realization of actuator coils. All aspects of this table are described in the following subsections.

3.3.1   Conductor Shape

A primary goal of the coil is to realize the highest possible current density. This is equal to get the best fill factor of the conductor inside the available space. We can easily imagine that a wire with a square cross-section is more efficient to fill the empty space efficiently than a round wire. In the same idea a conductor strip produces a very compact coil. Corners of this type of wire are indeed difficult to insulate and have many chances to create short-circuits between turns, they should be rounded to avoid problems. On the other side round wires are more often commercially available and a bit easier to handle. In terms of oxidation and surface diffusion, wires have less external surface for an equal cross section area than strips. This is the reason why wires are more stable than strips.

	Technical Alternatives					
Conductor Shape	Round	Square	Strip			
Conductor material	Copper	Silver	Gold	Aluminium	Nickel clad Copper	Nickel
Electrical Insulation	Organic ceramic (flexible)	Inorganic ceramic (hard)	Mica tape	Fibre glass		
Coil Holder	Full holder	Coils moulded in bloc	Bearing moulded in a bloc	Glass/Ceramic tapes	Plates	
Other insulating materials	Mica tape	Ceramic glue				
Electrical Connections	Welding	Clamping				

Table 3.1: Overview of the technological alternatives for actuator coils.

Choice criteria are also based on other aspects such as the amplifier and the system dynamic. A coil made of strips has obviously a low number of turns and a big cross-section area. That means that the amplifier has to deliver a high current to produce the same current density as with a round wire coil. Insulation aspect is interesting with strips because it is possible to insulate only one side of the band, which is a good way to increase the fill factor. The conductor shape depends on applicable technology, so the following sections give more selection criteria.

3.3.2 Conductor Materials

The aim of this section is to show the best conductive materials suitable for high temperature applications. Appendix A gives an overview of the material properties, especially the relative conductivity compared to copper with the temperature coefficient dependency. The second row of table 3.1 shows the materials usually used at high temperature.

In order to get information about the behavior of these materials at high temperature, wounded coils were put into a furnace for long term measurements. During this time, electrical resistance and inductance were measured. Tests have been done at three different temperatures: 500, 650 and 800°C. The tests were performed with the chosen material for at least 100 hours at different temperatures to prove their reliability. For comparison purpose, resistance values are always given relatively to the resistance after 2 hours at the given temperature.

Copper

Copper is a very good conductor but needs to be protected against oxidation. The measurements of figure 3.8 show that after 87 hours at 800°C a copper wire of 0.8 mm diameter is entirely oxidized and brakes up. A material usually used for high temperature wires is nickel clad copper. This wire has a much better life-span, but as we can see on figure 3.9, electrical resistance increases with time. Nickel and copper have a mutual solubility of 100% which makes them diffusing together very fast at high temperature. Anyhow, solutions to protect copper against oxygen should be found for using it at high temperature. A model based on tests of the resistance increasing in
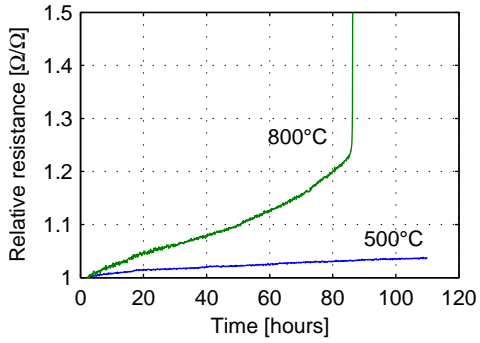
Figure 3.8: Relative resistance of copper at 500°C and 800°C in function of time. The copper wire broke up after 87 hours.
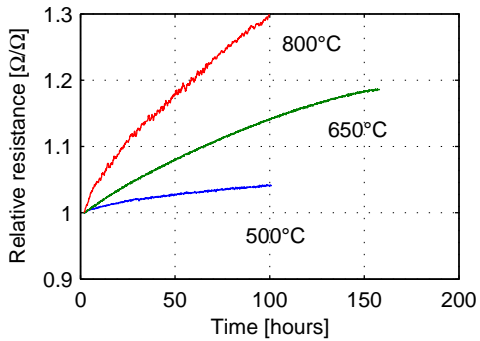
Figure 3.9: Relative resistance of 27% nickel-clad copper wire at 500°C, 650°C and 800°C in function of time.
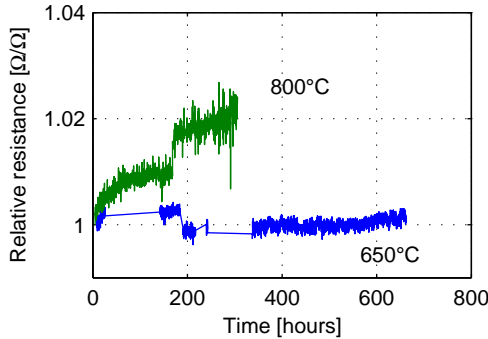
Figure 3.10: Relative resistance of silver at 650°C and 800°C in function of time

function of temperature and time is given in appendix B. Subsection 3.3.3 shows a wire type combining oxidation protection and electrical insulation.

Silver

Silver is the best conductor and even at high temperature its properties are still very good with a temperature coefficient α_1 (eq 2.20) of 0.0038 $[k^{-1}]$. The resistance is increasing only 2% at 800°C after 300 hours for a wire diameter of 0.8 mm (figure 3.10). It is common to use it up to 500°C. Beyond this point silver oxidizes and the formed oxide is not stable, it vaporizes. The cross section of the wire decreases consequently with time. This process is however very slow when no air stream is blowing on the surface. Cost of this material is quite high, so its use will be favored in small efficient machines, than in big non compact systems. Note that silver can be recycled, and resold, which could make silver also interesting in large systems.

Gold

It may be a strange idea to put gold into industrial machines. The very high cost of this material is a very strong argument against using gold in magnetic bearings. However, gold is a very stable material and also a quite good conductor with 65% of copper conductivity.

For cost reasons no tests have been lead in the frame of this work for actuator coils. Tests done with thick-film hybrid technology (section 4.2.2) show very promising results. In spite of its high cost, gold could be an interesting alternative, because it can be recycled.

Aluminium

Pure aluminium is the fourth best conductor with 59% of copper conductivity, which makes it a good candidate for actuator coils. Aluminium is also very light, with $2.7 \cdot 10^3 \frac{kg}{m^3}$ it is about three times lighter than copper, which makes it still lighter for the same conductivity. Low weight is exactly why aluminium is used in plane industry. Its oxide is very stable, resistant and has good insulating properties, which is used for electrical insulation. Anodized aluminium is commercially available and formed in many kinds of shapes; wire, strips, bars, etc. Its fusion temperature of 660˚C, makes it usable up to about 400˚C. Short time tests up to 480˚C have shown very good results in terms of insulation electrical resistance.

3.3.3 Insulations

Coil wire insulation is a critical point for high temperature actuators. Their specifications are to be a good electrical insulator, a good thermal conductor, flexible, compact, being reliable and supporting temperatures up to 800˚C. Beyond 260˚C, no plastic insulation is available. Solutions must be found with other material like glass, oxides or ceramics. Unfortunately, these specifications are somehow contradictory and also very difficult to fulfill for ceramics and glass. Limitations of ceramic insulated wires are shown in [18]. Montague and al. [26] have found a good way to solve this problem by building separate removable AMB poles with silver insulated wire, cast in a ceramic bloc. Existing industrial solutions are reviewed in the following paragraphs.

KD 500

This high temperature wire[6] was designed for high reliability coils. It can withstand short exposures up to 600˚C. The conductor is a nickel-clad copper wire from 0.07 to 1 mm diameter. Insulation thickness lies

---

[6]Karl Schupp AG Zumikon

between 8 and 10 μm and is designed for 150 V A.C. This wire should not be bent with a diameter lower than ten times its diameter. Once heated up, the KD 500 must not be moved anymore. The maximum allowed temperature of this wire is too low for the present application, so no further tests have been leaded.

Cercal

Cercal is an initially thin and flexible insulator. After curing at a temperature between 700 and 820°C, the material hardens and should not be moved anymore. It is available for nickel-clad copper and nickel wires. It is a vitreous anemal film made principally of lead oxide, titanium oxide, silicon dioxide and magnesium dioxide. This insulation is bonded to the wire conductor and it requires the same flexibility and temperature coefficient as the base wire. It is suitable for coil winding and lead wire applications in aerospace, nuclear, steam, chemical and other high temperature applications. Operating temperature is from -268°C to 540°C for continuous operation and up to 815°C for short periods. The coating is warranted not to crack when wound in a diameter at least 7 times the wire diameter. The thickness of the insulation is from 8 to 16 μm and is designed for up to 200 Volt D.C. current. The manufacturer[7] gives a lifespan of about 1000 hours for temperatures above 620°C, and only 500 hours at 700°C. Therefore, the given lifespan is too limited for the present application, so no further investigations have been done with this wire.

Alcal

Alcal Type E[8] ceramic insulation can be applied to many materials but is mainly used with platinum, gold, silver, palladium and nickel-clad copper. Made of alumina and silicon dioxide, this insulation has a thickness of less than 14 μm and is not moisture resistant. This ceramic coating is primarily a refractory-glass compound and can withstand bending and braiding requirements consistent with normal coil winding practices. It is flexible in its primary state and needs a curing at 700°C.

---

[7]Ceramawire
[8]California Fine Wire

Tests show that this insulation does not hold well to the wire after curing. It is very damageable, and for this reason does not fulfill the specifications of reliability of aero-engines.

Mica

An insulating tape made of mica and glass named SK650[9] is commercially available. Mica is a good electrical insulator, leads the heat well and can be manufactured in a reasonably compact way. This could be a good solution to insulate conductors in the shape of tape. It is also available for round wire. This tape is flexible due to organic ceramics at room temperature and sinters after the first heating. At this point this insulation becomes hard and brittle and the windings stick together thanks to the sintering of the organic ceramic. The result is a compact and quite strong coil. Mica has excellent properties up to 800˚C and resist thermal cycles well. Tests in electrical motors show that after about seven months, the material turns into powder and does no longer fulfill its function of electrical insulator. However, this lifespan is long enough to be tested in AMBs.

Ceramic-Braid

Insulation is commonly made with glass-braid. This insulation is flexible and easy to use, has an excellent thermal shock resistances, a maximum continuous use temperature over 1000˚C. Unfortunately this material is quite thick (0.5-5mm) and has a low thermal conductivity. This insulation is very suitable for leading wire, but is not recommended for coil windings.

Thermocoax

Thermocoax is composed of a copper core. A ceramic insulation powder is put around a copper core and maintained inside a stainless steel mantle (figure 3.11). Figure 3.12 shows how the relative electrical resistance at 800˚C in function of time. A life span of several month is guaranteed at 700˚C by the manufacturer[10]. Eddy current in the metallic insulation is limiting the dynamics of the bearing. They are

---

[9]Von Roll Isola
[10]Thermocoax
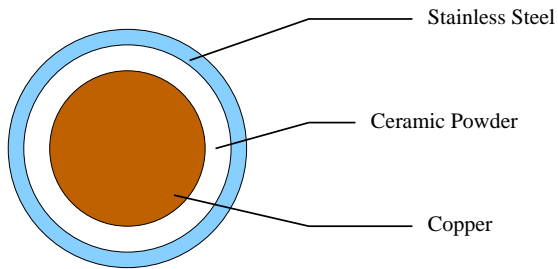
Figure 3.11: Thermocoax profile.
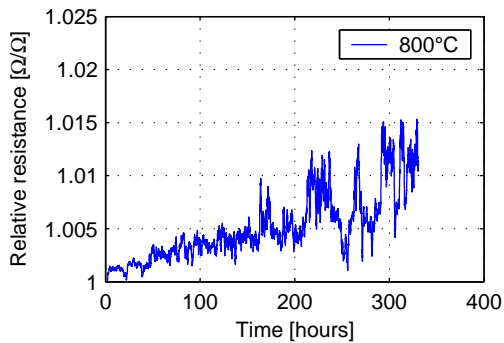
Figure 3.12: Relative resistance of Thermocoax at 800°C in function of time.

reduced by the oxidation of the mantle external surface. The fill factor is also limited due to relatively high insulation thickness. The thickness of this insulation is not advantageous; it is 0.3 mm of a 2.0 mm wire diameter. That means that the cross section of the conductor is only 49% of the whole cross section. This wire requires a larger outer diameter and high currents are for this reason required. Formability is limited to approximately five times the wire diameter. This solution is however mechanically robust and has a long expected lifespan.

3.3.4   Coil Formers

Actuator coils have to be formed and held in place on the stator. In the case of high temperature magnetic bearings with electromagnets having limited lifespan, it is a great advantage to be able to change them easily without having to disassemble the whole machine.

Coil formers have to prevent short circuits between stator and winding as well. They should be good electrical insulator to avoid short circuits and also to avoid eddy current. On the other hand they have to transfer the heat as well as possible to increase the cooling. In high temperature environment, the heat transfer from the coil to the stator should be reduced to avoid an over heating of the magnetic material. Table 3.1 shows alternatives for coil formers.

Full Coil Holder

First proposed solution is to build a full coil holder of ceramic, which can be mounted on the stator and on which a coil is wound. This solution has the advantage that a single defect coil can be changed without having to disassemble the whole system. Another advantage is that coils are not wound directly on the stator, which makes the winding process much easier. That is actually a good solution for prototyping, which allows to test different types of coils without having to change the soft magnetic alloy material. Concerning production cost, numerous series can be considered by casting the parts and prototypes by using machinable ceramics.

In case of machined coil holders, different materials are available on the market, such as: micanit, machinable ceramics or glass ceramics. A coil holder could be manufactured of metal. The problem in this

case is to avoid eddy current, and no reliable insulation between stator and rotor would be insured as well.

Coil in a Bloc of Ceramic, Bearing Actuator in a Bloc of Ceramic

As said in the beginning of this section, a tendency in magnetic bearing design is to mould the stator part into a plastic bloc. The same idea is also applicable for high temperature bearings using glass or ceramics instead of plastics. Cooling can be improved by using conduction instead of convection and radiation. To make that solution convenient for industrial applications, coils, magnet or pieces of magnets should be easily removable to decrease maintenance cost in case of failure in the actuator.

Plates, Tapes

Conventional magnetic bearings are usually constructed with very basic coil holders composed of insulation tape and cable fasteners made of plastic. Windings are finally glued together to get good mechanical stability and avoid frictions between turns, which create short-circuits. This low cost solution is a good example of what is quite difficult to realize for high temperature applications. Insulation tape is something very breakable if made of glass or ceramics, glue has a thermal expansion much smaller than good electrical conductors, plastic binders could be replaced by metal parts, but a short-circuit reliable system is then difficult to certify.

3.4   Rotor and Housing Material

Besides magnetic materials, materials for other parts such as: rotor, stator, housing and fixation parts, should also be considered. Table 3.2 shows an overview of the maximum use temperature for construction metals. For temperatures over 500°C, the choice of a metal is relatively restrained according to creep, stress-rupture and corrosion data. Murray [29] gives a general overview of material selection, especially in chapter nine, dedicated to heat-resistant alloys.

Alloy Type	Estimated maximum use temperature
Nickel-based superalloys	1200˚C
Cr-Mo-type	650˚C
Stainless steels	630˚C
Low-alloy steels	500˚C
Titanium alloys	500˚C
Carbon steels	400˚C
Copper alloys	300˚C
Aluminium (6xxx series)	275˚C

Table 3.2: Estimated maximum use temperature for selected metals

Precipitate stainless steels lose strength rapidly as the temperature increases beyond 425˚C. Martensitic stainless steels have good short time strengths up to about 590˚ but are not as corrosion resistant as the ferritic and austenitic stainless steels. Austenitic stainless steels have a good toughness, ductility and formability and are more corrosion resistant than ferritic and martensitic steels as well as having better high-temperature strength and oxidation resistance. They are used up to 630˚C in steam and gas turbines, turbine rotor, superheater tubes, steam pipes and pressure pipes.

Cr-Mo-type ferritic steels have good oxidation resistance due to Cr and improved creep resistance due to Mo (and V). They are widely used in petroleum and chemical industries for piping, heat exchangers and pressure vessels from 500˚C to 650˚C.

Superalloys are the best of the high temperature strength and oxidation resistance alloy group. They are subdivided in three groups. Iron-base alloys (ex: Haynes 556, Incoloys and A-286), which contain primarily iron, nickel and chromium, Nickel-base alloys (ex: Inconels, Hastelloys, Rene 41 and 95, Invar 36, M 252) and cobalt-base alloys (ex: Haynes 188, L-605, Mar-M 918 and MP35N). Nickel-base alloys are the most widely used. They have better performances than iron-nickel-chromium type and are less expensive than cobalt alloys. Superalloys are widely used in gas turbines, rocket motors, spacecraft, pumps, internal combustion engines, heat exchangers, industrial furnace applications. Of course many other applications are possible and there is no unique correct material for each application. Designers and vendors-suppliers should discuss the application specifications in order to get materials with the desired properties and quality.

3.5   Summary

Different aspects of mechatronic design for high temperature applications have been given in this section. Magnetic properties of a FeCo soft magnetic have been tested for a long exposure at high temperature. The results show temperature and time dependant magnetic properties. The literature gives that mechanical stress leads to creeping effect even under stress much lower than the maximal stress at room temperature. Special care has to be taken in account during the design phase, and further test done in realistic condition of use should be performed in order to estimate the material characteristic after the desired utilization time.

Several conductive materials as well as several insulating materials have been taken in review. Choosing an appropriate coil technology means that many parameters should be known, for example: the working conditions, the maximal temperature as well as the continuous temperatures, the working atmosphere, the number of temperature cycles, the amplifying electronic, the fill-factor, the cost, etc. All the presented solutions have their advantages and could be used in a high temperature application. Once again, in order to find an appropriate technology, long term test in real working condition should be done to be able to estimate and to ensure a satisfying life span.

Finally, ideas in the way of mounting coil windings on a magnetic stator are given so all the aspect of electromechanical construction elements have been treated.

Chapter 4

Thick-Film Eddy Current Position Sensors For High Temperature Applications

Inductive and eddy current sensors are widely used in AMBs as position sensors. State-of-the-art sensors for room temperature provide solutions with good robustness, but with quite low production reproducibility and often with high production cost. The proposed solutions are moreover not trivial to adapt to high temperature. This chapter describes a compact, reliable and low cost transverse flux eddy current position sensor, realized with thick-film technology for applications up to 600°C [6].

The present chapter is related to the design and characterization of the sensor performances. The integration of these sensors in a real application is shown in chapter 7.

4.1   State of the Art

AMB sensors are typically installed as several coils mounted symmetrically around the rotor. An interesting solution for high temperature eddy current position sensors based on standard technologies is shown in [47], where coils are wound on a non magnetic (ceramic) holder. The temperature compensation is done in this case by using the changing electrical properties of the sensor housing.

Recent developments carried out the concept of Transverse Flux Sensors (TFS^{TM} [23]), where conventional coils are replaced by inductors printed on a PCB[1] substrate. This technology is advantageous in terms of compactness, manufacturing reproducibility and production cost. The sensor length is reduced to the thickness of the PCB, furthermore one sensor unit is able to measure into two orthogonal directions.

Thick-film technology uses materials suitable for high temperature applications and enables to use the same layout as with PCB technology. Furthermore production cost with this technology is low and manufacturing precision and reproducibility are high.

Thick-film technology has already proved high life span at up to 550°C in the field of heating plates. Heating plates are on the other hand not so complex as sensors. They do not contain several conductive layers as needed for a sensing coil. Furthermore they do not have narrow lines and do not need any sensing capabilities. Therefore several modifications will be necessary to adapt this technology to sensors.

4.2   Thick-Film Technology Applied to High Temperature Position Sensors

This section offers an introduction to thick-film technology. Technical points concerning production and reliability of sensors for applications up to 600°C are shown here. This section ends with tong term tests showing the stability of these kind of sensors at high temperature.

---

[1]Printed Circuit Board

4.2.1   Introduction to Thick-Film Technology

The introduction to thick-film technology given here, is based on Chable [7] and Gupta [14] books. This technology is often called *thick-film hybrid technology*. In the term *hybrid* it is supposed that the devices integrate thick- and thin-film technology, components such as resistors, semiconductor or discrete devices. Sensors built during this work do not contain other technologies than thick-film, that is why the term used here is *thick-film*.

Thick-film technology is the art of screening, drying and firing an electrical circuit on a substrate. The term *thick-film* is derived from the fact that the fired film is fairly thick (5 to 50 μm) compared to thin-film (0.02 to 1 μm). Thick-films and PCB do have several similitude. The main one is that both of them use the notion of multilayer. The difference is that layers interconnections are done through metalized substrate holes in the case of PCB but done directly during the screen printing process with thick-film technology.

History

Developed from the 1940 for military applications, thick-film technology has found its first commercial applications in 1943 in the USA. Since 1965, Europe starts to develop this technology. From 1985, the growth is getting higher, until reaching today a great success thanks to performing screen printing pastes.

Substrate

The substrate is the support, on which the thick-films are deposed. It fills the function of mechanical support, electrical insulator and heat sink. The common substrate is a ceramic composed of 96% sintered alumina (Al_2O_3) mixed with 4% glass. The glassy grain boundaries react with the thick-film binder to give a significantly high bond strength.

The size of standard substrates is 4"x4" (101x101 mm) with 0.635 mm thickness. The substrate can be precut in order to cut them after the production process without any further machining as used for the axial sensor (subsection 4.3.1). Special shapes, as done for the radial position sensors (subsection 4.3.2), can be laser cut. General laser

cutting tolerances for ceramic substrate is ±0.05mm for longitudinal distances and for circle diameters, and is ±0.02mm for center-to-center distances. Nevertheless precautions have to be taken in the substrate geometry design phase in case of cut substrates. Internal sharp angles must be avoided in order to limit maximal local stresses, which could lead to breakage.

Pastes

There are different types of pastes (or inks), which are conductive, dielectric, resistive or protecting. They should have a low viscosity and appropriate wetting properties. For this special application of high temperature sensors, no resistive pastes have been used, only conductive and dielectric pastes.

Conductor pastes are composed of mixtures of particulates of metals, metal oxides, and fine glass powders suspended in organic binders. Dielectric pastes, on the other hand are composed of insulating materials such as oxides of metals, semiconductors and fine glass powders suspended in organic binders.

Screens

Screens are available in two different materials; silk and stainless steel. They are framed with uniform tension on wood or cast aluminium frames. The electrical pattern is reproduced on the screen with an emulsion in order to stop the zones where the paste should not go through. The screen mesh size, commonly 100-400 mesh, is adapted to the particle size of the paste and the desired image resolution (100-200 μm).

Printing

The image is transferred to the substrate by pushing the ink through the screen with a squeegee according to an appropriate speed, attack angle and pressure. The ink rheology is the key parameter to obtain the desired layer thickness and covering factor by keeping the highest resolution. The paste viscosity is the principle rheology influencing parameter.

Drying and Firing

Once each layer is deposed on the substrate it has to be dried during 10-15 minutes at 100-150°C before firing, depending on the material. Drying must allow the solvent, which composes 60 to 80% of the paste, to evaporate completely. While drying, the solvent must not be allowed to boil to avoid physical problems as voids or blisters.

After drying, the particles of various materials the film are bound together with a plastic like material called ethyl cellulose. This bonds the film to the substrate and the particles together until the substrate is fired.

During the firing process, the organic vehicle decomposes and the glass binder softens to wet the ceramic base and bond the metal particles together in a glass matrix. Firing occurs at 800-850°C for glass binder, during 10-12 minutes. The rate of ascent and descent should be comprised between 50-60°C/min. Each layer has to be fired before another layer can be deposited.

4.2.2   Position Sensor Manufacturing

Thick-film technology have first been tested in order to find a working solution for 550°C applications. Sensor prototypes have been developed for this purpose. Small inductors have been printed on Al_2O_3 substrates with varying track widths and materials.

Sensor Geometries

Printing a coil on a substrate means that a multiple of two conducting layers is needed in order to have the connectors outside the inductor. Figure 4.1 shows a schematic view of the sensor conception. A conducting layer is printed on the ceramic substrate, then a dielectric layer is printed as insulation. A second conducting layer is then printed. Both conducting layers are connected together in the center of the coil. A top protecting layer made of dielectric is needed to prevent conductor migration and oxidation.

A compromise between track thickness, which is limited by the technology, and high inductance has to be found. In case of radial sensor (subsection 4.3.2), the sensitivity is directly related to the inductor
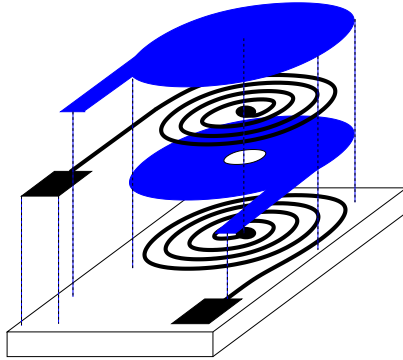
Figure 4.1: Realization of printed coils with thick-film technology on ceramic substrate. Two conductor layers are connected together in the center of a spiral. Dielectric layers are used as insulation between the conducting layers and as protection against migration and oxidation.

size. In this case the inductance has to be as high as possible and the coil as small as possible.

Standard thick-film resolution for the used inks is 200 μm line and 200 μm space width. In order to increase the inductance, tests have also been done with 150 μm line and 150 μm space widths. These tests show a strong color change of the sensors tracks and reduce life-span when current is applied at high temperature. The solution with 200 μm tracks has not shown such ageing.

Utilized Pastes

In order to find a reliable and low cost solution three commercially available conductive pastes (Ag: ESL[2] 9912-A, Ag-Pd: ESL 4913, Au: Dupond 5715) have been tested. A fourth material combination has been realized by cladding a gold layer on the top of the silver pads, in order to prevent oxidation of the silver pads. Doing so keeps the sensor cost low because only a small amount of gold is used.

Long term measurements have been performed to test the reliability and stability of the thick-film inductive sensor in the case of high temperature applications. Sensors of each conducting materials have

---

[2]ESL Electro-Science

been put in the furnace at 550°C. During the first experiment no electrical current has been applied on the sensors.

After 15 hours, inductance and resistance have been measured. No changes of the electrical properties have been measured so far.

After 650 hours at 550°C the same measurement has been performed again. It shows that none of the sensors with the combination Au-clad-Ag are working anymore. The color of the pads have changed and a small gap appears between the gold and the silver layers. Electrical conductivity is broken for all of these sensors. After 650 hours at 550°C, the Ag-Pd sensors show oxidation on the pads, and 30% of them are showing an increased electrical resistance. Because of a lack of reliability, tests were also stopped with Ag-Pd and Au-clad-Ag sensors.

However, sensors made of pure silver and gold are showing very good behaviour even after 2200 hours at 550°C. None of them are showing ageing. Their electrical resistance and inductance remain very stable when no voltage is applied.

The chosen solution for the sensors used in real application is realized with the combination of silver paste 9912-A and the dielectric paste 4913-G. The choice of using silver is motivated mainly by cost reasons. Wires have to be connected to the sensors. As shown in the previous tests, interfaces between gold and silver do not behave well at high temperature. In order to prevent an inter-diffusion between the connecting pads, the wire and the welding should be realized with the same material. Silver is a good compromise between performance and cost. Nevertheless silver is subjected to migration. This problem is described in section 4.7.

ESL 9912A is a mixed bonded silver paste particularly developed for chip resistors, consumer hybrid circuits, potentiometers and heater elements. The conducting layer has a thickness of 8-15 μm.

The dielectric paste ESL 4913-G is a non porous multilayer dielectric for use on alumina substrates based on calcium borosilicate and is cadmium-free, lead-free, and nickel-free. Three layers separately fired are used as insulation between the two conducting layers. The total thickness of these three insulating films is 50 μm. On top of the second conducting layer, a protecting film is needed, to prevent oxidation and silver migration. For this purpose two layers of dielectric are applied, with a total thickness of about 35 μm.
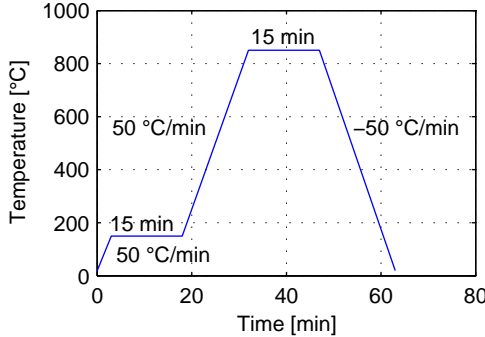
Figure 4.2: 60 minutes temperature profile of the soldering process.

Soldering Process

Connecting the leading wires to the sensors has been solved by using the thick-film conducting paste as soldering paste. This paste once fired consists essentially of silver and has naturally exactly the same composition as the sensor connecting pads. By using silver wire, the system is ensured not to suffer electrically of inter-metallic diffusion.

During the soldering process, the wires are maintained on the pads with clamps. Silver paste is applied over the soldering location and the system is put into a furnace. A 60 minutes standard thick-film profile (see figure 4.2) should be followed in order to guaranty a good drying during the first process half, and an accurate firing time and temperature during the second half of the process. Theoretical ascent and descent values of 50-60°C/min should be used. Actually the labor furnace utilized for the soldering process was not dynamical enough to reach such heating and cooling speeds. All prototypes have been achieved with 25°C/min heating rate and 10°C/min cooling rate. Soldering has not been done in clean room environment.

4.2.3   Behaviour of Thick-Film at High Temperature

Sensor Stability

A prototype sensor of silver with 200 μm track width, with silver wires and silver paste wire connections has been tested. Tests have
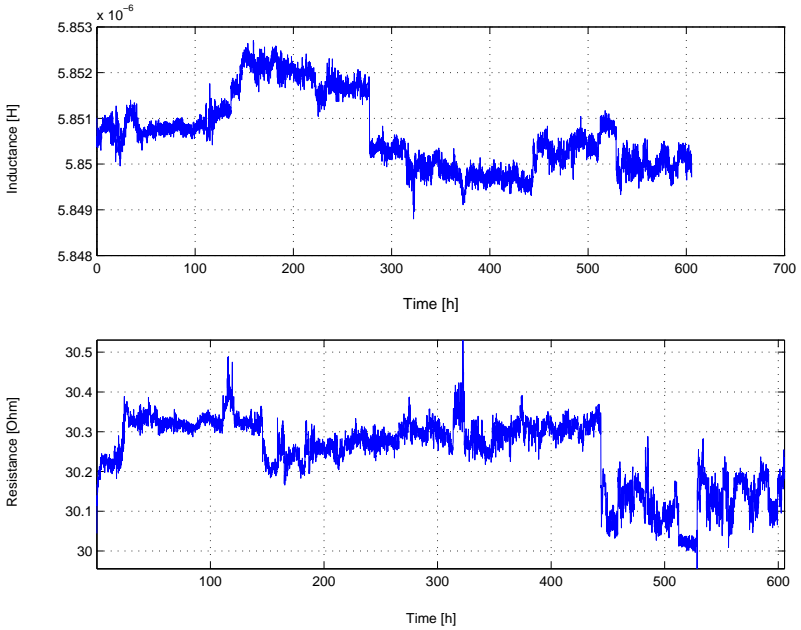
Figure 4.3: Sensor long term measurement at 550°C of the position sensor induction and resistance in function of the time.

been performed with electrical current. The sensor has been placed in a furnace at 550°C. A current of 100 mA DC ($\approx$3 V at 550°C) as well as an AC signal of 0.5 V, at 100 kHz has been continuously applied to the sensor.

Resistance and inductance have been measured every 5 minutes during 600 hours. Figure 4.3 shows a measurement of the electrical resistance and inductance in function of the time. The sensor inductance changes are lower than 0.1%, and the resistance measurement changes are lower than 2%, during the whole measurement.

Silver Migration

Migration of silver has been observed with a binocular magnifier between the connecting pads. This problem is described in section 4.7.
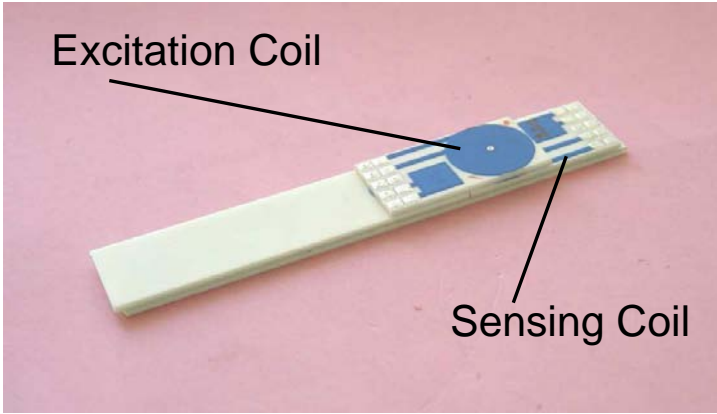
Figure 4.4: Axial sensor. Two planar coils are pasted on the top of each other.

4.3 Sensor Design

High temperature printed sensors are based on low temperature PCB sensors. The maximum using temperature for PCB sensors is about 150°C. Thick-film technology enables to realize the same sensor layout as with PCBs, with material suitable for high temperature applications.

The sensor working principle uses excitation and sensing inductors printed on ceramic substrates. This section is divided into two subsections in order to describe the working principle of the axial and radial sensors.

4.3.1 Axial Sensor

In common inductive eddy current position sensors, the position is estimated by measuring the response in a single coil. In order to enable the temperature compensation as presented in section 4.4, the excitation and measurement have been separated. The sensing principle of the axial sensor is based on two planar coils pasted one on the other. Figure 4.4 represents an axial sensor, where the top (excitation) coil can be seen as well as the connectors of the lower (sensing) one.

The excitation coil creates a high frequency magnetic field around the
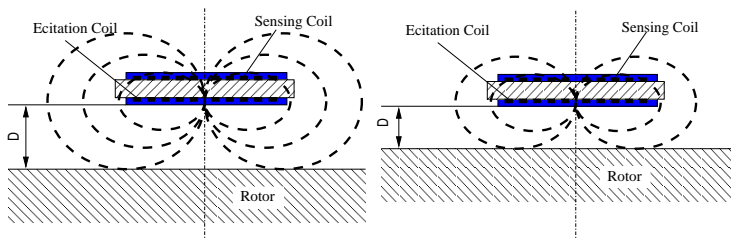
Figure 4.5: Axial sensor measuring principle. Schematic magnetic field distribution (dashed lines) when the rotor distance is changing.

sensor, which induce eddy current on the rotor surface. The eddy current creates an opposite field, which tends to decrease the excitation field. Obviously the magnetic flux depends on the distance between the rotor and the excitation coil.

The second coil measures the resulting field and creates a voltage dependent on the rotor position. Figure 4.5 shows the sensor arrangement and the changing magnetic field for two rotor positions. The sensor used in this way does not give a linear response. In order to improve the linearity a dummy sensor is connected in series to the measuring one.

The dummy sensor is composed as well of an excitation coil facing to a sensing coil. The system is then designed in order to get a half differential measurement. The distance between the two coils is chosen so as to get zero response when the rotor is in its middle position. A real differential measurement would give better results, especially regarding linearity. Sensors can be placed at both rotor ends, or can be placed for example at both sides of the thrust bearing disk.

The solution of one sensor and a dummy has been chosen, because it is comfortable to have the sensors outside the housing. Effectively for a prototype it is advantageous to have a comfortable access to the sensors. They can so be changed without having to open the whole system. The linearity with this solution is however good enough to guarantee the stability with a robust controller. Furthermore only one end of the rotor presented in chapter 7 is available as sensor target.
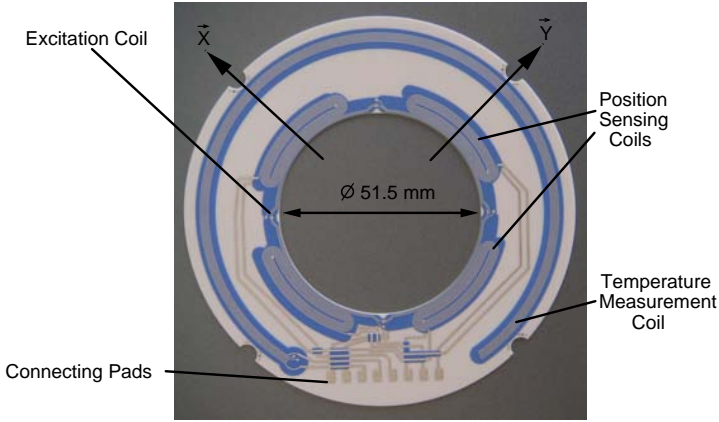
Figure 4.6: Radial sensor. Inductors are printed on a ceramic substrate.

4.3.2 Radial Sensor

The principle of the radial sensor is basically similar to the axial sensor. The excitation coil and sensing coils are printed on a substrate. The excitation coil embraces the rotor as shown in figure 4.6. It is supplied with an AC current source in order to create a high frequency magnetic field. Eddy currents are created on the rotor surface. They produce a magnetic field tending to attenuate the excitation. The final distribution of the magnetic field depends on the rotor position. Thus, when the rotor is centered (figure 4.7) the field is symmetrically distributed. When the rotor position is decentered (figure 4.8), the field is not distributed symmetrically anymore.

The position measurement is done differentially. Two coils facing one to the other are connected together in series, so that when the rotor is centered the output signal is zero. When the rotor is moving from the middle position, a voltage is measurable. The signal amplitude is proportional to the position and the measured signal sign is related to the displacement direction. The signal is then synchronously demodulated, so that a sample is taken at each signal peak.

The radial position sensor is able to measure along two orthogonal axis. This has been realized by placing two facing pairs of coil perpendicularly, as shown on figure 4.6.

Figure 4.7: Radial position sensor sensing principle. The high frequency magnetic field distribution in case of centered rotor is distributed homogeneously around the rotor.

Figure 4.8: Radial position sensor sensing principle. The high frequency magnetic field distribution in case of decentered rotor is no more symmetrically distributed. That induces a voltage on the sensing coils.

During the design phase a trade-off is done between inductance and sensibility. On radial printed sensors, the position is measured in the trans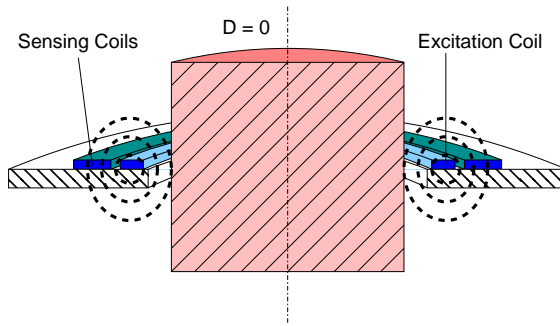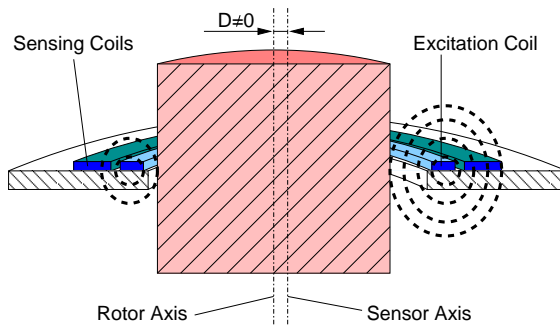verse direction. Consequently, the coil sizes influence the coil arrangement on the substrate. In order to get the best sensibility the measuring coils should be placed as close as possible from to rotor. At the same time the inductance should be as high as possible. Thick-film technology give the limitation in terms of coil miniaturization. Standard thick-film track line thickness is 200 μm, with a distance of 200 μm between two tracks.

For both cases, axial and radial sensors, there is no magnetic core. That makes the sensors interference proof against disturbances of the magnetic actuators. The target only needs to be an electrical conductor to induce eddy current; no magnetic rotor is needed. The working frequency of the sensors is in the range of 1 MHz. Thus, they are not disturbed by the low frequency field of the actuators.

4.4 Electronics for Temperature Compensation

Temperature has a non negligible influence on the sensor behaviour. Fortunately, the inductance remains almost constant, a small increase is possible due to the coil thermal expansion, but this effect is negligible. On the other hand, the sensor electrical resistance increases dramatically with the temperature. It is more than three time larger at 600˚C than at room temperature. However the measuring electronics has to give the same measuring signal independently on the temperature.

State-of-the-art electronics uses a RCL resonator to produce the excitation signal, which is obviously resistance depending. In order to get signals, which are not temperature dependant, an active circuitry has been designed.

The magnetic field depends on the current in the excitation coil. A current source able to deliver a constant current (independently of the sensor resistance) guarantees to produce a constant excitation whatever the temperature is. Such a device is represented on figure 4.9. A (synchronous) clock signal at 900kHz is given from the AMB controller and is filtered with a band-pass filter in order to get a harmonic signal.
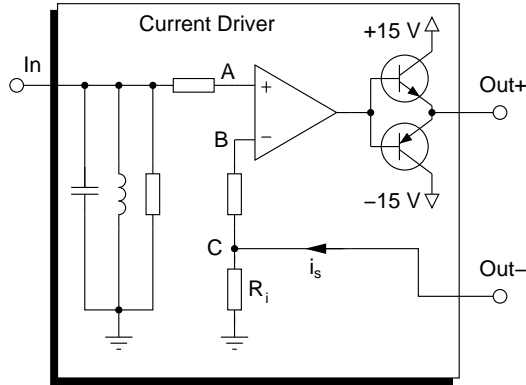
Figure 4.9: Current driver for sensor excitation, delivering a high frequency constant AC current. A clock signal is given as input and the excitation coil is plugged in the output.

An operational amplifier drives a push-pull transistor pair in order to keep the voltage of point A (V_A) equal to the voltage of point B (V_B). As long as the input impedance of the operational amplifier is considered as infinite, $I_{BC} = 0$. The voltage at point C, V_C, is also equal to V_A and V_B. From this point $I_s = \frac{V_A}{R_i}$, which means that the current I_s does not depend on the sensor resistance.

On the sensing side the current is kept as small as possible using high CMRR[3] (figure 4.10) with high input impedance amplifiers. They amplify the differential component of the measured signal with low common noise. Their high input impedance is much higher than the measuring sensor coil resistance, which leads to a current almost equal to zero. In this way the measured value does not depend on the temperature.

In order to reject noise component, a band-pass filter is put on the output. It is also combined with a transformer, which ensure a galvanic insulation.

In prevision of digital temperature compensation, the sensor temperature is estimated by resistance measurement. For this purpose a special track has been added on the external part of the sensor substrate (figure 4.6).

---

[3]Common Mode Rejection Ratio
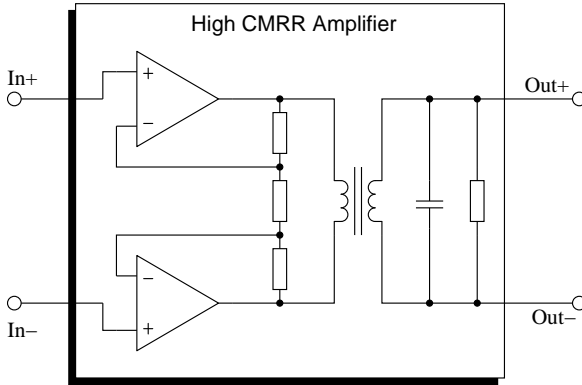
Figure 4.10: High CMRR amplifier with high impedance input. The measured sensor signal is amplified differentially, filtered and galvanic insulated in order to be demodulated.

The temperature can also be estimated by knowing the resistance of the sensing coils themselves. Since the position sensing principle is differential, a DC signal can be added to the AC signal without changing the position measurement. This signal combination enables to use the sensor as position as well as a temperature sensor.

Figure 4.11 shows the realized circuitry solving this problem. A current, practically independent on the temperature supplies the sensor, using a resistance bridge. The sensor resistance between 27Ω and 100Ω is small compared to the $40k\Omega$ resistance of the bridge. That brings a current difference of about 0.4%, which is acceptable for a temperature measurement. Thus the DC voltage created is directly proportional to the sensor temperature. That voltage is amplified differentially, with a ground reference.

4.5   Sensor Cables

Sensor cables have been realized with silver wires as discussed in subsection 4.2.2. Insulations have been realized with first a mica tape, type SK650[4] covered with an silica-alumina textile flexible tube.

---

[4]Von Roll Isola
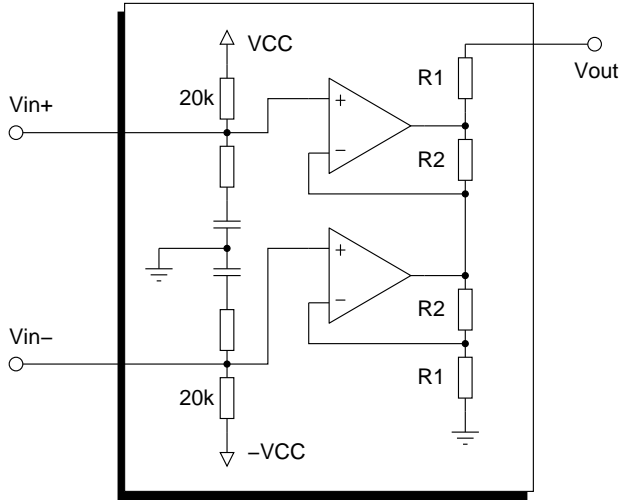
Figure 4.11: Temperature sensing electronics enabling the measurement of the sensor coil resistance.

In order to protect the sensor signal against high frequency noise, the conductors have been twisted. The sensors are relatively sensitive to the movements of the wires, that is why it important to keep the wires as close as possible from one another, and avoid relative movements. In order to fulfill this task and to give a good mechanical protection, glass sheath, which are mechanically much more robust than ceramic ones, have been put over the twisted pairs.

Tests have also been done regarding leading wires shielding. In this case experiments show that by winding another silver wire over the excitation pair of wire (over the glass sheath), noise is reduced to the minimum. The shielding has been connected only on the sensor electronic side and any electrical contacts with the environment have been avoided on the sensor side.

Such a configuration has given very good results in term of noise reduction, mechanical protection and electrical reliability.

Tests using only glass insulation have shown that glass does not insulate good enough above about 300˚C. At this temperature ionic conduction makes the insulation not reliable any more. That is why in the final configuration glass is used only as mechanical protection.
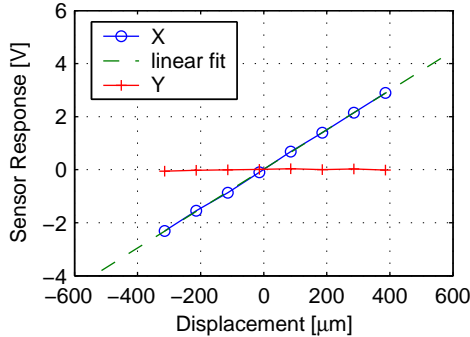
Figure 4.12: Sensor response when the rotor is moving along X axis.
Measurement done at 600˚C.

4.6   Measurements

In order to provide measurements of the sensor response at different
temperatures in function of a metric displacement, a special setup
device has been built. The sensor has been put into a furnace. It
has been mounted on a bar, going through the furnace wall. That
enabling to move it from a room temperature region. The sensor has
been displaced with an X-Y table aligned with the two orthogonal
sensor sensing axis. A non-magnetic metallic cylinder has been put
into the furnace as well, playing the role of sensor target.

Obviously, the thermal expansion of this setup is quite high and dif-
ficult to model, especially because of the temperature gradient along
the bar. That is why the measurements have been done differentially
by moving the sensor until touching both ends of the target. Thermal
expansion of the bar has been adjusted by moving the table and by
rotating the sensor support.

The sensor sensitivity was measured in this manner from 20˚C to
600˚C. Figure 4.12 show a measurement done at 600˚C where the rotor
is moving along one sensing axis. A linear fitting line gives the sensor
linearity. Residuals between the linear fit and the sensor response of
figure 4.12, are 1.5% of the full response range[5]. The two sensing axis
are well decoupled.

---

[5]Actually the sensor resolution of 0.17 μm/Digit, is much higher than the
resolution of the used measurement device (5 μm). So 30 Digits of measurement
error correspond to 5 μm, which is the resolution of the measurement device.
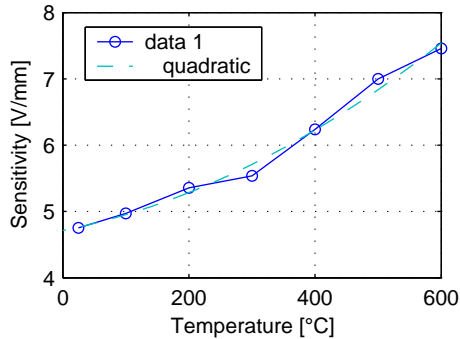
Figure 4.13: Sensor sensitivity (solid line) and quadratic fitting (dashed line) in function of the temperature.

The sensitivity has been studied in function of the temperature. Sensitivity measurements have been performed from room temperature up to 600°C and plotted in figure 4.13. A non-negligible sensitivity augmentation in function of the temperature is measured. Considering the temperature compensation electronic presented in section 4.4, the sensitivity change is not due to the sensor circuitry. This augmentation can be explained with the fact that sensor and rotor are made of two different materials having different thermal expansion coefficients. This means that the air-gap sensor-rotor is reduced at high temperature, what leads to a higher sensitivity.

A compensation is possible in order to get a constant sensitivity over the whole temperature range of operation. It should be adapted to the application, considering namely the temperature variation speed, the possibility to recalibrate the sensor at the working temperature, the robustness of the controller. In gas turbines, it is not possible to recalibrate the sensor at the working temperature during operation. Moreover the heating speed is very high; the turbine reaches the steady temperature during the first minutes of operation.

Nevertheless a digital compensation is possible. By measuring the sensor temperature and estimating the rotor temperature, an algorithm, which regulates the sensor gain, could be integrated into the AMB controller. Another possibility would be to regulate the gain electronically. This is possible by designing an excitation electronic having an amplitude decreasing in a controlled way in function of the temperature.

In this work no temperature compensation has been implemented. Temperature changes are slow and it is always possible to lift down the rotor to perform a sensor calibration.

4.7 Silver Migration on Ceramic Substrates at High Temperature

Metallic electromigration is the movement of metallic material - usually through or across a non-metallic medium - under the influence of an electric field [21]. The material that migrates is considered to be in metallic state. The migrated material can cause short circuits.

Silver migration can be classified as solid state (electron momentum transfer) and electrolytic (ionic) migration depending upon the environmental conditions of occurrence [44]. Solid state occurs at high temperature ($>150^\circ$C) or with high current densities ($> 10^4$ A/cm^2). Electrolytic migration occurs at ambient temperature and low current densities, most of the time due to moisture or humidity. Silver migration decreases by approximately hundred times when the Palladium content in the conductor is increased from 10%-19% [30].

4.7.1 Silver Migration Between Wire Connections

ESL 9912-A paste (subsection 4.2.2) is subject to silver migration. Figure 4.14 shows migration of silver particle on 1.1 mm distance between two wire connections. In this case a conductive bridge has been created, making a short-circuit between the sensors poles.

Migration process was stronger between the excitation wire connections than for sensing wires. For excitation wires, the voltage between the poles is ±13V at 600°C for the current source of 100mA at 900kHz. The voltage between sensing wire connections is about 3V at 900kHz, and the current is zero. Short circuits on the excitation signal are quite difficult to detect. The bridges are immediately burned by the current going through them. The excitation signal noise produces noise on the measurement signals. In the case of radial sensor, this noise is correlated between the two position measuring canals.
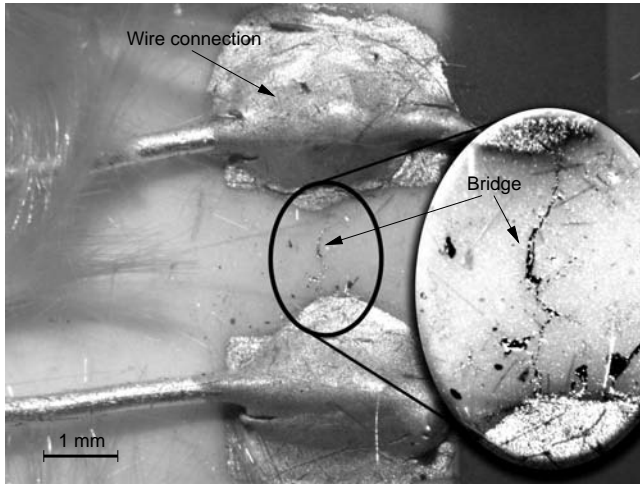
Figure 4.14: Migration of silver particles on 96% Al_2O_3 sensor ceramic substrate. A conductive bridge is created between the sensor connecting areas creating a short-circuit.

4.7.2 Migration Stopping with Protective Pastes

For high temperature applications, the conductor layer and the solderings have to be covered with a dielectric to prevent silver migration. For this purpose the same dielectric (ESL 4913) as for the sensors manufacturing has been used. The sensors have been inserted into the AMB under real working conditions: 550°C, 100mA current supply at 900kHz. Due to probably a too low heating speed during the firing, the ESL 4913 could wet the connection surface enough before sintering. The result is a porous dielectric and silver has diffused into it. The consequences are short-circuits and sensor noise. Cracks on the wires are visible, due to the high thermal expansion difference of silver and ESL 4913.

ESL 4924, ESL 4904 and ESL 4903 have been tested as cover for the sensor soldering areas. For each paste three layers have been applied and separately fired. They have been tested at 600°C, with a DC current of 100mA applied on the sensors. After 220h, sensors with ESL 4903 were short circuited and they were not working any more. At this time one sensor with ESL 4904 was short circuited as well. Nevertheless after 760h, one of the ESL 4904 and both ESL 4924
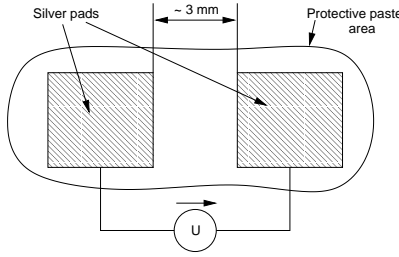
Figure 4.15: Migration testing procedure.

covers gave a good barrier against migration.

Tests with other covering pastes have been done. Silver connection pads (ESL 590G) have been covered by several pastes, in order to test barriers against migration (figure 4.15). A voltage of 15V has been applied on the pads during 220h, and then 50V during 540h. The testing device has been done in a furnace at 600°C. Two tests have been done.

First a passive barrier has been tested by covering the silver pads with dielectric pastes. The aim of this test is to produce an ion-proof protection. The protection has to be dense, and do not suffer from the high thermal expansion of the silver wire. Effectively thermal expansion is a source of crack in the dielectric. A cracked barrier could let the silver ions going through. Two dielectric pastes were tested on this device: the ESL 4913 and the ESL 4904. Only one fired layer has been applied for each paste. ESL 4904 has shown short circuits after 300h tests. Dendrites, as shown on figure 4.16, are clearly visible after this test. ESL 4913 has not shown any migration after 720 hours.

Secondly, resistive pastes have been tested to cover the silver pads. The idea is to produce a lightly conductive area around the pads making a screened room. The electrical field on the silver region is then zero and the migration is by this manner "actively" stopped. Two pastes have been tested: ESL 3915 and ESL R315. With ESL 3915 tests have been done with pastes connecting the pads together, which creates a small current and with separation between the paste areas. After 100h the, ESL 3915 is no more conducting between the so-connected pads. After 600h, the pads with disconnected ESL 3915 are conducting. After 720h a current is measurable again between the pads connected with ESL 3915. That means that this paste is
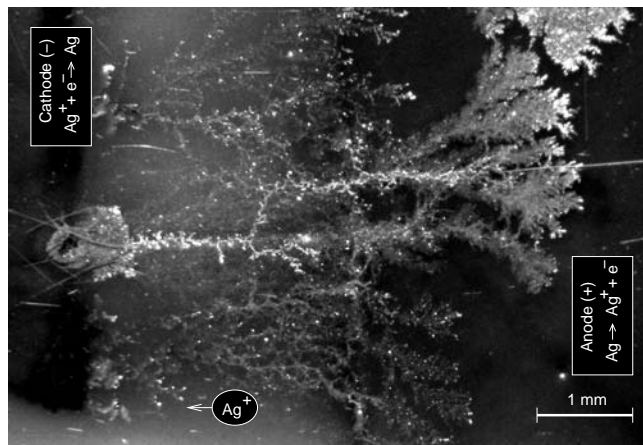
Figure 4.16: Silver migration dendrite growing principle.

not stable at high temperature. Optically, large traces of metallic migration are visible. The ESL R315, with disconnected protective areas, showed clear traces of metallic migration between the pads, but with no electrical contact.

A last test has been performed with pads without any protection. After 720h no migration and electrical contact have been detected. This last test gives an indication on the test validity. Effectively, with no migration on the non covered pads, the test is actually not valid for the position sensor working conditions. It was however easier to supply DC voltage than a 900kHz current source and easier to measure the current peaks than noise on a high frequency signal.

4.8   Summary and Outlook

A technology has been tested and suitable materials have been found for thick-film printed eddy current sensors. Two sensing principles, axial and radial, have been presented. Measurements done with the radial sensor have been presented. They show extremely good results in terms of linearity. The sensitivity has been characterized in function of the temperature.

Sensors have to be connected to leading wires, and that point is much more critical due to silver migration. Dendrites are growing quite fast

in the electric field between two connector pads at high temperature. Thus short circuits are created. Solutions to slow down this effect have been tested. They show that with an accurate protection, sensors are still working after 700 hours at 600˚C.

A new sensor design should be done with wire connections far away from each other in order to limit the migration phenomena. Cutting the substrate between the connecting pad or putting the them on each sides of the substrate are possible good solutions.

Chapter 5

Thermal Model for High Temperature AMBs

In order to design an AMB working at high temperature, the thermal aspect has to be explored. The limitation of current must be determined as well as the working temperature of the materials. A steady state model including the thermal radiation has been built on the basis of a thermal network.

Basic thermal networks are proposed in [41] where the model is reduced to it's minimum. Traxler [43] proposes a coil model, simplifying the coil as a torus and integrating the thermal characteristics along the winding radius. Paychère [35] gives a network model suitable for precise temperature predictions in electrical motors. However none of the above-mentioned projects presented as been validated for designing high temperature magnetic bearings.

This chapter presents a thermal model, which allows the layout and optimization of high temperature AMBs. It is based on a thermal network and is implemented in MATLAB. It is able to cope with temperature dependent parameters in a non-linear way. This simplified, but powerful layout tool is used for the design of a high temperature bearing running at up to 550°C ambient temperature. The algorithms shall be programmed effectively in order to keep computation time small. The results have been verified on a high temperature AMB demonstrator rig [5].

5.1 Physical Basics

This section describes the thermal physical phenomena, which occur in an AMB. Losses in AMBs are heat sources and all the produced heat has to be dissipated in order to reach the thermal equilibrium. AMBs are often designed to be able to carry the highest amplifier current continuously, which should avoid any overheating in the electromechanical parts. This correspond to a steady state model, taking the worst case into account. Such a model is simplified by skipping thermal capacities, in order to reduce the number of parameters. No extra cooling other than the natural air convection and the radiation is foreseen, thus no assumptions about forced air cooling are proposed.

5.1.1 Heat Sources

Heat sources are related with the system losses. The losses have been presented in subsection 2.2.3. They occur under hysteresis, eddy-current, air-losses and resistance losses. Since in this special case the rotor is not rotating, the main losses are stator losses. They are dominated by the ohmic losses. The heat source taken into account in this model is only due to resistance losses. Equations 2.18, 2.19 and 2.20 give the resistance losses equation:

$$P_{Cu} = \rho_0(1 + \alpha_1 T + \alpha_2 T^2)\frac{A}{l}i^2 \tag{5.1}$$

5.1.2 Heat Sinks

Basically the global heat sink of the AMB is achieved by the housing external surfaces. Internal parts, for example the coils, do have their proper heat sinks; the air inside the housing and the iron. It is obviously possible to increase the cooling of the system using for example liquid coolant, or by blowing air on the rotor and the coils. Other solutions are possible, such as cooling the coils internally.

In the case of the demonstrator built during this work, the system complexity is kept as low as possible. Fastening parts and sinks external to the oven are reduced to the minimum in order to keep the entire system at high temperature and to avoid unmodeled temperature gradients. Moreover the system benefits from the advantageous heat transfer through radiation.

Since the furnace temperature is regulated by a controller. As far as the AMB heat losses are sufficiently low that the temperature can still be regulated, the furnace temperature is assumed to be constant. The furnace heat capacity is considered as infinite.

5.1.3 Heat Transfers

Heat transfer can be described by three principles: conduction, convection and radiation. The transfer thermal power is defined by $\dot{Q}$ [W]. The particularity for a thermal model valid from room to high temperature, is that the thermal coefficient are temperature dependant. The thermal radiation is by itself temperature dependant.

Conduction

The conduction, or the heat transfer in solid materials is given by:

$$\dot{Q}_{cond} = \frac{\vartheta \cdot A}{L} \Delta T \qquad (5.2)$$

Where ϑ [$\frac{W}{mK}$] is the thermal conductivity of the material, L [m] is the length between two points with temperatures T_1 and T_2 [K], ΔT is the temperature difference $(T_2 - T_1)$ and A [m^2] is the cross section of the material parts.

Convection

Natural convection is expressed by the heat transfer between solids and fluids.

$$\dot{Q}_{conv} = \alpha \cdot S \cdot \Delta T \qquad (5.3)$$

The coefficient α[$\frac{W}{m^2 K}$] describes both the thermal conduction of the fluid and its motion. S [m^2] is the surface of the solid in contact with the fluid.

Radiation

The thermal radiation is electromagnetic radiation emitted from the surface of an object that is simply caused by its temperature.

For the case of the radiation some assumptions have been made. All the materials are considered as gray body, they absorb only part of the thermal radiation reaching their surface. They are characterized by their coefficient of emission ε, which is considered equal to the coefficient of absorption of a gray body. The radiation to the environment is given by [15]

$$\dot{Q}_{rad} = \varepsilon \sigma \left(T_1^4 - T_a^4 \right) S_1 \tag{5.4}$$

Where T is the temperature in Kelvin, S_1 is the emitting surface and σ is Stefan Boltzmann's constant, $\sigma = 5.67e^{-8} \ [\frac{W}{m^2 K^4}]$.

5.2   Thermal Model

The bearing model has been realized as a thermal network. All elements are discrete, and transformed into heat resistances and heat sources (Figure 5.1). In this study, the problem has been restrained to the static case, so the heat capacitance in the network can be skipped as explained in [35], and the number of unknowns is by this way minimized.

In order to be able to supply DC current without having stability problems, the rotor has been fixed on the system housing. Since the rotor has a rotation speed equal to zero, $f_r = 0$, the rotor hysteresis (eq. 2.16) and eddy current losses (eq. 2.17) are zero.

The thermal resistances of the network elements are transformed from equations 5.2, 5.3 and 5.4 into:

- Conduction

$$G_{cond} = \frac{L}{\vartheta \cdot A} \tag{5.5}$$

- Convection
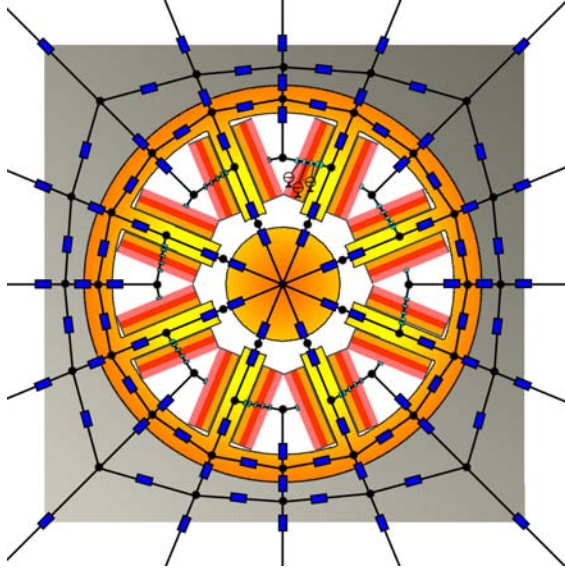
Figure 5.1: Thermal Network of the AMB

$$G_{conv} = \frac{1}{\alpha \cdot S} \tag{5.6}$$

- Radiation

$$G_{rad} = \frac{\Delta T}{\varepsilon \sigma (T_1^4 - T_a^4)} \tag{5.7}$$

Thermal parameters ϑ, α and ε, in equations 5.5, 5.6 and 5.7 are temperature dependant. This dependency is expressed by polynomials of first or second order.

The electromagnetic system is discretized in a finite number of elements K_i. The states of the model are the temperatures T_i of each element. They are connected together by the thermal conductances G_{mn} of the matrix G (equation 5.8).

$$\begin{pmatrix} G_{11} & G_{12} & \cdots & G_{1n} \\ G_{21} & G_{22} & \cdots & G_{2n} \\ \vdots & \vdots & \ddots & \vdots \\ G_{m1} & G_{m2} & \cdots & G_{mn} \end{pmatrix} \begin{pmatrix} T_1 \\ T_2 \\ \vdots \\ T_m \end{pmatrix} = \begin{pmatrix} \dot{Q}_1 \\ \dot{Q}_2 \\ \vdots \\ \dot{Q}_m \end{pmatrix} \tag{5.8}$$
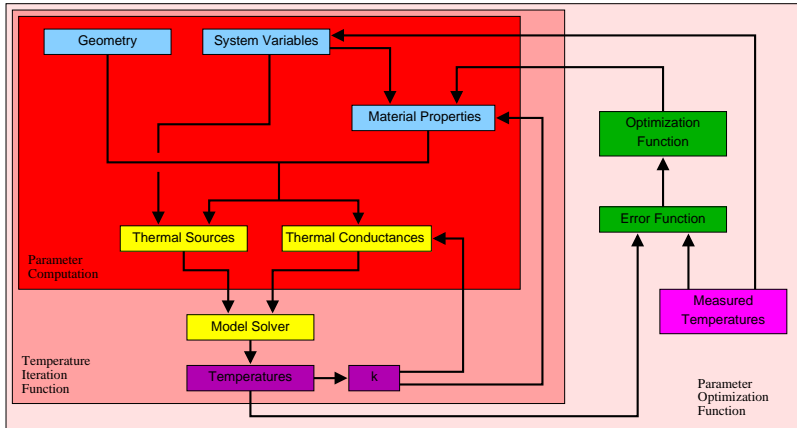
Figure 5.2: Block diagram of the thermal model.

This matrix G is square and symmetric and is inverted in order to get the temperatures T_i; $T = G^{-1}\dot{Q}$.

5.2.1   Thermal Network

The model has been built up in two steps. First a simplified coil model (subsection 5.2.2) has been developed and validated. Secondly a model including coils, iron core, housing and rotor (subsection 5.2.3) has been developed and validated.

The block diagram of figure 5.2 shows the three main blocks in the model structure. The first one reads the values from a file containing all the parameters of the AMB and build the T and G matrices. At this stage, the material temperatures are defined equal to the ambient temperature.

The second block calculates the temperature from the given matrices. Since some parameters and the thermal radiation conductances are temperature dependent, the calculated matrices T and G of the first block must be redefined. The second block proceeds by iterations and tries to converge to equilibrium. The convergence of the system is ensured by a factor allowing to tune the closed loop gain.

The third block is an optimization loop, which compares the model predictions with measurements and tunes the polynomial coefficients

of the material properties accordingly. The measurement conditions, i.e: coil currents and ambient temperature, are given to the model as well as the value of the parameter to fit. A temperature computation is done and compared to the measurement data. The function *fmincon* of Matlab tries, using a medium-scale algorithm (line search), to find an optimum parameter value reducing the error between the measured and the calculated temperatures.

5.2.2 Coil Model

The aim of the coil model is to be able to model and to validate only a part of the whole system. A simple coil has been put at high temperature with thermal sensors in the winding and on the surface. The thermal parameters of a simplified model can be found by this way.

The system to model is a coil composed of conductor windings made of ceramic insulated wire, wound on a ceramic support. The coil heat source is given by the conductor resistance losses, which depends on the cable material, diameter, length and temperature. The heat sink is the ambient air and the furnace environment. The coil is cooled by natural convection and by thermal radiation.

In order to decrease the model complexity, a simple coil model has been chosen. The temperature in the coil is considered as constant in each layer of windings. That means that in term of thermal flux, the coil is modeled as it has been made of alternating conducting and insulating strips (see figure 5.3). The conduction parameters describing this simplification have been found experimentally.

Since the thermal conductivity of the coil ($\lambda_{Cu} = 401 \, [\frac{W}{mK}]$, $\lambda_{Ag} = 427 \, [\frac{W}{mK}]$) is much higher than the insulation materials conductivity ($\lambda_{ins} = 0.5$ - $16.3 \, [\frac{W}{mK}]$) and the insulation relatively thick, the thermal resistance of the copper is neglected in the direction perpendicular to the windings. The parameter λ_{ins} depends on the winding compactness as well. In order to make this parameter repetitive, the same windings compactness has been kept for experimental and test rig coils.

The coils have been wound on ceramic coil holders (figure 5.3). Low thermal conduction of the relatively thick maintaining parts on the sides of the coil holders, and the flat shape of the coils, permit to
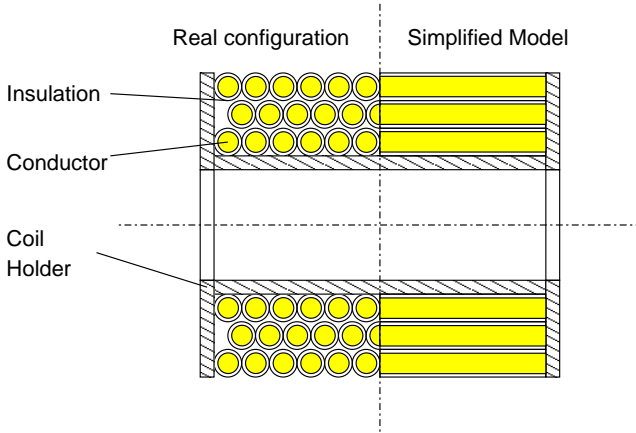
Figure 5.3: Cut of a coil with real configuration and simplified model for heat transfer calculation.

restrain the number of thermal elements of one per layer by neglecting the side effects.

Coil wires with different insulations have been used; a nickel-clad copper wire with an insulation of mica-fiberglass tape and Thermocoax (see subsection 3.3.2).

5.2.3 AMB Model

The coil model has been inserted into a whole system model containing the housing, the stator laminations and the rotor. Heat transfer coefficients for thermal conduction in function of the temperature are precisely given in the literature for most materials and coil internal parameters have been defined in the previous test (subsection 5.2.2). Nevertheless coil holders conduction, internal convection, and radiation have to be defined experimentally. An experimental rig has been built in order to validate the model.

For simplicity reasons the rotor has been fixed on the housing, enabling to change the coil current without stability problems. The model correspond to the experimental rig, which is consequently not exactly a real AMB. However doing so gives an idea of the coil heating in function of the temperature and the current.

Without rotor rotation and any forced airflow inside the furnace, the thermal convection is in this case only due to natural convection. In this case Wong [46] and Hofmann [15] give elaborated methods to model natural convection. Analytical cases are given for simple surface geometries as planes or tubes. No reasonable analytical model can be developed for AMBs.

Natural convection is related to the gravity field, and each parts of the stator have a different orientation compared to the gravity direction. A special analytical model should be used for each coil. In order to keep the model complexity low, this phenomenon was approximated with a single parameter α for all the areas where convection takes place. An exception was however made for the small air gap between stator teeth and rotor. Without rotor motion it is meaningful to consider a heat transfer mainly due to conduction of the air and not due to air-flows. The parameter of the air conduction was used to model this case.

The whole AMB was modeled including thermal radiation and absorption. The values of the thermal radiation parameters are not given precisely in data sheets. They actually depend on the temperature and the surface colors (which may change due to oxidation). The largest heat transfer due to the radiation happens at the hottest spots of the system, which are the coils in the case of AMB.

The coils are divided into two parts, the coils head and the flat longitudinal parts. The coil heads radiate directly into the oven without reflection, so equation 5.4 is used. In order to obtain a simple model, the longitudinal parts are considered as triangular spaces. The walls S_1 and S_2 (figure 5.4) are considered as the coils surface and S_3 the visible area of the stator. The illuminance $J\left[\frac{W}{m^2}\right]$ is a function of the emission flux φ_2 and of the reflection flux of the three surfaces [46].

$$J_1 = \varphi_1 + (1 - \varepsilon_1)\left[F_{12}J_2 + F_{13}J_3\right] \qquad (5.9)$$

$$J_2 = \varphi_2 + (1 - \varepsilon_2)\left[F_{21}J_1 + F_{23}J_3\right] \qquad (5.10)$$

$$J_3 = \varphi_3 + (1 - \varepsilon_3)\left[F_{31}J_1 + F_{32}J_2\right] \qquad (5.11)$$

F_{mn} is the factor, which considers the angular orientation of surface S_m to surface S_n and ε_n their radiation coefficients. Equations 5.12, 5.13 and 5.14 express the heat transfer from one surface to the others.
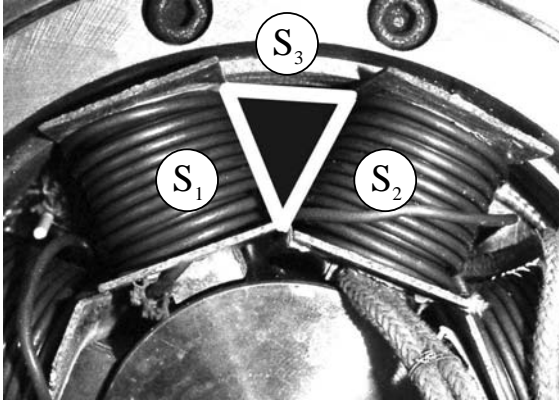
Figure 5.4: Areas of thermal reflection

$$\dot{Q}_{12} = F_{12}S_1(J_1 - J_2) \tag{5.12}$$

$$\dot{Q}_{13} = F_{13}S_1(J_1 - J_3) \tag{5.13}$$

$$\dot{Q}_{1,23} = S_1(J_1 - F_{12}J_2 - F_{13}J_3) = \dot{Q}_{12} + \dot{Q}_{13} \tag{5.14}$$

By permutation of the indices the heat transfer of the other surfaces is obtained. In the present case the areas S_1, S_2 and S_3 are considered to be equal (assuming that the coil holder doesn't emit), so the factors F_{mn} are equal to 0.5.

5.2.4   Model Reduction

AMBs have the particularity to be symmetrical, with their coils placed regularly around the rotor. The maximum current allowed in the coils is the maximum current deliverable by the amplifiers.

A simplification of the model is possible according to symmetry properties of the system. The system model can be divided into two symmetrical parts along a vertical axes, going through the center of the stator. The model size is by this way divided by a factor two.
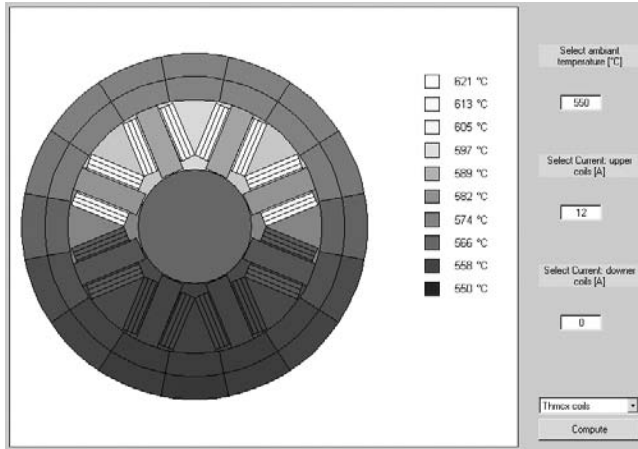
Figure 5.5: Thermal model graphical user interface.

5.2.5 Result Visualization

A Graphical User Interface (GUI) has been programmed (figure 5.5) enabling to chose between the two types of radial bearings used in the developed AMB prototype (section 7.1.2). The ambient temperature can be set, as well as the current in the upper coils and lower coils. The temperatures are finally represented with the modeled elements color, from dark to bright, respectively to their low and high temperature.

5.3 Model Validation

First, single coils wound on coil holders of ceramic have been put into a furnace. Their resistance in function of the temperature has been measured using a small current, in order to use the coil resistance as temperature sensors for the next experiments. Then a DC current has been applied and the coil temperature has been measured.

For the purpose to validate the AMB model, a real radial bearing equipped with temperature resistance detectors has been used. The temperature sensors locations were: Within the housing, inside a tooth, in the air between two coils, in the centre of the rotor and within a coil. The coil temperature was also estimated by measuring its electrical resistance.
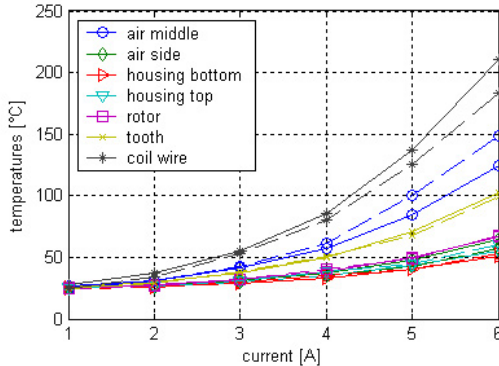
Figure 5.6: Comparison between the measured (dashed lines) and the model temperatures (solid lines) for the steady state at room temperature in function of the current.

The rotor has been fixed within the bearing enabling current variations without rotor motion. Rotor fastening parts have been designed as thin as possible to avoid heat transfer to the housing. Nevertheless, they have been included in the model.

A special care has been taken to thermally isolate the system as much as possible from the environment. The AMB housing was standing on thin ceramic parts having thus a low cross section, a high length and a low thermal conduction parameter. It has not been fixed with any metallic screws. Therefore there has been no metallic contact of the housing with a base plate and thus no unmodeled heat losses.

The system has been put into a furnace and heated up until reaching the steady state. The temperature data have been acquired with a digital data acquisition system (Dspace) as well as a LCR meter linked to Matlab during long-term measurements. For each applied DC current, data were acquired until reaching the steady state.

The results are summarized in figures 5.6, 5.7 and 5.8 for three ambient temperatures (25°C, 200°C and 460°C). For each one of these tests the same setup and the same model with the same parameters were used.

A maximum deviation error of 20% is obtain in the worst case, which is the temperature of the air between the coils at low temperature in figure 5.6. The phenomenon for this case is only due to the convection
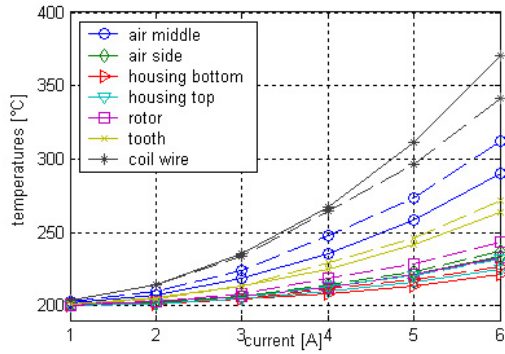
Figure 5.7: Comparison between the measured (dashed lines) and the model (solid lines) temperatures for the steady state at 200˚C ambient temperature in function of the current.
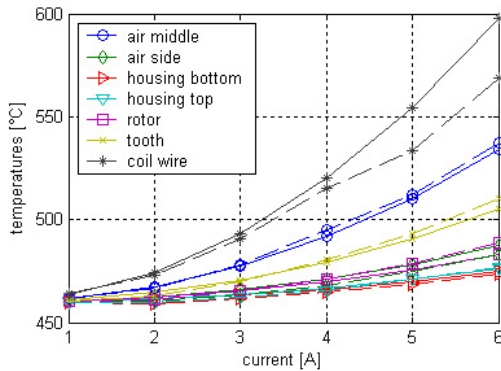
Figure 5.8: Comparison between the measured (dashed lines) and the model (solid lines) temperatures for the steady state at 460˚C ambient temperature in function of the current.

of the air between the coils. A more analytical model should be done to obtain better results or to use forced airflow in order to have a clearly defined airflow. The coil temperature is also accurate only with 12.5 % between the prediction and the measure. Estimating the coil temperature by measuring its electrical resistance does not give precise results. Effectively the coil resistance is low ($< 1\Omega$ at 25°C) and its temperature coefficient is low as well. The measurement precision depends as well on the previous calibration, which is another error source.

The parameters values of the coefficient λ_{ins}, λ_{Mica}, α, $\varepsilon_{1,2,3}$ estimated by using the optimization function are in the ranges given in the literature [46]. The computation time is also very small, between 2.5 and 4 seconds depending on the current and environmental temperature.

5.4   Summary

The presented thermal model permits to calculate the increase of temperature resulting from the thermal losses in a wide temperature range. The innovation is the inclusion of the thermal radiation effect in a relatively simple model. The fast and effectively programmed algorithms make it suitable for AMB design optimization. Modeling first the coils to find their specific parameters and secondly the whole system model is the iteration step done in this development.

Finally validation of the model has been done, by using a radial AMB and measuring temperatures in several locations.

Chapter 6

Toward Diagnosis of High Temperature AMB

6.1   Introduction

Magnetic bearings have the reputation to be very reliable. At room temperature they can work properly during decades, without encountering any problems. They can be used at high temperature, but only at the cost of reduced life span. In order to avoid failures due to high temperature exposition, fitting of the controller has to be done in function of the system changing characteristics. Nevertheless, the failures that can occur have to be known and diagnosis procedures have to be developed. For this purpose, typical failures related to high temperature are studied (see subsection 6.2.1).

The present chapter does not claim to show a complete solution catalogue of diagnosis procedures, nevertheless an example of diagnosis is given: coil characterization (see section 6.2). Current ripple is an inevitable outcome of the pulse width modulation (PWM) signal and the basic idea here is to exploit this natural excitation for purposes of identification and diagnostics. Subsection 6.2.4 shows the simulation of the developed diagnosis procedure.

Experiment and knowledge of the material physical properties evolution allow the introduction of prognosis procedures. An outline of

this approach is developed in section 6.3. An outlook about correction strategies is finally given in section 6.4.

6.2   Diagnosis

In the field of diagnosis of high temperature active magnetic bearings, research has already been done. Redundant systems [10] are proposed with adaptive controller for the realization of a reliable system.

Procedures not directly related to high temperature, which use AMBs as sensors have been developed. Approaches using the frequency response caused by the PWM voltage as shown in [39, 31] and a protocol linking the rotor inertia to the AMB actuator [24] can be adapted to estimate the actuator properties.

In this work, AMB characteristics are considered not only to be dependant on temperature, but dependant on time as well.

6.2.1   Failures Related to High Temperature

In order to be able to perform diagnosis, the failures to detect have to be known. Failures can occur in different locations of the magnetic bearing and some of them take place suddenly whereas other ones rise slowly in function of time [3]. The consequences on the AMB behaviour is different for each case, going from small changes compensated by the controller to critical faults that suddenly stop the AMB from working. In order to have an overview of the encountered cases, table 6.1 shows a summary of the failures related to high temperature.

Diagnosis implies to use sensors, and obviously at high temperature, the available sensor choice is very limited. Major points are considered; the coils aspect, the magnetic material properties, the position sensors and the rotor.

6.2.2   Coil Failure Diagnosis Example

Coil diagnosis is taken as example. The aim of this subsection is to estimate the coil number of turns. This one could change at high temperature due to insulation failures. Coil ageing is determined through

Location	Type of failure	Consequences
Actuator Coil	Oxidation of the conductor	Slow increase of electrical resistance
	Diffusion in wire	Slow increase of electrical resistance
	Short-circuits between turns	Inductance and electrical resistance changes
	Wire over heating	Wire breaks up
	Short-circuits between coils and stator, housing	Loss of inductivity
Soft Magnetic Alloy	Short-circuits in the insulations between the laminations	Eddy currents losses changes
	Creep or clearance	Mechanical contact between rotor and stator possible
	Modification of the saturation	Loss of magnetic force
	Modification of the permeability	Light change of AMB constant k
	Modification of the hysteresis losses	Heat and loss of controllability
	Mechanical properties modifications, elasticity	Eigen frequencies become lower
Position Sensors	Oxidation of the conductor	Slow increase of resistance, drift
	Diffusion of the conductor in the dielectric	Diminution of conductivity, drift
	Silver migration	Sensor noise
	Insulation failure	Decrease of inductance, noise
	Cracks in the ceramic substrate	Sudden sensor critical failure
Rotor	Modification of the rotor material flexibility	Decrease of the eigen frequency
	Retainer bearings degradation	Possible whirl in case of controller failure
	Rotor dilatation	Plastic deforming of the lamination, loss of magnetic properties

Table 6.1: Possible failures in high temperature magnetic bearings.

electrical resistance and inductance. Coil electrical resistance (equation 2.19) depends on the temperature and the section of the conductor. The wire section could change with phenomenon of oxidation and diffusion.

Current Ripples Technique

The change of inductance of the actuator coil can be estimated using the modulation of the control current with a high-frequency signal. The advantage of this method is that the sensing information is not coupled to the control signal. This approach is used in Self-sensing AMBs [39, 31, 32] and shows good results. Since an industrial AMB already uses a PWM amplifier, the modulation approach using this signal requires less additional hardware for its implementation. For these reasons, this diagnosis concentrates on the PWM modulation approach. Using this principle, the properties of the transducer could be used as well as an actuator and as a sensor.

The PWM frequency response depends on three parameters; the actuator inductance, rotor position and the PWM duty-cycle. To compensate the effect of duty-cycle changes, the voltage ripple is also measured and divides the demodulated current [16].

6.2.3   System Identification Procedure

System linear frequency response

The goal of this procedure is to obtain an estimation of the number of turns of the actuator coils in order to detect short circuits. This can be done of course only with measurable values, in our case the voltage U [V], the current i [A] and the rotor position x [m] (see figure 2.5 and 6.2). A basic model of the coil is

$$U = L\frac{di}{dt} + Ri \qquad (6.1)$$

The idea of the system identification is to fit the frequency response of the actuator with the model, in order to find the parameters L [H] and R [Ω]. This estimation induces the measurement of the voltage signal. The transfer function of the system is given by:

$$H = \frac{i}{U} = \frac{1}{Ls + R} \tag{6.2}$$

Replacing $\frac{L}{R}$ by τ, the relation 6.3 is obtained:

$$H = \frac{\frac{1}{R}}{\tau s + 1} = \frac{\frac{1}{\tau R}}{s + \frac{1}{\tau}} \tag{6.3}$$

This model is not valid when the rotor is moving. A way to take care of the velocity of the rotor is described in equation 6.4:

$$U = L\frac{di}{dt} + Ri + k_u\frac{dx}{dt} \tag{6.4}$$

To still be able to perform the parameter estimation, equation 6.4 is transformed into equation 6.5:

$$\tilde{U} = U - k_u\frac{dx}{dt} = L\frac{di}{dt} + Ri \tag{6.5}$$

From this point the same analysis is done for $\tilde{U}$ as for U, when the term $k_u\frac{dx}{dt} = 0$.

The transfer function of equation 6.2 is a first order linear system. The frequency of the PWM is above the cut off frequency of the system; a low pass filter in this case. It is not possible to estimate factor τ precisely. The way to solve this problem is to measure the resistance of the actuator coil and then set the static gain of the transfer function.

Once the inductance is known, the coil number of turns is estimated using the relation 6.7.

$$L = \frac{A\mu_0 N^2}{\left(2x_g + \frac{l_m}{\mu_r}\right)} \tag{6.6}$$

$$N = \sqrt{\frac{L\left(2x_g + \frac{l_m}{\mu_r}\right)}{A\mu_0}} \tag{6.7}$$
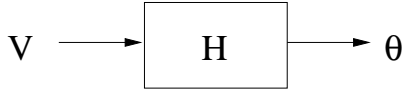
Figure 6.1: Single-input single-output linear system to analyse.

Frequency Response Estimation Using Stepped Sine

The proposed solution is to perform a system identification of the linear system by a frequency response estimation using stepped sine.

A single-input single-output linear system is analysed (figure), where the input (voltage) is:

$$V = \rho_1 \cos \omega t + \rho_2 \sin \omega t \tag{6.8}$$

and the resulted response is

$$\theta = \theta_1 \cos \omega t + \theta_2 \sin \omega t \tag{6.9}$$

The linear system can be described by means of its transfer function $H_a = |H|\, e^{j\phi}$, therefore, the output is related to the input V by:

$$\theta = |H|\, (\rho_1 \cos(\omega t + \phi) + \rho_2 \sin(\omega t + \phi)) \tag{6.10}$$

Or

$$\theta = |H|\, ((\rho_1 \cos \omega t + \rho_2 \sin \omega t) \cos \phi + (\rho_2 \cos \omega t - \rho_1 \sin \omega t) \sin \phi) \tag{6.11}$$

Making use of the identities, $H_R = |H| \cos \phi$, $H_I = |H| \sin \phi$, yields

$$\theta = (H_R \rho_1 + H_I \rho_2) \cos \omega t + (H_R \rho_2 - H_I \rho_1) \sin \omega t \tag{6.12}$$

Hence $\theta_1 = (H_R \rho_1 + H_I \rho_2)$ and $\theta_2 = (H_R \rho_2 - H_I \rho_1)$

Also:

$$\frac{\theta_1 - j\theta_2}{\rho_1 - j\rho_2} = H_R + jH_I \equiv H \qquad (6.13)$$

Estimation of the Inductance

The input voltage and current output are decomposed into Fourier series.

$$f(x) = \frac{1}{2}a_0 + \sum_{n=1}^{\infty}[a_n \cos(nx) + b_n \sin(nx)] \qquad (6.14)$$

The Fourier amplitudes a_n and b_n are obtained. Using equation 6.13, the transfer function of the system is estimated. In the simulation, good estimation is obtained for $n \geq 8$.

The estimated transfer function can be compared to the model transfer function (equation 6.3). This comparison has been done using a *MATLAB* analog filter least squares fit to frequency response data (*invfreqs*). The system physical values are so estimated.

6.2.4   Simulation

In order to develop a diagnosis procedure to detect failure in the actuator coils of a magnetic bearing, a simulator of an AMB actuator composed of a controller, amplifier, a pair of electromagnets and a punctual mass has been developed (Figure 2.6). The first aim of this simulator is to estimate the coil inductance. This will enable to detect short-circuits between turns inside the coil. A simulation has been programmed in *SIMULINK* to generate AMB data. This data is saved and analysed with a *MATLAB* algorithm in the frequency domain.

The AMB is simulated in closed-loop. The controller structure is shown in Figure 6.2. A PID controller tries to keep the rotor in the middle position between the two magnets. It delivers the current set points for each actuator from the rotor position. Each magnet is composed of a current controller, which measures the current in the coils and regulates the PWM duty cycle. The duty cycle is then transformed into PWM voltage thanks to the power amplifiers. Actuators generate the magnetic force and the rotor position is calculated. The coil inductance is calculated, and is given to the AMB actuators.
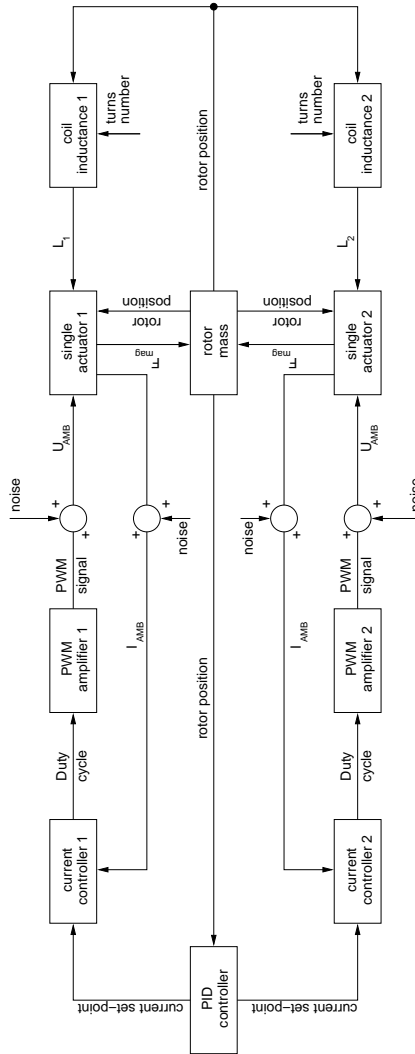
Figure 6.2: Schema of the simulator for generation of data for diagnostic purpose. A pair of magnets with rotor and controller are simulated.
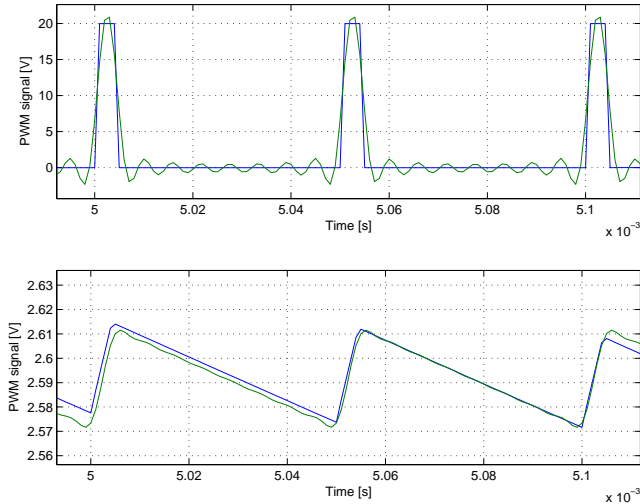
Figure 6.3: Estimation of PWM and AMB current signal with Fourier series for n=8.

The two magnets are modelled separately and without linearization. All the parameters can be modified in the simulation. The simulation generates the signals U_{AMB} and I_{AMB}, which are used for the system identification. Figure 6.3 shows the transformed simulated signals in Fourier series with the eight first harmonics. PWM frequency is 20 kHz and a minimum sampling frequency of 1 MHz is needed for an accurate estimation of the PWM. The Frequency response of the coil is given in figure 6.4. Since the PWM frequency is higher than the cut-off frequency of the actuator, the low frequency gain can not be estimated. The latter is set by using a measurement of the coil resistance. A recursive least square algorithm is able to filter a coil resistance measurement, with being fast enough to detect sudden changes of the resistance.

Matlab fitting function gives the estimated transfer function. The coil inductance is then estimated and the physical parameters, as the coil number of turns can be estimated. Figure 6.5 gives the coil number of turns estimation in function the length of the computed data. It can be seen that a sample length of 0.015s is needed to obtain an estimation with less than 2% error.

This procedure has shown a way to perform an estimation of a phys-

Figure 6.4: Frequency response of the coil.

Figure 6.5: Estimation of the coil number of turns in function of the sample length.

ical parameter of the AMB. The estimation has been done in the frequency domain, but could also be done in the time domain us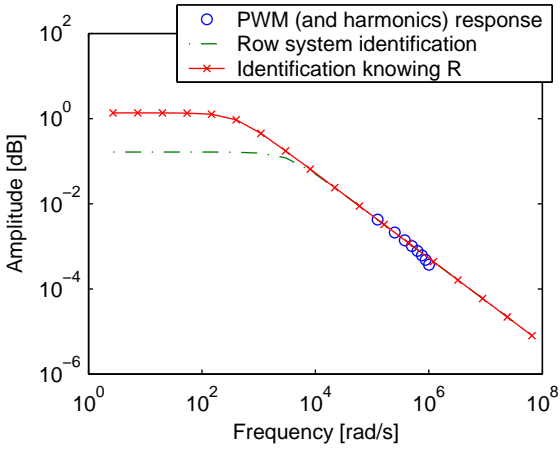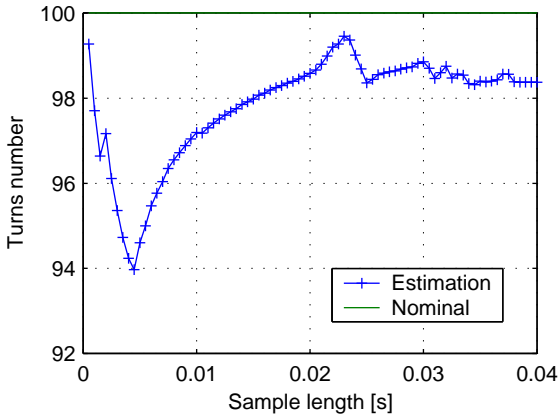ing for example observers. The PWM signal has been taken as high frequency excitation. In reality, many power amplifiers use three state PWM, which give too small current ripples for such a procedure. Nevertheless digital controller, due to their high modularity, are able to generate frequency signals at other frequencies. Redundant diagnosis, with several excitation frequencies is possible as well for a high accuracy.

6.3 Prognosis

Diagnosis of the system enables the prognosis of the changing characteristics in function of the time. With experience on magnetic bearing for high temperature applications, prognosis on the state of the system can be done. Obviously the more experience we get about a system, the more precise is the prognosis. Furthermore there are aging effects, which occur suddenly and others, which occur slowly.

Coil evolution is somewhat predictable for failures appearing slowly. If the conductor is nickel-clad copper, it's resistance can be estimated in function of temperature and time as shown in appendix B.

In the same way, magnetic properties of the soft magnetic alloy, using measurements as shown in subsection 3.2.2, can be predicted.

On the other hand, it is not trivial to get data corresponding exactly to the real working conditions, especially for aging effects.

6.4 Correction Strategies

According to diagnosis and prognosis, corrections strategies can be developed for the control of the AMB. Slow changing characteristics, can be compensated by a robust controller, or with an adaptive control.

Correction strategies can be based as well on redundant hardware. For aero-engine, six poles AMBs have been already developed [10, 17], with a switching controller able to keep the rotor levitating in case of failure.

Redundancy can be applied on the position sensors as well. The position sensors showed in this work (see chapter 4) are very suitable for such an application. Effectively their compactness and their low cost enable to put several of them in parallel and to switch off the channel giving meaningless response.

6.5 Outlook

A main feature of AMBs is related to their abilities of analysis and self-tuning. Effectively AMBs with their digital controllers, they can be used as a sensor, in order to monitor the system characteristics. In order to enable diagnosis a list of failures due to exposition at high temperature has been done. A plausible case of short-circuits between turns has then been studied. A procedure estimating the coil inductance has been developed, using system identification.

Diagnosis offers its full advantages of monitoring only when prognosis and corrections strategies are associated. These two last points have been briefly presented.

Chapter 7

Experimental Validation

This chapter is related to the construction and the measurements of a high temperature AMB rig. The manufacturing technologies and modelling tools presented in previous chapters find their application here. A test rig has been built and tested at ambient temperature from 25°C up to 550°C.

The following sections describe step by step how the test rig has been realized, with an accentuation on design solutions directly related to the high temperature problematics. This chapter ends with measurements characterising the behaviour of a high temperature magnetic bearing (section 7.3).

7.1 Test Rig General Characteristics

First, a description of the whole system is done. Its specifications are summarized in subsection 7.1.1. Secondly, in subsection 7.1.2, the configuration and arrangement of all the components needed for such a system is presented.

7.1.1 Global Specifications

In order to prove the feasibility of magnetic bearing working at high temperature for gas turbines application, a five degree-of-freedom

(DOF) active magnetic bearing has to be realized. Five DOFs means that the rotor is maintained in levitation along the three spacial translation directions and on two rotations. The last DOF, in order to get the six DOFs defining the position of a solid in a three dimensional coordinate system, is the rotor rotation. In standard AMB applications, the rotor rotation is actuated by an electrical motor integrated into the system. Obviously, in gas turbines the rotation is generated by the turbine. That is why a prototype actuating only five DOFs at high temperature has been realized.

In this work, the electrical drive and the AMB electronics stay in a room temperature environment. Temperature sensors have to be mounted in the system at several locations. Temperature monitoring has to be done on-line.

The target working temperature is 550°C. High temperature AMBs should prove their abilities to keep a rotor levitating with high rotational speeds; the target speed here is 15'000 rpm.

7.1.2   AMB Configuration

A magnetic bearing with five DOF has been realized. Figure 7.1 shows a general view of the AMB system. The rotor is supported with two radial bearings and a thrust bearing. Position sensors are positioned in the system along each rotor actuation direction. The whole system is shown on figure 7.2 with the opened furnace.

The rotor is maintained in levitation with a digital controller. The position is measured for each magnetic actuators and sent to the digital controller. The controller computes the position signal and gives a set point current to the amplifiers. The amplifiers thanks to an internal current control loop, supply the actuators.

Retainer bearings are used to avoid contact between rotor and stator when the rotor is not levitating or in case of controller failure. The retainer bearing 1, is able to retain the rotor axially and radially. The retainer bearing 2, retains the rotor radially. With this manner, the rotor is able to rotate inside the retainer bearings without contact with the actuators.

Since this system is a prototype, it is convenient to be able to open it easily in case of failure. For this purpose the axial bearing has been put at one rotor end. The axial bearing disk, as well as the retainer
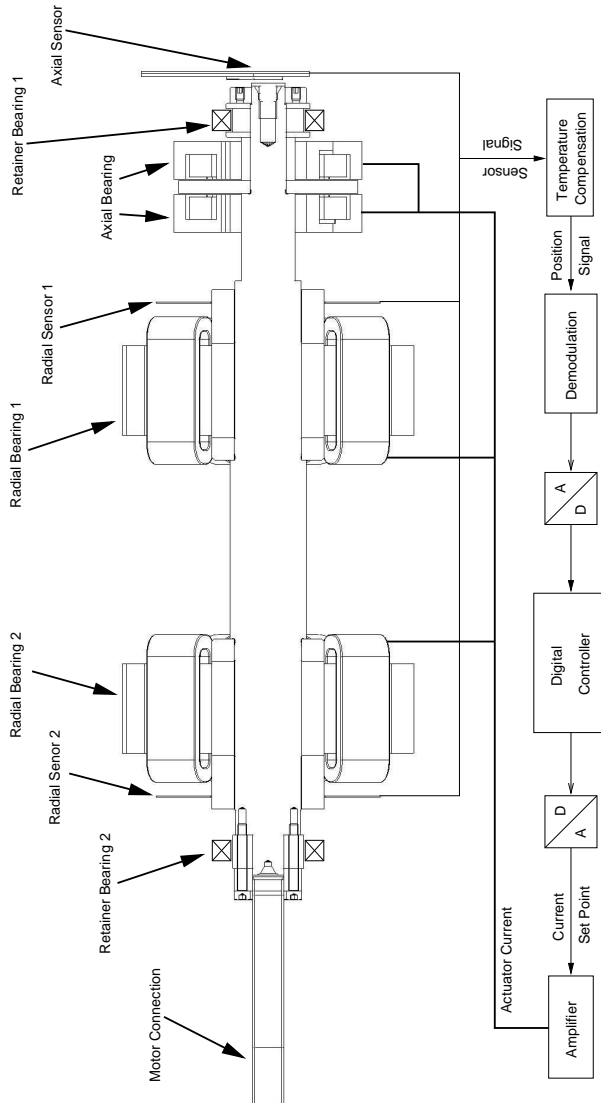
Figure 7.1: Configuration of a 5 DOF AMB for high temperature application.
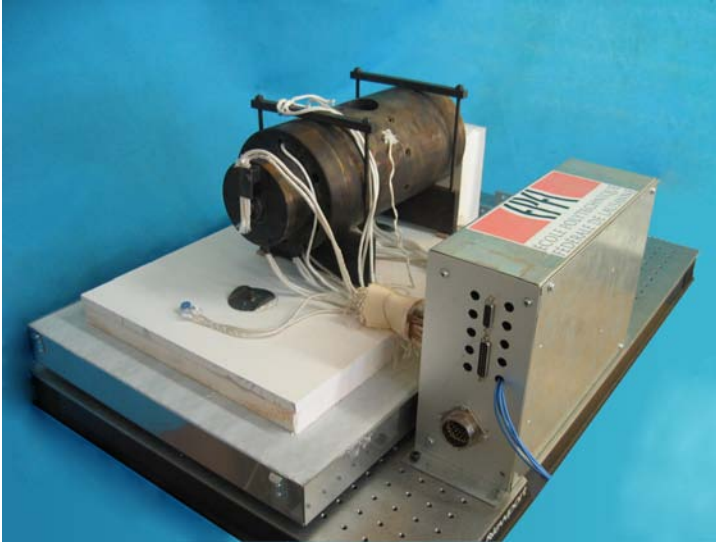
Figure 7.2: 5 DOF high temperature AMB.

bearing 1 are held on the rotor with a lock nut and can be easily removed. The rotor can then be removed from both sides, without disassembling the radial bearings.

Since the electrical drive is located outside the furnace, the drive shaft has to go through the furnace insulation. This arrangement has to be realized with the lowest heat conduction through the shaft. For this purpose, an hollow tube with thin walls has been connected to the main shaft.

The high temperature environment is generated by a furnace. Figure 7.3 shows an overview of the AMB, the motor and the furnace. The AMB is mounted in a housing (section 7.2.6), and fastened inside the furnace. Information about the furnace is given in section 7.2.7. The electrical motor is connected to the rotor with a flexible coupling[1].

---

[1]BDS-Thomas miniature coupling
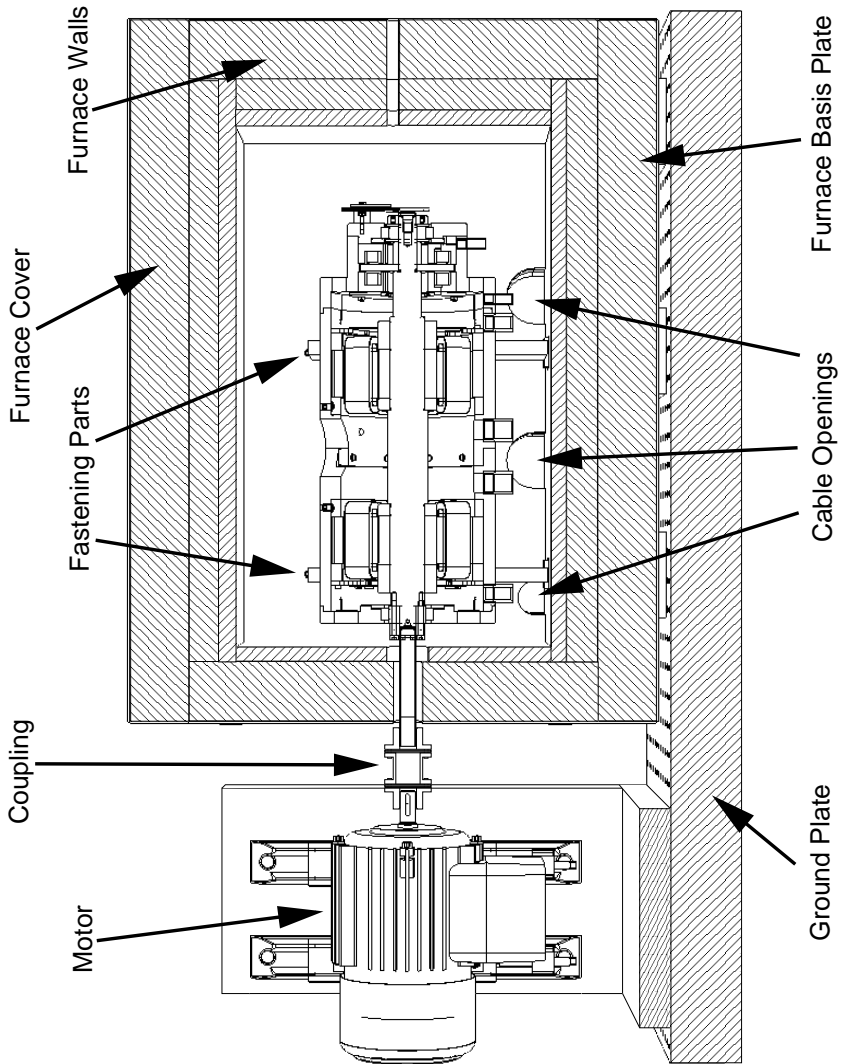
Figure 7.3: 5 DOF AMB with furnace and motor.

7.2   High Temperature AMB Components

This section describes the particularities and the solutions chosen for the realization of the high temperature magnetic bearing components.

7.2.1   Radial Actuators

The present radial actuators are based on stator of insulated sheets and removable coils wound on coil holders. Both radial bearings are four poles (NS-SN-NS-SN) stators. They have been realized with 0.35 mm laminated AFK502. The stator lamination is hold between two screwed rings.

Coil Holders

Actuator coils have been wound on coil holders. The choice has been done to be able to remove the coils easily, and to keep the stator in place. The coil holders have been made with Micanit plates and Stumatit rounded parts as shown on figure 7.4. Their assembly is self stable and the parts are maintained together without screws or glue. Made of ceramic, they insure a reliable electrical insulation between windings and stator, and low Eddy currents losses.

Windings

Two different types of wire have been selected for the actuator windings: silver wire with mica insulation (figure 7.5) and Thermocoax (see subsection 3.3.2) wire (figure 7.6). The choices of wires and insulations have been done for the following reasons.

First, silver wire has an excellent conduction and is quite stable at high temperature. On the other hand, this wire suffers of the instability of silver at high temperature. Silver migration and evaporation are on the other hand possible failure sources. The mica insulation is relatively thin, easy to handle and is a good insulator. Once sintered it is breakable, and can suffer from the system vibrations and from thermal cycles. With this solution a fill-factor of 0.64 can be achieved. It has to be tested in order to get experience on its performances in real applications.
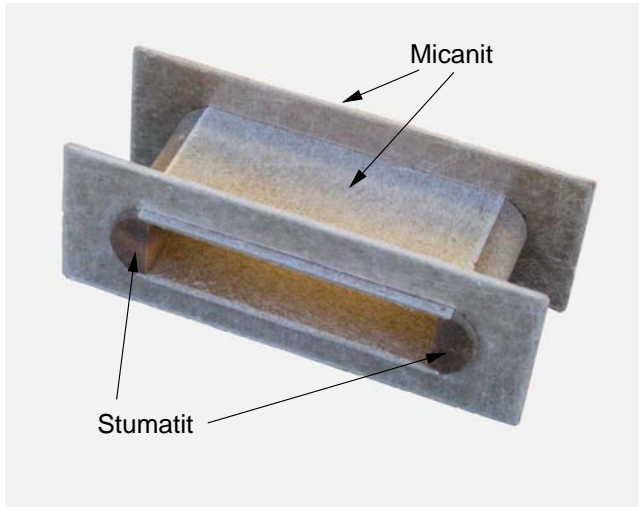
Figure 7.4: Coil former made of Micanit (flat parts) and Stumatit (rounded parts). The structure does not need glue to hold together.

Figure 7.5: Radial bearing with silver wire and mica insulation.

Figure 7.6: Radial bearing with Thermocoax wire.

Secondly, Thermocoax has the advantages of being a product commercially available, and developed for high temperature applications. Despite of a low fill-factor of 0.42, it is an interesting candidate because of its reliability. This wire is guaranteed to work several month continuously at 700°C and a maximum temperature of 800°C can be achieved. The stainless steel tube is a source of eddy current losses. Nevertheless, its surface oxidize at high temperature, which produces kind of surface electrical insulation. The losses are by this way reduced during operation.

No internal connections between coil wires have been done. That means that the pair of coils of each actuator pole is wound with a single wire. This ensure perfect conductivity and avoid local hot spots or material diffusion. It would be for example difficult to connect two Thermocoax wires together, because the stainless steel protection has to be cut and the protection against oxidation would be locally lost.

Bearing Characteristics

Both radial bearings do have exactly the same stator laminations. Their characteristics are the following:

- Internal diameter: 50.8 mm

- External diameter: 130 mm

- Bearing length: 40 mm

- Magnetic flux cross section A_a: 400 mm^2

- Nominal air gap s_0: 0.4 mm

The characteristics, which are different between the bearings 1 and 2 are summarized in table 7.1.

	Silver coils	Thermocoax coils
Conductor diameter	0.8 mm	1.3 mm
Insulation thickness	0.05 mm	0.3 mm
Number of windings	100	32
Maximum current	6 A	12 A
Maximum voltage	50 V	50 V
Nominal maximum force	1000 N	408 N

Table 7.1: Characteristics changing between actuator 1 and 2.

Radial Bearing Centering

Since the thermal expansion of the FeCo stator laminations (λ_{FeCo}=9.8·10^{-6} K^{-1}) is smaller than the one of the housing (Hastelloy X, λ_{Hast}=15.2·10^{-6} K^{-1}, see section 7.2.6), a diametrical bearing clearance between housing and stator ($\sim$0.37 mm) appears at 550°C.

The way to guarantee centering, or at least mechanical stability of the system, is to clamp the laminations between two rings having the same thermal expansion coefficient as the housing (figure 7.7). The laminations have to be pressed axially sufficiently strong, in order to produce friction force. By this way no lamination can move in the radial direction due to the AMB force.

The screws, which maintains the two stator rings together, should have the same thermal expansion as the laminations. They have to insure the minimum sheet friction force independent of the temperature.
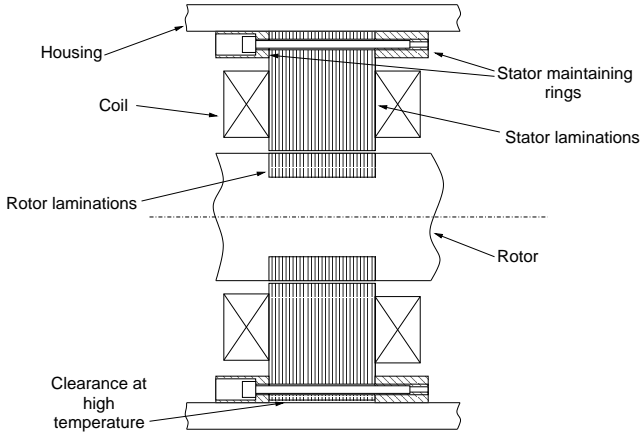
Figure 7.7: Radial bearing lamination fastening principle.

Standard stainless steel screws have a thermal expansion coefficient of $18 \cdot 10^{-6} \ K^{-1}$ at 550°C. Only special screws are fulfilling these specifications, for example Fe/Cr12.5 screws ($12 \cdot 10^{-6} \ K^{-1}$). With sufficient preload applied at room temperature, the load at high temperature is still high enough. Screws of this material are not available for small quantity. The chosen solution are nickel-plated standard steel screws, which have a thermal coefficient of $13 \cdot 10^{-6} \ K^{-1}$.

7.2.2   Axial Bearing

An axial bearing for high temperature application has been developed. A schematic view is shown on figure 7.8. Two identical actuators pull a soft magnetic disk of AFK502 mounted on the rotor. The axial bearing has been realized with a solid core of AFK502 and Thermocoax wire. The winding holds inside the core thanks to an insulated Ni-clad Cu wire bound around it. One of these actuators is shown in figure 7.9.

The axial bearing characteristics are:

- Internal diameter: 36 mm

- External diameter: 80 mm

- Actuator length: 17 mm

Figure 7.8: Axial bearing schematic overview

Figure 7.9: Axial bearing actuator. The soft magnetic core is made of solid FeCo. The winding has been realized with Thermocoax.

- Magnetic flux cross section: 791 mm^2

- Nominal air gap: 0.4 mm

- Number of windings: 42

- Maximum current: 6 A

- Maximum voltage: 50 V

- Nominal maximum force: 87 N

7.2.3   Position Sensor Fasteners

This section is related to the utilization of the thick-film position sensors presented in chapter 4. Obviously ceramic and metals do have very different thermal expansion. Here is presented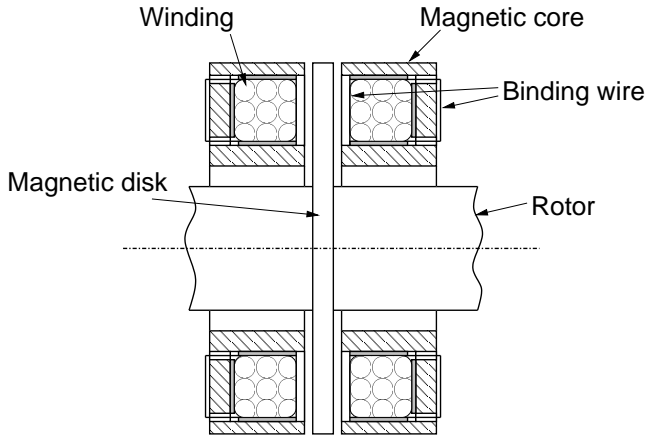 how the radial position sensors are mounted and kept centered in the system by compensating the thermal expansion differences.

Radial Position Sensor Centering Fasteners

Thermal expansion at 550°C of the sensor alumina substrate is $7 \cdot 10^{-6}$ K^{-1}, which is much smaller than the one of Hastelloy X ($15.2 \cdot 10^{-6}$ K^{-1}). There is also a thermal expansion difference of 0.45 mm between the sensor external diameter and the housing at 550°C.

An elastic structure, which compensates the thermal expansion and keeps the sensor centered in the housing has been realized. The system symmetry is the key point of this structure. This compliant support is composed of four fingers pulling on the sensor sides along four orthogonal directions (figure 7.10). The pushing force has to be low in order to keep low stress on the sensor substrate and to avoid cracks in the ceramic. It is 6 N at room temperature and 2.7 N at 550°C. Long fingers are used in order to reduce the difference of pushing force between room temperature and 550°C (figure 7.11).

Since the structure is elastic, its resonance frequency has to be high enough in order to be not excited by the rotor rotation. It has been designed to be at 400 Hz for each single finger, which is sufficient for the present application (max. rotation speed is 250 Hz). Since the fingers push in four different directions, the eigenfrequency of the whole
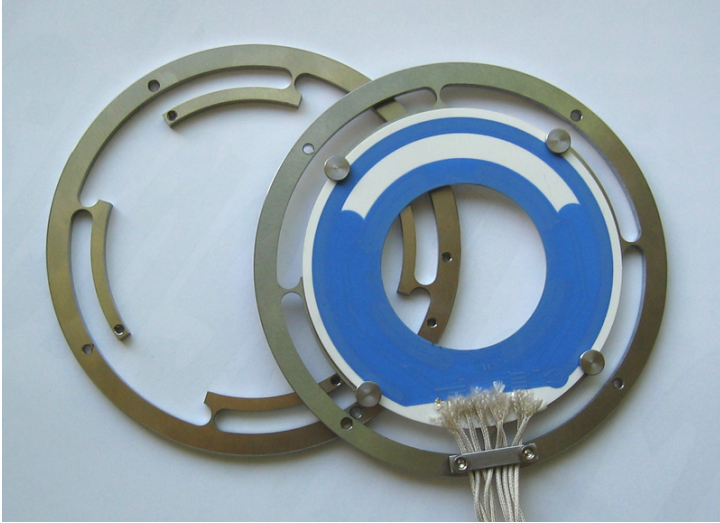
Figure 7.10: Sensor holder for thermal expansion compensation, with and without position sensor
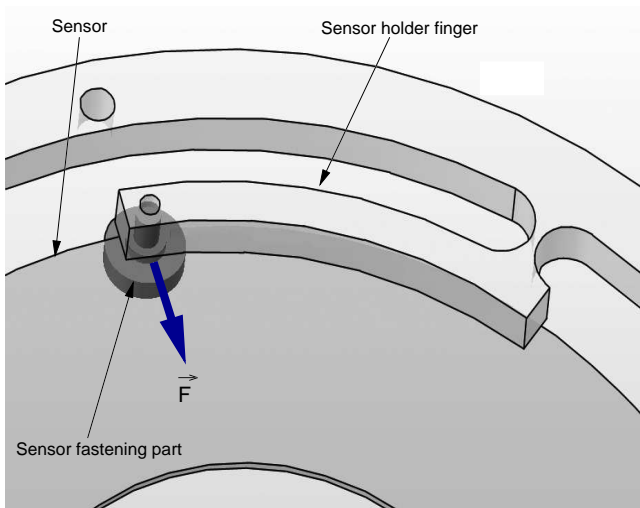

Figure 7.11: Position sensor positioning parts

system is much higher. The sensor rotation due to finger movements is negligible and does not affect the whole system behaviour.

Optimizations of this design are possible. The eigen frequency can be increased, for example by reducing the finger mass. The geometry used here is actually not advantageous. The structure deformation is done at a localised point and it concentrates the strains in a small material volume. An optimized design geometry should distribute the strain inside the whole finger length in order to prevent creep at high temperature.

Ceramic Substrate Positioning Parts

Four notches have been cut on the external part of the ceramic substrates in order to position the fastening parts (figure 4.6). The concave shape of the notches enables a precise positioning, with however moderate surface stress on the contact point.

Axially, the sensor is held with static friction force. Its stroke is limited by the screw length, which is a bit longer than the sensor thickness. The axial fixation can be improved by using elastic devices.

Position Sensor Wires

On the sensor holder, a clamper is screwed and maintains the sensor electrical wires. A good wire fixation is important to avoid mechanical stress on the weldings. Clamper and sensor holder are recovered with a mica plate in order to insure a reliable electrical insulation.

7.2.4   Rotor

The rotor designed here is based on a subcritical Hastelloy X shaft. 0.35 mm AFK502 ceramic insulated laminations have been used for the radial bearings. The axial bearing is realized with a solid AFK502 disk. The whole rotor assembly is represented on Figure 7.12.

A rotor prolongation, consisting of a tube, has the purpose of connecting an electrical motor from outside the furnace and driving the rotor. This rotor part has to have the lowest cross section as possible in order to minimize the heat transfer from hot to cold temperature.

Figure 7.12: Rotor for high temperature AMB.

Rotor Shrinking

In standard AMB designs, rotor laminations for radial bearings are shrunk on the shaft. The thermal expansion of the shaft (Hastelloy X, $15.2 \cdot 10^{-6}$ K^{-1}) is larger the one of AFK502 ($9.8 \cdot 10^{-6}$ K^{-1}). Shrinking the rotor laminations how it is done generally, would lead to plastic deformation of the laminations. That would lead to lower magnetic properties and a clearance between shaft and lamination will appear after cooling down.

Lamination stress has to be kept below 200 MPa (see subsection 3.2.2) at 550°C and at a rotor rotation speed of 15'000 RPM (250 Hz). The way to do that is to have a clearance between the shaft and the laminations at room temperature. The lamination internal diameter has to be 70 ± 10 μm larger than the rotor diameter (30 mm). Narrow mechanical tolerances (± 10 μm) are necessary to stay below the maximum stress and to avoid clearance at 550°C.

Despite the clearance at room temperature between rotor and laminations, the last one can not move. The laminations holds between two Hastelloy X shrunken rings. In order that the laminations hold together without moving at room temperature an axial load of 10'000 N (7.96 MPa) has been applied on the maintaining rings during the shrinking. Furthermore, the laminations are not perfectly flat, which gives a certain elasticity to the lamination stack. That is why in practice there is an (undefined) axial load keeping the stack in place at any temperature.

Axial Bearing Disk Fixation

The axial soft magnetic disk is made of solid AFK502. It is removable in order to be able to dismount the system easily in case of failure.
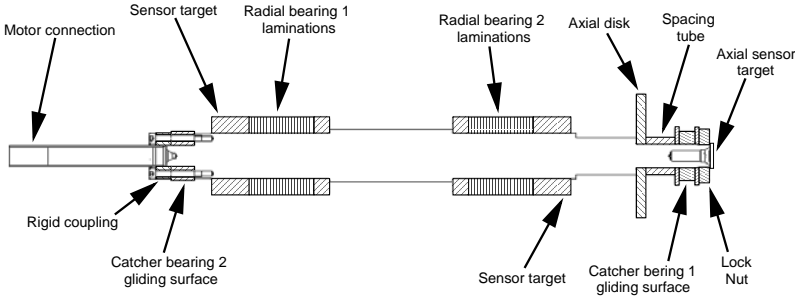
Figure 7.13: High temperature AMB rotor.

For that purpose the axial disk as well as the retainer bearing 1 (figure 7.13) are fastened with a lock nut.

Rotor Physical Characteristics

The rotor mass is 4 kg. Its Length is 454 mm (352 mm without motor connection). The rotor diameter at the radial bearing locations is 50 mm. The axial disk has a diameter of 80 mm.

Using a finite element model, the resonance frequencies have been calculated. Since the maximum rotation frequency is 250 Hz, the rotor's first bending mode has to be over this frequency.

Figure 7.14 shows the eigen forms of the two first bending modes. The calculated frequency for the first bending mode is 403 Hz, the second one is located at 818 Hz. Rotor balancing is possible by adding weights at both rotor ends.

7.2.5   Retainer Bearings

Retainer bearings are used in magnetic bearings to catch the rotor if the rotor is suddenly no more levitating. Fumagalli [13] and Orth [33, 34] show modeling and experimentation of the behaviour of a rotating rotor falling down on retainer bearings.

Usually ball bearings are used for this purpose. Unfortunately there are no ball bearings available for applications at 550˚C.
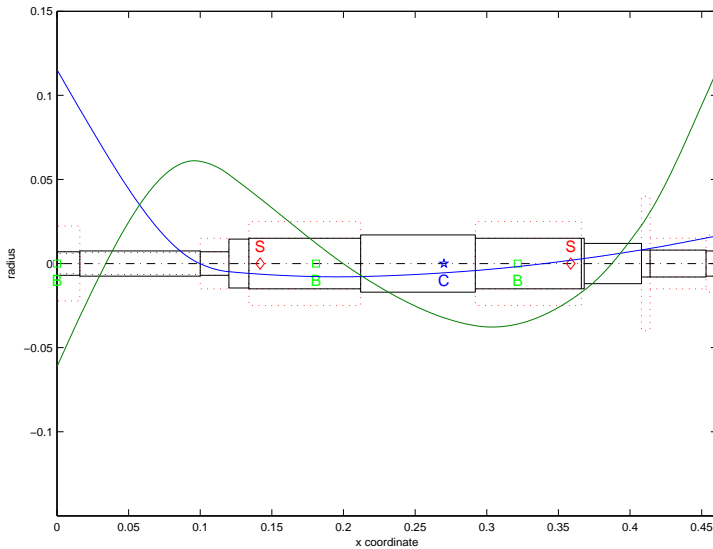
Figure 7.14: Eigen modes of the high temperature rotor at 550°C with motor connection and coupling.

Solution Used in the Prototype

The retainer bearing 1 (figure 7.13) is a slide bearing and is composed of three parts; a cylinder and two disks. The cylinder has been designed to carry the radial forces in case of radial bearing failure. The radial nominal air gap is 0.25 mm for both radial retainer bearings.

The two disks are located on each sides of the cylinder. They carry the axial force in case of axial bearing failure by touching the retainer bearing sides. The nominal air gap in the axial retainer bearings is 0.25 mm.

These parts are easily removable. It is also possible to change the sliding surfaces without having to change the whole rotor.

Because of its hardness of 80-200 Brinell, Hastelloy X is to soft to fulfill the task of gliding bearing. Furthermore after several working hours at high temperature, the surface oxidizes and the friction coefficient becomes quite high. No good sliding properties are then guaranteed.

Figure 7.15: Housing separate parts.

Possible Alternatives

In order to be able to do load sharing tests, other alternatives have to be found. A major problem is to keep the friction losses as low as possible, and thus being able to dissipate the heat produced by the friction.

The used gliding bearing could be improved by treating the sliding surfaces. A way to do that is to spray a hard material (Co-Mo-Cr-Si powder, Ni-Cr-Al powder) on the gliding surfaces. This treatment reduces the friction coefficient and improves the life span. However, for cost and time reasons, no test has been performed with this solution.

7.2.6   Housing

The housing has been designed to hold the two radial AMBs, the axial AMB and the two retainer bearings. It consists of a tube, where the AMB components are inserted. It has been realized with five Hastelloy X parts, as shown on figure 7.15. Each part receives a separate component of the magnetic bearing. The radial bearings are

kept centered in the big tubes, as explained in subsection 7.2.1. Both parts of the axial bearing are inserted in the tube with the smaller diameter. The retainer bearings are mounted in the two disks, which close the housing.

Cable Anchorage

In common AMB systems, there are many cables to connect from the actuators and from the sensors to the amplifying electronic. The problem is not trivial at high temperature, because the cables are difficult to handle and because there are only few possibilities to anchor the cables. Clampers have been used to guide the wires from the actuators to the housing outputs and as relief of traction.

High temperature wires are not so flexible as common cables, furthermore the insulation are quite damageable. However the wires have to pass through the housing. Since it is hardly possible to reeve the cable through a hole, the problem has been solved by making slots from the housing edges to the holes. The wires can be bent through the slots into the holes, without having to reeve them. Finally a screwed tube maintains the wires in position and avoids insulation damage.

7.2.7   Furnace

A special furnace has been developed for this test rig. The furnace has to be big enough for the AMB. The motor drive shaft, cables and measuring devices require holes in the furnace side at specific locations. The furnace specifications are the following.

Specifications

- Maximum temperature: 700˚C.

- Furnace outside wall maximum temperature: 70˚C.

- Time to reach the maximum temperature: one hour.

- Holes are foreseen to pass the AMB electrical cables through.

- Since the motor drive is external, a hole is foreseen for the motor drive shaft.

- Force measurements require a hole in the wall at the rotor height.

- Realized in three parts, it can be opened without disassembling the test rig.

- Low thermal conduction of the fastening parts, ensuring minimum thermal losses.

Construction

The furnace has been realized in three parts, a basis plate, a part including the walls and the cover. Figure 7.3 shows a section of the furnace. It can be opened with the cover. Furthermore, when a comfortable space around the AMB is needed, the furnace walls can be removed without disconnecting any other device. For this purpose the wall part located under the motor connection is interdependent to the furnace base plate.

Four heating elements are located at the bottom of a wall side. They deliver a heating power of 2500 W. A temperature controller linked to a temperature sensor enable a precise temperature control.

AMB Fastening Elements

The aim of the fastening elements is to provide a good fixation with however a low thermal conduction.

The AMB is posed on four ceramic (Stumatit) feet. Their maximum continuous working temperature is 1400˚C. They have good mechanical properties, especially in compression with as E module: 800 MPa. With their low thermal conduction ($2.1\text{-}2.2{\cdot}10^{-6}\ K^{-1}$) and a cross section of $6.25{\cdot}10^{-4}\ m^2$ for 95 mm length, the feet give a high thermal insulation. They have been manufactured with a hole, in order to receive a threaded rod. The AMB is by this manner screwed on the base plate. This combination of ceramic and steel provides high compression and pulling stiffness, with low thermal conduction.

7.3   Experimental Results

This section presents measurements done with the AMB. They have been done from room temperature up to 550˚C. This section is divided

in two subsections. The first with static measurements, and the second with dynamic ones.

7.3.1   Static Force Measurements

The goal of the static measurements is to compare the current-force relation of the AMB with the simulation. There are not many possibilities to measure the force at high temperature. Several methods have been developed for this purpose, for example by using a load cell [1]. Unfortunately none of these sensors are available for high temperature applications. Other methods have to be found.

The measurements have been done by pulling the rotor with a cable. This method has been already used for high temperature bearing characterization [19]. Holes in the housing and in the furnace wall enable to pull from a room temperature environment. The cable has been attached in the middle of both radial bearings. The pulling force direction was horizontal and perpendicular to the rotor rotation axis. The force has been measured with a dynamometer. Since the application point of the force is in the center of the two radial bearing and the force direction has an angle of $\pm 45°$ with the actuators, the measured force has been divided by the factor $2\sqrt{2}$ in order to get the force of a single actuator. The current has been measured by the AMB power amplifiers current sensors.

Measurements have been performed during rotor levitation. The force could not be measured up to saturation, because the system became unstable before. Measurements done at $25°$C and at $300°$ are shown in figure 7.16 and compared with the simulation. The measurements have been done for three rotor positions, which are $x = 0.1$ mm, $x = 0$ and $x = -0.1$ mm. The bias current was 2.3 A, which is much below half of the maximum current. This implies that the force-current relation is not linear. However two conclusions can be done: First the measured force coincide quite well with the simulation. Secondly, the static force does not depend on the temperature.

7.3.2   Dynamic Measurements

The frequency response of the system has been measured at all temperature, in order to study the dynamic system behaviour.
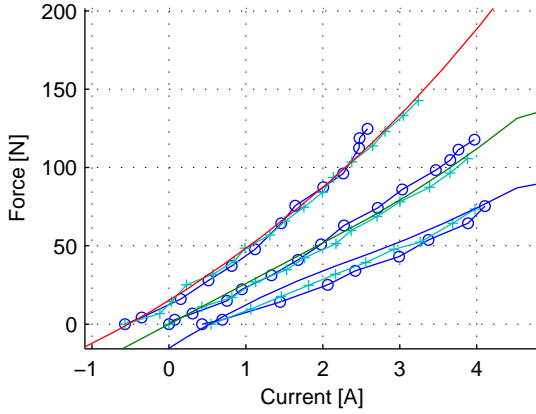
Figure 7.16: Comparison between simulation and measured force of the radial bearing with Thermocoax wire at 25˚C (circles) and at 300˚C (crosses), for the nominal positions: $x = 0.1$ mm, $x = 0$ mm and $x = -0.1$ mm.
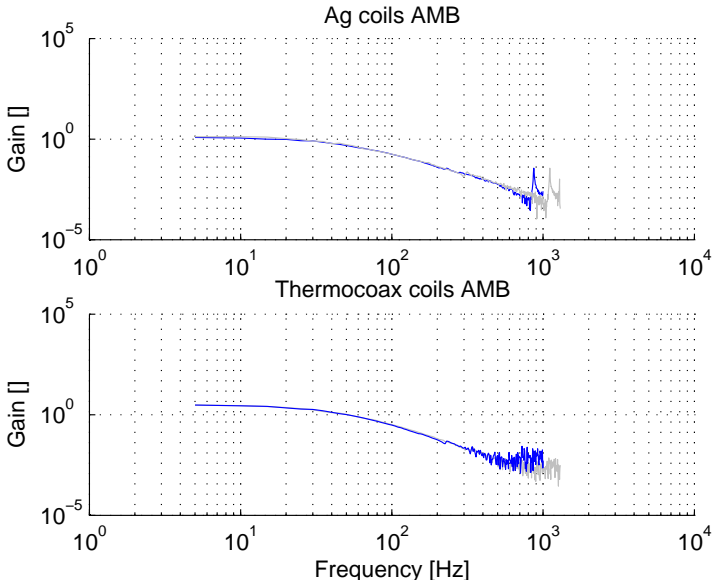
Figure 7.17: Plant frequency response at 550˚C (dark line) and at 25˚C (bright line) of both radial bearings.
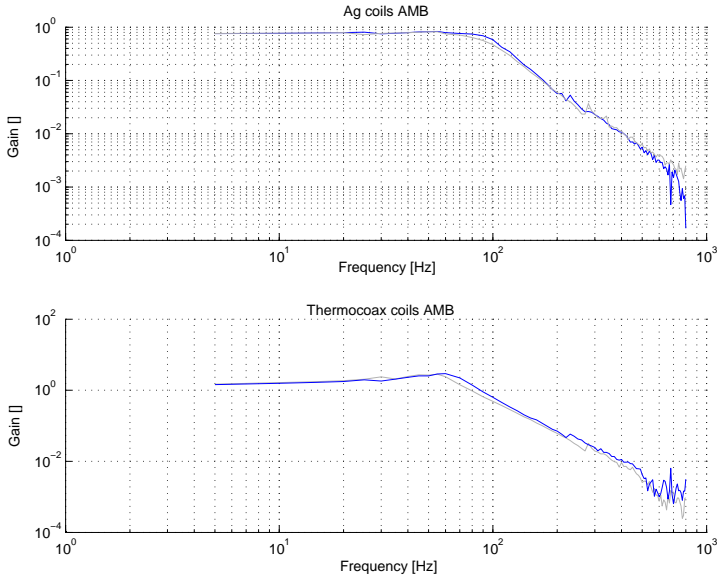
Figure 7.18: Closed loop frequency response at 550°C (dark line) and at 25°C (bright line) of both radial bearings.

The frequency response of the plant is shown in figure 7.17. The plant response is defined as the frequency response of the rotor position over the actuator current. The figure shows on the top part the plant response of the Ag coils AMB and on the bottom part the measurements for the Thermocoax AMB. The dark and bright lines are measurements done at 550°C and 25°C respectively.

The behaviour of the electro-mechanical system is quite stable with respect to the temperature. The first bending mode for the rotor without motor connection has been calculated at 646 Hz and 602 Hz for room and high temperature respectively. The first bending mode is measured at 870Hz at high temperature. This difference is due to the fact that in the simulation, the lamination stack is defined as a mass element without stiffness added to the rotor. Since the laminations have been axially preloaded, the resultant stiffness is higher.

The closed-loop response of the system is given here as well. This is the behaviour of the whole system including control and electromagnetic system. Figure 7.18 show the measurements, in dark and bright at
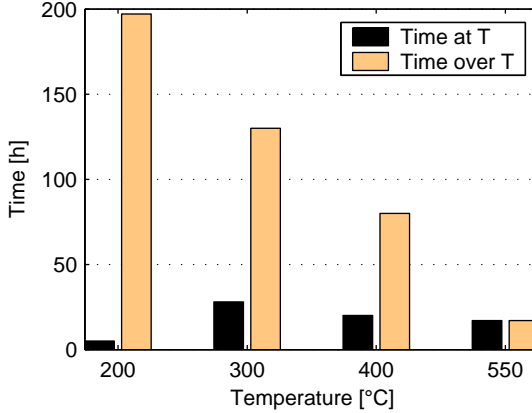
Figure 7.19: Current exposition time of the AMB prototype at high temperature.

550°C and 25°C respectively for both bearings. The temperature do not influence the whole system behaviour as well.

These measurements show that the system is able to levitate at high temperature. The current amplifiers are able to deliver an accurate current independently of the actuator coils resistances.

It is important to notice that the position sensors have been recalibrated during the heating phase. A position offset of only 60 μm has been measured between 25°C and 550°C in the worst case.

7.3.3   Long Term Measurements

The high temperature test rig did five complete thermal cycles from room temperature up to 550°C. Figure 7.19 shows the history of the temperature exposure. Measurements have been performed at defined temperature. Quite a long time is needed to get a stabilized temperature in the whole system after heating or cooling phases. The times at stabilized temperature are represented in black. The bright bars show the duration where the system temperature was over or equal at the given temperature.

The system operated seventeen hours at 550°C, and no electro-magnetic properties have changed so far. It is interesting to notice that for only

seventeen hours at 550°C, the system has been about 200 hours over 200°C. This last temperature is actually about the maximum temperature, at which a standard system can be exposed without degradation.

In order to get a meaningful information about system aging, tests should be performed during several thousands of hours. Unfortunately, due to problems of silver electro-migration on the sensor substrates, levitation has been possible only for a short time (about one hour) at high temperature.

However the AMB should not show important aging effects during the first thousand hours. For evaluating this, force measurements and the frequency response of the system should be studied in function of time.

Assumptions on the AMB behaviour with aging are the following. In a first period, the Thermocoax wire should show a bit less eddy current losses. Effectively, the stainless steel shielding before the first heating cycle has a conductive surface. After some time at high temperature, the stainless steel surface oxidizes, and so an insulating layer appears. The stainless steel windings are then no more connected between each other, which tends to decrease the eddy current losses.

In a second period, the magnetic saturation of the magnetic alloy will decrease. Slow changes of the AMB characteristics when the control current is maximum will be observed, especially in case of magnetically decentered rotor.

Due to a decreasing permeability of the magnetic material, small changes of the AMB constant k_i and k_s could be observed after a long exposure duration.

7.4   Summary

Thanks to the research and tests presented in chapter 3, an active magnetic bearing with five degrees of freedom has been manufactured. A general view of the whole system including AMB, furnace and motor has been presented.

Each separate system component has been described. The construction difficulties related to the high temperature aspects were presented. Solutions have been chosen for a real system and construction

details given. Dealing with thermal expansion differences between different materials is the key point of such a system.

The rotor has been kept levitating from room up to 550°C furnace temperature. Measurements have been performed, which prove that the AMB still levitates at such an environmental temperature.

Due to silver migration problems of the sensors, there was no time to perform long term measurements. Unfortunately no rotation tests could be presented in this work. However 15'000 RPM rotation is not such a high speed for an AMB and should not be critical to reach. Tests are planned for the future.

Chapter 8

Conclusion

8.1   Summary

This thesis decribed the way a high temperature active magnetic bearing system has been realized. The needs of developing such a system have been shown. Aero industry and all gas turbines need technical solutions to improve its profitability. A way to do that is to improve the aero-engine by replacing the ball bearings by AMBs working at high temperature. A literature survey has been presented, which has shown research in the same field led by other laboratories.

The working principle of AMBs have then been presented. The main features of AMB theory have been taken in review, and the most important equations for AMB design have been given.

This report has continued with the design aspects related to high temperature applications. This chapter (3) has shown the ground research necessary to build high temperature electro-mechanical systems. A survey of the available materials has been done, giving their advantages, disadvantages and limitations.

Materials for high temperature applications are often limited in life span. The properties of high temperature systems depend not only on the working temperature, but strongly on the working time as well. Several long term measurements were performed during this work and are available in chapter 3.

AMB controllers need an information about the rotor position in order to control the actuators. For this purpose, eddy current position sensors for high temperature applications have been developed. They are made of silver coils printed on ceramic substrates. Tests done up to 600˚C have shown their high performances.

Since the AMB performances are highly limited by the temperature rise, a high temperature thermal model has been implemented. This model has been validated with tests done on a radial AMB at high temperature.

A survey of the failures, which can occur due to high temperature exposure, has been done. The notion of diagnosis has been introduced. A way to detect modification of the coil inductance has been presented.

The knowledge acquired in the whole work has found its application in the design of a prototype. The construction of this AMB has been shown, with explanations of the manufacturing details related to high temperature. Finally, tests have shown that AMBs are still able to levitate at 550˚C.

8.2   Outlook

The task of building an AMB working at high temperature is quite ambitious. AMBs are actually pure mechatronic systems. They are based on three very different domains: electro-mechanic, electronic and control. The development of a high temperature electro-mechanical systems requires further knowledge, especially in the field of advanced materials and manufacturing technologies.

Developing a system for high temperature is not done as it is usually done for room temperature systems. Before a component can be put into a system, it has to be certified to survive at high temperature. This research field is relatively new and few data about the materials are available. High temperature applications are very specific, and the working conditions play quite an important role on the material behaviour. The time is another very important parameter and temperature cycles are relevant as well. For all these reasons, it is hardly possible to acquire material data for high temperature application.

Basic research on the materials with the most realistic working conditions are needed. Development of materials with high performance

and high life span should be continued. Experience on real system applications has to be acquired, and by this way new material specifications could be set. Such iterative developments have still to be done in this field. Unfortunately, this testing is very time consuming and expensive.

However, thanks to the know-how of material properties acquired during this research, a complete system has been built. This system has proven that AMB can still levitate at $550°$C. Unfortunately, sensor signal noise appears after a short time and levitation has not been possible anymore. It is a bit frustrating not to be able to prove that the rotor could levitate at least for thousand hours at $550°$C. Instead of using the time to study the AMB behaviour after a long exposure time at high temperature, basic research on silver diffusion on ceramic substrate had to be carried out.

Silver diffusion is actually not a new phenomena. Its effects has been studied, more often at room temperature under humid working conditions and with different voltages. The effect of silver diffusion has not been considered during the conception phase. When the technology has been tested at high temperature in the previous design stage, the actual working conditions were not met to activate the electromigration process. Finally, further tests have shown that the position sensors are able to operate at least seven hundred hours at $600°$C.

Failures such as short-circuits due to silver migration show the importance of system diagnosis. Monitoring the state of a system having components with limited life span is important for safety reasons. Diagnosis can have other benefits. The reliability can be improved with the use of correction strategies. For the sensor case, it is imaginable to put several sensors in parallel in order to create redundancy. Only one sensor would be supplied with current, thus only one sensor would suffer from silver migration. It would be possible, in case of failure, to switch to another sensor, which has not been under voltage. This correction strategy would give a life span twice longer on the global position sensing device.

The work for a next future is to test the present solution, and study more precisely the effect of the temperature on the system behaviour. Rotation tests have to be carried out. Magnetic materials with stable characteristics in function of time have to be developed and tested magnetically and mechanically. The fill factor of coil conductive material can be improved. A trade-off between reliability and performance has to be found.

Thermal measurements have to be done as well. The heat sources
have to be characterized precisely in function of temperature, rotation
speed and time. The thermal modelling has to be improved by this
way, and finally a design approaching the limit of each component
could be done. Power electronic adapted to the actuators has to be
designed. Due to relatively thick insulation of the winding wires, high
currents give better performance. A new sensor design could easily
avoid silver migration between the connections. Once having all these
elements put together, control, diagnosis, prognosis and correction
strategies have to be developed and tested on real systems under real
conditions.

Appendix A

Properties of Metals

Metal	Relative Conductiv-ity[1]	Temperature Coefficient of Resistance[2]	Tensile Strength (lbs./sq. in.)	Composition of Earth's Crust (% by Weight)
Aluminum (2S; pure)	59	0.0039	30	8.1
Aluminum (alloys):				
Soft-annealed	45-50	-	-	-
Heat-treated	30-45	-	-	-
Brass	28	0.002-0.007	70	-
Cadmium	19	0.0038	-	0.0001
Chromium	55	-	-	0.02
Climax	1.83	0.0007	150	-
Cobalt	16.3	0.0033	-	0.002
Constantin	3.24	0.00001	120	-
Copper:				
Hard drawn	89.5	0.00382	60	-
Annealed	100	0.00393	30	0.007
Gold	65	0.0034	20	0.0000005
Iron:				
Pure	17.7	0.005	-	5.0
Cast	2-12	-	-	-
Wrought	11.4	-	-	-
Lead	7	0.0039	3	0.002
Magnesium	-	0.004	33	2.1

---

[1]At 20º Celsius, based on copper as 100

[2]Per degree C at 20º C. Note: The conductivity of various metals is subject to variation according to processing and alloy composition

Manganin	3.7	0.00001	150	-
Mercury	1.66	0.00089	-	0.00005
Molybdenum	33.2	0.004	-	0.001
Monel	4	0.002	160	-
Nichrome	1.45	0.0004	150	-
Nickel	12-16	0.006	120	0.008
Nickel silver (18%)	5.3	0.00014	150	-
Phosphor bronze	36	0.0018	25	-
Platinum	15	0.003	55	0.0000005
Silver	106	0.00038	42	0.00001
Steel	3-15	0.004	42 - 230	-
Tin	13	0.0042	4	0.004
Titanium	5	-	50	0.4
Titanium, 6A14V	5	-	130	-
Tungsten	28.9	0.0045	500	0.007
Zinc	28.2	0.0037	10	0.01

Appendix B

Resistance of 27% Ni-clad Cu in function of the time and the temperature

B.1   Model of the Increase of Resistance of Nickel-Clad Copper in Function of Time and Temperature.

For a constant temperature it is also possible to build a model of the ageing process of the nickel clad copper wire. It could be done with the theory of the diffusion and then correlated to the resistance through the resistivity of the nickel-copper alloy in function of its concentration. In this report we will restrain this analysis to an approximation based on the physical model. The diffusion process is proportional to the square root of the time, and proportional to the exponential of the temperature:

- Diffusion $\approx \sqrt{time}$
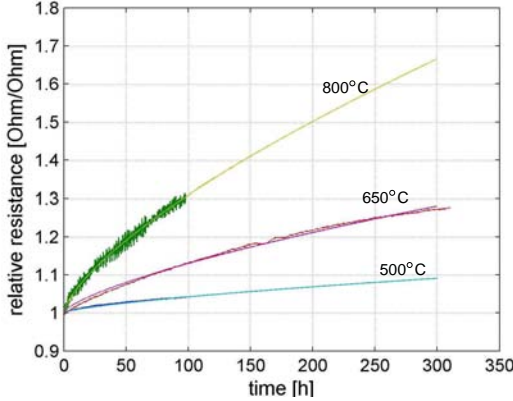- Diffusion $\approx e^{Temperature}$

Figure B.1: Extrapolation of the electrical resistance

From this point we have searched a good approximation of the curves, for each temperature. The equation, which was used has the following form:

$$R_{relative} = (e^{-\frac{\alpha}{T}}t)^P, P \simeq 0.5 \qquad\qquad (B.1)$$

The only unknown parameter is α. So for the tests with the 27% Ni clad Cu, we can obtain three values for α, one for each temperature. If the model was accurate, the values would be equal. Figure B.1 shows the approximation for three temperatures. To compare graphically if the model is accurate, we can extrapolate the curves for each temperature for the two other temperatures and see the accuracy, as it is done in figure . We can see that this basic model gives a good approximation. We can notice too, that it is better to extrapolate the result obtained of highest temperature. We can also compare the values of the coefficient α:

- $\alpha_{500} = 7058$

- $\alpha_{650} = 6940$

- $\alpha_{800} = 6743$

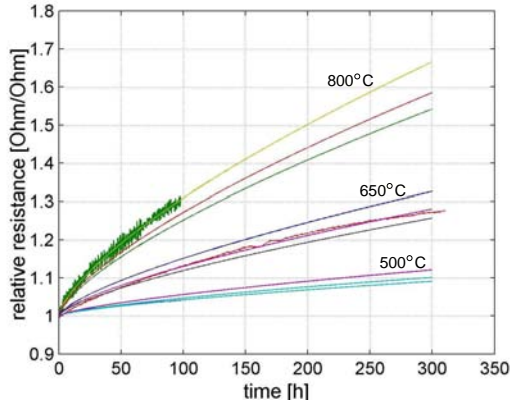The maximal difference between the coefficients is only 4.6%.

Figure B.2: Comparison of each model parameter results

B.2 Life Span Estimation

As said before, the ageing of the material is a non-neglectable factor at high temperature. For example in the case of nickel-clad copper wire, there is diffusion between the conductor and the cladding, which causes an increase of electrical resistance of the coils. Tests have been made at different temperatures for different materials during hundreds of hours and the curves have been approximated in order to predict the behavior of the materials after a very long time (figure B.1). Test with cyclic thermal loading still have to be done. The thermal model gives for example the temperature inside the coil layers in function of the current. So using the resistance estimation and the thermal model, it is possible to estimate the life span in function of the current.

B.3 Conclusion

In order to find a conductor for high temperatures, static high temperature tests have been done. If copper wire is used, it has to be protected against oxidation. This protection has to be very stable in temperature and not diffusing into the conductor, even at high temperature. The coating has to be thick enough to not diffuse entirely into the copper. The tests made with 27% nickel-clad copper wire

show that it is not a stable solution for high temperatures applications. After operation at high temperature, the resistance of the wire increased considerably. This wire may only be used with an accurate diffusion model in order to estimate the increasing of resistance in function of time. Approximations made here allow to accelerate life span testing by performing tests at a very high temperature. The results can be extrapolated to the real operating temperature. Another material for the coating should be found, a material which can stop the oxidation and which does not diffuse into the copper, as stainless steel or ceramic do.

Bibliography

[1] M. Aenis and R. Nordmann. A precise force measurement in magnetic bearings for diagnosis purposes. In *ISMT 5*, 1999.

[2] Beat Aeschlimann. *Control Aspects of High Precision Active Magnetic Bearings*. Phd dissertation, Ecole Polytechnique Fédérale de Lausanne, Switzerland, 2001. Thèse Nr. 2489.

[3] Michèle Basseville, Albert Benveniste, and Qinghua Zhang. Surveillance d'installations industrielles: Démarche générale et conception de l'algorithmique. Technical report, IRISA, Campus universitaire de Beaulieu, Rennes, France, 1996.

[4] A. C. Beiler. Magnetic materials for space power systems. *Journal of Applied Physics*, Vol. 38(No. 3), March 1967.

[5] Luc Burdet, Beat Aeschlimann, and Roland Siegwart. Thermal model for a high temperature magnetic bearing. In *International Symposium of Magnetic Bearings (ISMB 9)*, 2004.

[6] Luc Burdet, Thomas Maeder, Roland Siegwart, Philipp Buehler, and Beat Aeschlimann. Thick-Film Radial Position Sensor for High Temperature Magnetic Bearings. In *Tenth International Symposium on Magnetic Bearings*. Martigny, Switzerland, 2006.

[7] Y. Chable. *Circuits hybrides à couches épaisses*. Masson, 1993.

[8] David Colling. Soft magnetic structural alloys for elevated-temperature applications. *IEEE Transactions on Magnetics*, Vol. Mag 7(No. 1), 1971.

[9] European Research Project. MagFly - Active Magnetic Bearing for Turbo Machinery, 2002 - 2006. Competitive and Sustainable Growth Program, GRD1-2001-40191.

[10] R. J. Field and V. Iannello. A reliable magnetic bearing system for turbomachinery. In *Seventh International Symposium on Magnetic Bearings*. ETH Zürich, 2000.

[11] Richard T. Fingers and C. Scott Rubertus. Application of high temperature magnetic materials. *IEEE Transactions on Magnetics*, Vol. 36(No. 5):3373, September 2000.

[12] Richard Todd Fingers. *Creep Behavior of Thin Laminates of Iron-Cobalt Alloys for Use in Switched Reluctance Motors and Generators*. PhD thesis, Virginia Polytechnic Institute and State University, Blacksburg, Virginia, June 1998.

[13] M. A. Fumagalli. *Modelling and Measurement Analysis of the Contact Interaction between a High Speed Rotor and its Stator*. PhD thesis, Swiss Federal Institute of Technolgy, Zürich, Zürich, 1997. Diss.-No. 12509.

[14] Tapan K. Gupta. *Handbook of thick- and thin-film hybrid microelectronics*. John Wiley & Sons, inc., 2003.

[15] H. Hofmann. *Phénomènes de Transfert*. Laboratoire de Technologie des Poudres, EPFL/IMX.

[16] V. Iannello. Sensorless position for an active magnetic bearing. Technical report, United States Patent No. 5,696,412, 1997.

[17] Mark Jansen, Gerald Montague, Andrew Provenza, and Alan Palazzolo. High speed, high temperature, fault tolerant operation of a combination magnetic-hydrostatic bearing rotor support system for turbomachinery. Technical report, John H. Glenn research center, Cleveland, Ohio, 2004.

[18] S. Jumonhi, J. Senoo, K Ueda, S. Chabata, S. Amano, and A. Ono. Super heat resistant ceramic insulated wire. *Electrical Electronics Insulation Conference, 1995, and Electrical Manufacturing and Coil Winding Conference. Proceedings*, 1995.

[19] Jonas Jung. Performance test of high temperature magnetic bearings. Master's thesis, Swiss Federal Institute of Technology, Zurich, Institut für Robotik, 2000.

[20] Anthony S. Kondoleon and William P. Kelleher. Soft magnetic alloys for high temperature radial magnetic bearings. In *Seventh International Symposium on Magnetic Bearings*. ETH Zürich, August 2000.

[21] Simeon J. Krumbein. Tutorial: Elecrolytic models for metallic electromigration failure mechanisms. *IEEE Transactions on Reliability*, Vol. 44(No. 4), 1995.

[22] P. Kueser. Properties of magnetic materials for use in high-temperature space power systems. Technical report, NASA SP-3043, 1967.

[23] René Larsonneur and Philipp Bühler. New radial sensor for active magnetic bearings. In *Ninth International Symposium on Magnetic Bearings*. Lenxington, Kentucky, August 2004.

[24] Florian Lösch. *Identification and automated controller design for active magnetic bearing systems.* Phd dissertation, Swiss Federal Institute of Technology, Zurich, Switzerland, 2001. Diss. ETH Zurich Nr. 14474.

[25] Mouhoub Mekhiche, Stephen Nichols, John Oleksy, John Young, Jerome Kiley, and Douglas Havenhill. 50 krpm, 1100 °f, magnetic bearings for jet turbine engines. In *Seventh International Symposium on Magnetic Bearings*. ETH Zürich, August 2000.

[26] Gerald Montague, Mark Jansen, Ben Ebihara, Ralph Jansen, Alan Palazzolo, Randy Tucker, Jason Preuss, Andrew Hunt, Jeff Trudell, and Andrew Provenza. Design and fabrication of high-temperature, radial magnetic bearing for turbomachinery. Technical Report E-13861, National Aeronautics and Space Administration, John H. Glenn Research Center at Lewis Field, Cleveland, Ohio, 2003.

[27] Gerald Montague, Mark Jansen, Ralph Jansen, Ben Ebihara, Andrew Provenza, and Dr. Alan Palazzolo. Experimental high temperature characterization of a magnetic bearing for turbomachinery. In *American Helicopter Society 59th Annual Forum*, NASA Glenn Research Center, Cleveland, Ohio. University of Toledo, Ohio. Texas AM University, College Station, Texas, 2003.

[28] Gerald Montague, Mark Jansen, Andrew Provenza, Ralph Jansen, Ben Ebihara, and Alan Palazzolo. Room temperature characterization of a magnetic bearing for turbomachinery. Technical report, John H. Glenn Research Center at Lewis Field, Cleveland, Ohio, 10 2002.

[29] G.T. Murray. *Handbook of materials selection for engineering applications.* Macel Dekker, Inc., 1997.

[30] Hussein M. Naguib and Blair K. MacLaurin. Silver migration and the reliability of pd/ag conductors in thick-film dielectric crossover structures. *IEEE Transactions on Components, Hybrids, and Manufacturing Technology*, Vol. CHMT-2(No. 2), 1979.

[31] Myounggyu D. Noh. *Self Sensing Magnetic Bearings Driven by a Switching Power Amplifier*. Phd thesis, University of Virginia, 1996.

[32] Y. Okada, K. Matsuda, and B. Nagai. Sensorless magnetic levitation control by measuring the pwm carrier frequency component. In *Proceedings of the Third International Symposium on Magnetic Bearings*. Alexandria, USA, 1992.

[33] Matthias Orth, Rainer Erb, and Rainer Nordmann. Investigations of the behaviour of a magnetically suspended rotor during contact with retainer bearings. In *Seventh International Symposium on Magnetic Bearings*. ETH Zürich, 2000.

[34] Matthias Orth and Rainer Nordmann. ANEAS, A Modeling Tool for Nonlinear Analysis of Active Magnetic Bearing Systems. In *Proceedings of the Mechatronic Systems Conference*. Berkeley, California, Dec. 2002.

[35] Cédric Paychère. *Conception d'entraînements électriques intégrés pour dispositifs multi-axiaux*. PhD dissertation, Ecole Polytechnique Fédérale de Lausanne, Switzerland, 1997. Thèse Nr. 1693.

[36] Béatrice Peyrani. Jean-Cyril Spinetta - Le Conquistador du Ciel. *Le Point*, May 2005.

[37] J.M. Provost. The more electric aero-engine: a general overview from an engine manufacturer. In *International Conference on Power Electronics Machines and Drives*. Bath, UK, 2002.

[38] Roland Siegwart, Hannes Bleuler, and Alfons Traxler. *Mechatronic Systems Techniques and Applications*, volume Vol. 4, chapter Industrial Magnetic Bearings - Basics and Applications. Gordon Breach Science Publisher, 2000.

[39] Alexandre Schammass. *Self-Sensing Active Magnetic Bearing : Modulation Approach*. PhD dissertation, Ecole Polytechnique Fédérale de Lausanne, Switzerland, 2003. Thèse no. 2841.

[40] Gerhard Schweitzer. Active magnetic bearings - chances and limitations. In *Sixth International Conference on Rotor Dynamics*, pages pp. 1–14. FTOMA, Sydney, 2002.

[41] Gerhard Schweitzer, Hannes Bleuler, and Alfons Traxler. *Active Magnetic Bearings*. Number ISBN 3 7281 2132 0. Hochschulverlag AG der ETH Zürich, 1994.

[42] Roland Siegwart. *Aktive magnetische Lagerung einer Hochleistungs-Frässpindel mit digitaler Regelung*. Diss. eth nr. 8962, Swiss Federal Institute of Technolgy, Zürich, 1989.

[43] Alfons Traxler. *Eigenschaften und Auslegung von Berührungsfreien Elektromagnetischen Lagern*. Phd dissertation, Swiss Federal Institute of Technolgy, Zürich, Switzerland, 1986. Diss ETH Nr. 7851.

[44] Kim Vu. Silver migration - the mechanism and effects on thick-film conductors. Technical report, College of Engineering - Chemical and Material Science Engineering Department, San Jose State University, 2003.

[45] Letian Wang, Lonxiang Xu, and Gerhard Schweitzer. AMB Temperature Restrictions - 1.3 Report on High Temperature Prototype AMB Development. Technical report, ETH, September 1999. EU Project.

[46] H. Y. Wong. *Heat Transfer for Engineers*. Longman Group Limited, 1977.

[47] L. Xu and J. Zhang. A Study on High Temperature Displacement Sensor. *IEEE Trans. on Instrumentation and Measurement*, 2000.

[48] Longxiang Xu and Gerhard Schweitzer. AMB Temperature Restrictions – 1.1 Identify Temperature Limitations in Current AMB Designs. Technical report, ETH, September 1998. EU Project.

[49] Longxiang Xu, Letian Wang, and Gerhard Schweitzer. Development of Magnetic Bearings for High Temperature Suspension. In *Seventh International Symposium on Magnetic Bearings*. ETH Zürich, 2000.

[50] Lonxiang Xu, Letian Wang, and Gerhard Schweitzer. AMB Temperature Restricions – 1.2 Report on Alternative Materials. Technical report, ETH, June 1999. EU Project.

[51] R. H. Yu, S. Basu, Y. Zang, and J. Q. Xiao. Magnetic Domains and Coercivity in FeCo Doft Magnetic Alloys. *Journal of Applied Physics*, Vol. 85(No. 8), April 1999.

Curriculum Vitae

I was born on 19 June 1978 in Lausanne, Switzerland. I did my primary and secondary school in the school arrondissement of Moudon (Switzerland). In 1993, I went to the Gymnase du Bugnon in Lausanne, where I got a scientific Maturity (C) in 1997. In 1997 to 2002 I started my degree in microtechnics in the EPFL (Swiss Federal Institute of technology, Lausanne). During my studies I was very interested in robotics and I participated to two robotic teams for robotic competitions. I was in charge principally of the robots hardware design. In 2002, after writing my degree diploma thesis at the company Daimler-Chrysler in Germany, I got my degree with a specialization in production techniques.

Since 2002, I started to work in the Autonomous System Lab as PhD student under the conduction of the Prof. R. Siegwart. I was involved in an European project related to active magnetic bearings for high temperature applications. I did the major part of my research at the company MECOS Traxler AG, as EU project partner. For this purpose I lived in Zurich (Switzerland) until late 2005. In 2006, I came back to live in Lausanne. I wrote the present thesis mainly at the EPFL.